



Universiteit
Leiden
The Netherlands

The holographic glass bead game : from superconductivity to time machines

Bagrov, A.

Citation

Bagrov, A. (2015, September 23). *The holographic glass bead game : from superconductivity to time machines. Casimir PhD Series*. Retrieved from <https://hdl.handle.net/1887/35436>

Version: Not Applicable (or Unknown)

License: [Leiden University Non-exclusive license](#)

Downloaded from: <https://hdl.handle.net/1887/35436>

Note: To cite this publication please use the final published version (if applicable).

Cover Page



Universiteit Leiden



The handle <http://hdl.handle.net/1887/35436> holds various files of this Leiden University dissertation

Author: Bagrov, Andrey

Title: The holographic glass bead game : from superconductivity to time machines

Issue Date: 2015-09-23

**The holographic glass bead game:
from superconductivity to time machines**

PROEFSCHRIFT

TER VERKRIJGING VAN
DE GRAAD VAN DOCTOR AAN DE UNIVERSITEIT LEIDEN,
OP GEZAG VAN RECTOR MAGNIFICUS
PROF. MR. C.J.J.M. STOLKER,
VOLGENS BESLUIT VAN HET COLLEGE VOOR PROMOTIES
TE VERDEDIGEN OP WOENSDAG 23 SEPTEMBER 2015
KLOKKE 11.15 UUR

DOOR

Andrey Bagrov

GEBOREN TE ZHELEZNODOROZHNY, SOVJET-UNIE IN 1987

Promotores: Prof. Dr. J. Zaanen
Prof. Dr. K. E. Schalm
Promotiecommissie: Dr. A. Starinets (Oxford University, Oxford, VK)
Prof. Dr. S. Vandoren (Utrecht University)
Prof. Dr. A. Achucarro
Prof. Dr. T. H. Oosterkamp
Dr. V. Cheianov
Prof. Dr. E. R. Eliel

Casimir PhD series Delft-Leiden 2015-19

ISBN 978-90-8593-227-7

An electronic version of this thesis can be found at

<https://openaccess.leidenuniv.nl>

Printed & Lay Out by: Proefschriftmaken.nl — Uitgeverij BOXPress

The work described in this thesis is part of the research programme of the Foundation for Fundamental Research on Matter (FOM), which is part of the Netherlands Organisation for Scientific Research (NWO).

The cover shows an allegoric representation of the holographic correspondence as Plato's cave. The material physical reality on the wall of the cave is a projection of ideal holographic archetypes in the bulk. The concept of the cover design is due to Olga Basha, and the concrete realisation is by Marina Vorontsova.

*To my parents Alexander and Valentina,
my wife Olga,
and my sister Anastasia*

Contents

1	Introduction	1
1.1	Preface	1
1.2	The holographic principle: the idea.	5
1.3	The AdS/CFT dictionary	11
1.3.1	Anti-de Sitter spacetime	11
1.3.2	Holographic interpretation of <i>AdS</i> spacetime	13
1.3.3	The Gubser-Klebanov-Polyakov-Witten rule	15
1.3.4	AdS/CFT and thermodynamics	18
1.3.5	Correlation functions from holography	21
1.4	The correspondence as a method	25
1.4.1	Minimal viscosity	25
1.4.2	The holographic superconductor	28
1.4.3	AdS/CFT and fermionic matter	32
1.5	This thesis	35
2	Pairing induced superconductivity in holography	45
2.1	Introduction	45
2.2	Review of fermion spectra in the AdS dual: spin splitting	48
2.3	Self interacting fermions in AdS and a bulk BCS theory	53
2.3.1	Majorana interaction	53
2.3.2	Nambu-Gorkov formalism	53
2.3.3	Perturbative calculation of the scalar source	56
2.3.4	Analytical study of the non-dynamical scalar: double gap equation	58
2.4	Fermionic ordering in holography	61
2.4.1	Purely scalar holographic superconductor	63
2.4.2	Bose-Fermi competition	63
2.4.3	A dynamical BCS scalar and a BCS/BEC crossover	65
2.5	Conclusions	74
2.A	Green's functions and charge densities	75
2.B	Perturbative solution	77
2.B.1	Perturbative fermion spectrum, AdS-gap equation	77
2.B.2	Simplified Gap equation	79

2.C	Numerical methods	80
2.C.1	General strategy	80
3	Holographic phase diagram of quark-gluon plasma formed in heavy-ions collisions	87
3.1	Introduction	87
3.2	Set up	90
3.2.1	Dual conjectures	90
3.2.2	Remarks about the regularization of TS calculations in the case of wall-on-wall collisions	100
3.3	Holographic QGP phase diagram for the central heavy-ions collisions	105
3.4	Holographic QGP phase diagram in the wall-wall dual model of heavy-ions collisions	107
3.4.1	Charged wall as a dual model for a heavy-ion	107
3.4.2	Charged wall-on-wall collision as a dual model for heavy-ions collisions	109
3.4.3	Comparison of the results	111
3.4.4	The square trapped surface calculation	113
3.4.5	Remarks about the regularization	114
3.5	Conclusion	117
3.5.1	Summary	117
3.5.2	Further directions	119
4	Holographic dual of a time machine	127
4.1	Introduction	127
4.2	Time machine in AdS_3	129
4.3	Entwinement of geodesics and causality violations	134
4.4	Quasigeodesics connecting boundary points	139
4.5	The two point Green's function	147
4.5.1	The algorithm	147
4.5.2	Phenomenology and discussion	152
4.6	Phases of the boundary field theory	156
4.7	Conclusions	159
5	Discussion	165
5.1	Holographic fermions and superconductivity	165
5.2	Holography and the non-equilibrium quark-gluon plasma	167
5.3	Theoretical aspects of time travelling	168

Samenvatting	173
Summary	175
List of Publications	177
Curriculum Vitæ	179
Acknowledgments	181

Chapter 1

Introduction

Cognoscibility of the Universe is the basic axiom of beingness of our civilization. Real progress in understanding fundamental principles governing Nature at various scales, from microscopic physics to the dynamical processes in society, can be possible only under one assumption: any conceivable problem we might ever face in our research must be soluble in one way or another. In the novel “The glass bead game”, Hermann Hesse described a surreal world where people have managed to figure out a universal language that allows for establishing precise connections between all branches of human knowledge, and is powerful enough to provide a solution to any problem once it is reformulated in terms of the glass bead game. This fictional concept is a good illustration of what the actual goal of theoretical science should be: not just to solve a problem that seems to be difficult, but rather to find a proper language that automatically makes it almost trivial.

1.1 Preface

A wide class of longstanding open problems in theoretical physics that have proven themselves to be unsolvable with existing methods belongs to the area of strongly interacting quantum systems. The most famous of them include the problem of confinement in quantum chromodynamics, and the question about the physical mechanisms of high Tc superconductivity. After decades spent in efforts to crack these puzzles by standard techniques, it is becoming clear that if we wish to get a handle on strongly correlated quantum dynamics, we should seek a completely new theoretical paradigm.

The problems we are facing in our attempts to analyze physics of strongly interacting systems are caused by two factors - the large value of the coupling constant, and finite fermion density. The first factor manifests itself in the absence of a small parameter that we could use to

construct a perturbative analytic description of a model. If this was the only issue, we still might hope that the equations governing the evolution of a strongly coupled system could be solved at least numerically. This is possible for bosonic models (or models that allow for the effective reformulation in bosonic variables). However, a finite density of quantum fermionic matter leads to an obstacle that may be considered more severe than just the strong correlations. The standard numerical approach to simulation of many-body systems is the (Quantum) Monte Carlo method, which consists of calculating the quantum field theoretical observables by random sampling of the Euclidean phase space configurations, and averaging over them with the Boltzmann distribution. If we are studying a fermionic system, however, the anticommutativity of fermionic operators, along with the finite density, spoils the charge conjugation symmetry of the corresponding Hamiltonian. On the numerical level it leads to the Fermion Sign Problem [1] - uncontrollable sign oscillations of the sampled quantum partition function. This problem is conjectured to be non-polynomially hard [2], and thus it puts very strong limitations even on our ability to perform numerical simulations.

This thesis is dedicated to a new framework, a new language that has demonstrated an unexpected naturalness in dealing with models of many body systems both at strong coupling and finite density. This framework is the holographic correspondence. The holographic principle emerged from attempts to understand the applicability of the laws of quantum theory to black holes in papers by G. 't Hooft [3] and L. Susskind [4]. In its most generic form, the principle states that a theory of quantum gravity in $D + 1$ dimensions should be equivalent to a quantum field theory in D dimensions, in the sense that the degrees of freedom of the two theories can be precisely mapped to each other, and all observables of each of the theories are encoded in its dual partner. Phrased this way, the principle seems to be unrelated to real life phenomenological problems. But we can try to revert this statement and ask when it is possible to represent a quantum field theory in dual gravitational form, and what we can gain from it for our understanding of the QFT?

Nowadays we know several concrete examples of holographic dualities [5–8], among which the most developed and understood one relates gravity in spacetimes with a negative cosmological constant (Anti-de-Sitter spacetimes) to conformal field theories, the *AdS/CFT* correspondence. Even before the holographic principle was proposed, in 1986 J. Brown

and M. Henneaux demonstrated that the asymptotic symmetry group of three dimensional anti-de Sitter space coincides with the two dimensional conformal group [9]. But the actual realization of the correspondence was proposed in 1997 by J. Maldacena [5], who seminally conjectured that the $N = 4$ supersymmetric $SU(N)$ Yang-Mills theory in $D = 4$ in the strong coupling limit is exactly dual to type IIB string theory on the $AdS_5 \times S_5$ background at weak coupling (and vice versa). The concrete rigorous mathematical formulation of the correspondence was developed by S. Gubser, I. Klebanov, and A. Polyakov in [10], and E. Witten [11]. They emphasized an equivalence of partition functions of the two dual theories that provides a way to calculate correlation functions, now known as the GKPW-rule.

We should remark that the idea of weak/strong dualities is not novel in physics. Already in 1941, H. Kramers and G. Wannier discovered that a two dimensional Ising model on a square lattice at small coupling is dual to itself at strong coupling [12]. Since that time, plenty of other dualities in many areas of theoretical physics have been figured out and played a great role in the history of science. Some of them relate only two particular models, some are broader and applicable to large classes of theories. The latter include the Seiberg duality [13] that equates infrared fixed points of $N = 1$ supersymmetric field theories with different number of flavors and colors, and the particle-vortex duality [14], relating the dynamics of point-like and non-local objects in statistical systems. However, as we will see further, holographic duality has so far demonstrated the largest flexibility and universality in description of various models in completely different areas of theoretical physics.

Originally the AdS/CFT correspondence was an important string theoretical construction, though unrelated to quantum many-body phenomenology. A key observation was made by G. Policastro, A. Starinets, D. T. Son in [15], and then elaborated on by P. Kovtun, A. Starinets, D. T. Son in [16]. Using the AdS/CFT correspondence, they calculated the shear viscosity of the $N = 4$ supersymmetric quark-gluon plasma, and it turned out to be not a value specific for the particular toy model, but a universal quantity equal to $\hbar/4\pi k_B$, which they conjectured to be a lower bound for the shear viscosity of an ideal quantum liquid. This calculation and this conjecture were of huge importance since they demonstrated that the holographic correspondence, in principle, can be used to get insights into the physics of experimentally accessible strongly cor-

related field theories. The era of applied holography had begun. The *AdS/CFT* correspondence was successfully applied to plenty of different physical phenomena, from non-equilibrium processes in the quark-gluon plasma [17] and meson spectra in QCD [18], to the transport properties of high temperature superconductors [19, 20] and the evolution of open quantum systems [21]. Holographic quantum chromodynamics and holographic condensed matter theory evolved into broad independent areas of physics [22, 23].

Among other achievements we can mention the following:

- The theory of hydrodynamics has been fully reformulated holographically [24, 25]. That opened a natural and simple way to describe dissipative forces in quantum systems, that is hard to do within the standard field theoretical formalism. In particular, accurate simulations of turbulence in quantum liquids have been performed with the holographic approach [26, 27].
- Transport coefficients of unconventional superconductors have been calculated. The linear temperature dependence of electric resistivity of non-Fermi liquids, that can not be derived within the standard Landau Fermi liquid paradigm, was demonstrated to naturally come out of holographic setups [20, 28], as well as the Hall angle [29].
- A framework for simulations of the non-equilibrium quark-gluon plasma, using advances of numerical relativity, has been developed [30]. This opened a possibility to study real-time processes in the QGP theoretically.
- A language to describe phases of fermionic quantum matter, that does not rely on the paradigm of weakly coupled Fermi liquids, has been suggested [31, 32].

After more than ten years of research, the applied *AdS/CFT* correspondence is still a young and actively developing area of physics. Being a drastically new, and not completely established, language, it attracted both attention and enthusiasm, and justified criticism and skepticism of theoretical physicists. It still remains to be seen whether holographic duality really has the capacity to become The Glass Bead Game of strongly coupled quantum field theory. But we have very good reasons to hope so.

This thesis is organized as follows. In section 1.2 of the introductory chapter we review basic ideas of the holographic principle closely following

the original paper by L. Susskind [4]. In 1.3 we briefly introduce technical aspects of the *AdS/CFT* correspondence, the so called *AdS/CFT* dictionary that translates quantum field theoretical objects to the language of the theory of gravity. In 1.4 we recall the most important steps in the history of the applied “phenomenological” holography. Chapters 2, 3, and 4 are based on research papers and form the core of this thesis.

1.2 The holographic principle: the idea.

The idea of the holographic principle is based on the fundamental fact first emphasized by J. Bekenstein [33], that if we wish to account for quantum properties of matter interacting with a black hole, we should unavoidably impose that the black hole must be subject to the laws of thermodynamics. To understand this statement, recall that the black hole event horizon is not a singular surface. A freely falling observer crossing the horizon will not experience anything qualitatively new at this moment. It is always possible to make a simple coordinate change that makes this explicit. Therefore if we wish to construct a self-consistent theory of a quantum field evolving in the background of a black hole, we should properly define it not only outside of the horizon, but also behind it.

This was done by S. Hawking [34], and the outcome of his calculation was that quantum effects would lead to evaporation of the black hole. Without getting into formal mathematical details, we can see it from the following reasoning. A classical signal from behind the horizon cannot leave the black hole and reach the outer region. However quantum phenomena are more subtle. Quantum fluctuations can lead to formation of a virtual pair near the horizon. Under normal circumstances these particles would not be observable and would immediately annihilate, since for a very short time they violate the energy conservation law. But if they emerged from a vacuum on the opposite sides of the black hole horizon, the physical picture becomes more complicated. The signature of the space-time alternates across the horizon, and the timelike direction ∂_t becomes spacelike behind the horizon. Since the energy of a particle is associated with the symmetry of translations in time, this sign change would lead to the fact that the virtual particles on either sides of the horizon will have energies of opposite signs. From the point of view of an external observer the particle behind the horizon has negative energy, and the conservation law is not violated. Thus if the outer particle has speed large enough to

leave the vicinity of the black hole (for light-like particles that's always true), it will not annihilate with its counterpart.

This particle emission due to quantum fluctuations near the horizon is known as Hawking radiation. The radiation takes away energy from the black hole, thus causing its evaporation. Hawking famously demonstrated that this black hole radiation has a black body thermal spectrum with a temperature (in the natural $k_B = \hbar = c = 1$ unit system):

$$T = \frac{1}{8\pi GM}. \quad (1.1)$$

Because a black hole has a temperature and energy (equal to its mass, $M = E$), it would be natural to define its entropy in accordance with the first law of thermodynamics:

$$dM = dE = TdS. \quad (1.2)$$

supporting Bekenstein's conjecture. So,

$$dM = \frac{1}{8\pi GM} dS, \quad (1.3)$$

and finally for the entropy we get

$$S = 4\pi M^2 G = \frac{\pi R_s^2}{4G} = \frac{A}{4G}, \quad (1.4)$$

where $R_s = 4GM$ is the Schwarzschild radius, and A is the area of the event horizon.

The next natural question to ask is what kind of microscopic statistical physics is behind a black hole's thermodynamic properties? This area-law scaling is very puzzling from the perspective of general physics wisdom. We do not have a complete theory of quantum gravity yet, but it would be natural to assume that a unit cell of a quantum gravity phase space must be set by the Planck scale, $l_P = \sqrt{G}$. If each Planck cell encodes k degrees of freedom, then the naive counting tells us that the total number of possible different microstates corresponding to the macroscopic black hole should be proportional to

$$\Gamma_{\text{naive}} = k^{\frac{4\pi R_s^3}{3l_P^3}}. \quad (1.5)$$

The black hole entropy scales then with the volume of the black hole, and not with the area:

$$S_{\text{naive}} = \frac{V}{G^{3/2}} \log k. \quad (1.6)$$

A radical solution to this contradiction has been suggested by G. 't Hooft [3] and L. Susskind [4]. They conjectured that the actual number of states in a theory of quantum gravity should be lower than the naive estimation, and that any quantum state of a subregion of the $3 + 1$ dimensional spacetime can be completely encoded in a state of its $2 + 1$ dimensional boundary. In this language, the number of microstates n inside a spatial volume $V = \frac{4}{3}\pi R^3$ can not exceed the maximal possible value set by (1.4):

$$n \leq \exp(S) = \exp(\pi R^2 / 4G). \quad (1.7)$$

When this bound, called the entropic bound, is saturated, a black hole forms, and any further increase of the number of microstates is impossible without growing of the black hole volume/area.

Because the number of microstates of a black hole is the maximal for a given volume, if the 't Hooft-Susskind holographic conjecture is correct for a black hole, it should also be correct for any other macroscopic state of a spacetime. In the limit of an infinitely large region, the state of the whole spacetime can be reconstructed from the state of a lower dimensional surface at spatial infinity. From here on, we will call the higher dimensional space the “bulk”, and its encoding boundary surface the “boundary”. An elementary Planckian volume $\sim l_P^3$ in the bulk then corresponds to an elementary area $\sim l_P^2$ on the boundary. We will refer to this elementary boundary area as a “pixel”.

This holographic principle sounds very counterintuitive. A simple counterexample to it appears to be a collection of black holes where one of them is shielded by others from the boundary. Nevertheless configurations of this kind can be holographically projected onto the boundary in an unambiguous manner. If we have a number of black holes in the bulk, their horizons still form a disconnected surface of a finite area, and can be injectively mapped pixel-by-pixel to the boundary. The easiest way to show this is by tracing classical light rays emerging from the horizons. The gravitational field of a black hole has the property that nothing can be hidden in the “shadow” of a black hole. Light rays approaching the black hole from behind would be strongly deflected and reach the observer

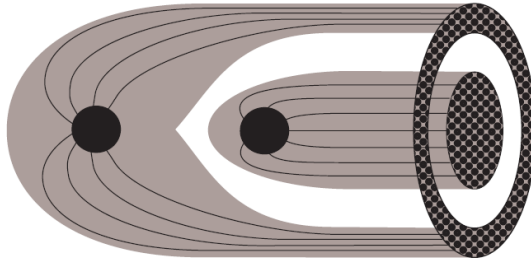


Figure 1.1. The horizons of two black holes, after the holographic mapping, form a picture on the boundary. Nothing can be hidden behind a black hole, so each Planckian pixel on both of the horizons can be connected with a unique pixel on the boundary without any overlap.

in front of the black hole (see Fig. 1.1). In particular, it can be explicitly calculated that, for an arbitrary distribution of black holes in the bulk, information about the states of their horizon pixels can be unambiguously transmitted to the boundary by light-like geodesics orthogonal to it [4].

What we have discussed so far is related to the physics of black holes. The natural question to ask is whether an arbitrary configuration of gravitational fields *and* matter possesses a holographic description. It is natural to expect that if we have non-gravitational degrees of freedom in the bulk, we can map them onto the boundary only if the dual holographic quantum field theory also contains matter. Here we face a new puzzle. If a point-like particle (we will call it a parton) is located somewhere in the bulk, its projection on the boundary screen at first sight seems to occupy a single boundary pixel, independently of its bulk coordinates. So, how would we encode the parton's distance to the boundary? A possible resolution of this problem has been proposed by L. Susskind [4]. Consider the holographic extra bulk dimension in the momentum representation, i.e. partons with larger values of the holographic coordinate have higher momenta. We must take into account that a parton is a quantum object. If we boost it up to high enough energy, the interplay of quantum and relativistic effects causes particle number non-conservation, and the parton can split into multiple partons (see Fig. 1.2). Thus, in the rest frame of a static observer at the boundary, we see a spatially distributed cloud of apparent partons instead of the original single point-like particle. To estimate the growth of the cloud's transversal area under Lorentzian

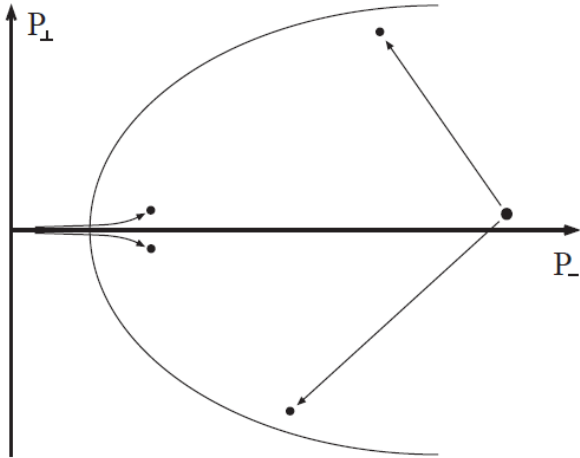


Figure 1.2. Momentum space representation: the larger is the “holographic” momentum P_{\parallel} , the stronger is the effect of partonic cloud spreading in the transversal “boundary” directions, P_{\perp} .

boosts, we can use different models of relativistic partons. In particular, if we treat the parton as a free string in the context of string theory, the dependence of its transversal size on the momentum can be shown to be logarithmic [4] (when the energy of the parton is much lower than the Planckian limit):

$$R_{\perp}^2 \sim l_s^2 \log \frac{P_{\parallel}}{\epsilon}, \quad (1.8)$$

where l_s is the string length, and ϵ is an IR cut-off. Hence information about the holographic momentum of a parton can be stored in the size of its boundary projection.

This picture can be rephrased in terms of the coordinate representation. Consider a parton falling into a black hole in the bulk. The further away it is from the boundary, and closer to the horizon, the larger are its momentum and transversal spreading. In the rest frame of a static observer, the transversal size of the parton grows in time as [4]

$$R_{\perp}^2 \sim l_s^2 \frac{t}{4GM}, \quad (1.9)$$

when the energy is much smaller than the Planckian limit, and

$$R_{\perp}^2 \sim l_s^2 e^{\frac{t}{4GM}}, \quad (1.10)$$

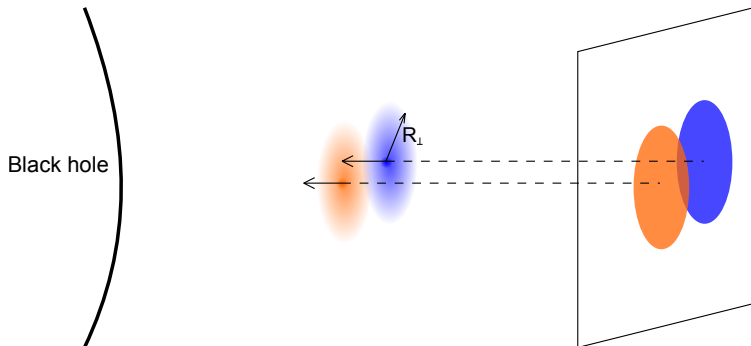


Figure 1.3. Overlapping partonic clouds and their holographic projection. Transversal size grows in time as the parton approaches the black hole.

in the ultra-relativistic transplanckian regime. So the distance to the screen is encoded in this quantity.

The last point to be discussed is how to describe holographically a many-particle bulk state. When a number of partons are boosted by the gravitational forces to very high energies, their images on the screen start overlapping, as shown on Fig. 1.3. As they approach the horizon, the overlap becomes stronger, and at some point the partons lose their identity. Information about their bulk state can not be any more recovered just from local probes of the holographic boundary. In the dual boundary language, the pixels on the screen start getting entangled, and in order to reconstruct the full bulk state we have to analyze non-local correlations. If the boost is extremely strong, we might expect a situation where the partonic clouds spread over the whole horizon, forming infinitely thin identical shells (as is clear from (1.10), this would happen in a finite time). If it happens, partons will become holographically indistinguishable, and even the non-local correlations would not provide us with enough information to reconstruct the bulk state. Nevertheless, the holographic principle still can be saved. As was argued in [4], the apparent partons forming the cloud are not subject to Lorentz contraction. Therefore, when approaching the black hole horizon, each partonic cloud occupies a unique shell of a finite radial thickness, and interpenetration of the two clouds is impossible (we could say they behave as an incompressible liquid). As a result, different partons have different holographic radial positions, and the corresponding pattern imprinted on the holographic screen is unique and unambiguous.

That concludes the generic discussion of the ideas behind the holo-

graphic principle, and we can proceed further to its concrete constructive realisation - the Anti-de-Sitter/Conformal Field Theory correspondence (*AdS/CFT*).

1.3 The AdS/CFT dictionary

In this section we provide a brief introduction to technical aspects of the AdS/CFT correspondence. We start with reviewing basic facts about anti-de Sitter spacetime, and provide a holographic interpretation of its geometric features. Then we introduce the holographic prescription for a quantum field theory partition function (the Gubser-Klebanov-Polyakov-Witten formula), and demonstrate how it can be used both to describe collective thermodynamic properties of the QFT and to calculate microscopic correlation functions.

1.3.1 Anti-de Sitter spacetime

Anti-de Sitter space is a maximally symmetric space of a constant negative curvature, which can be thought of as a one sheet hyperbolic surface embedded into $\mathbb{R}^{(2,d)}$ space. In physics it naturally appears as a vacuum solution to the Einstein-Hilbert equations with negative cosmological constant. The embedding into the higher-dimensional flat space is given by the equation

$$-X_0^2 - X_{d+1}^2 + \sum_{i=0}^d X_i^2 = -L^2. \quad (1.11)$$

By construction, this surface is a homogeneous and isotropic Riemannian manifold with the $SO(2,d)$ isometry group. L here is the *AdS* radius, and hereinafter we set it to be $L = 1$. The induced metric on this surface can be obtained by parameterizing these $d + 2$ dimensional coordinates in terms of $d + 1$ independent variables:

$$X_0 = \sqrt{1+r^2} \cos(t), \quad (1.12)$$

$$X_{d+1} = \sqrt{1+r^2} \sin(t), \quad (1.13)$$

$$X_i = r\Omega_i, \quad (1.14)$$

where Ω_i are coordinates on a d -dimensional sphere. The induced metric on the hypersurface is the

$$ds^2 = -(1+r^2)dt^2 + \frac{dr^2}{1+r^2} + r^2 d\Omega_{d-1}^2. \quad (1.15)$$

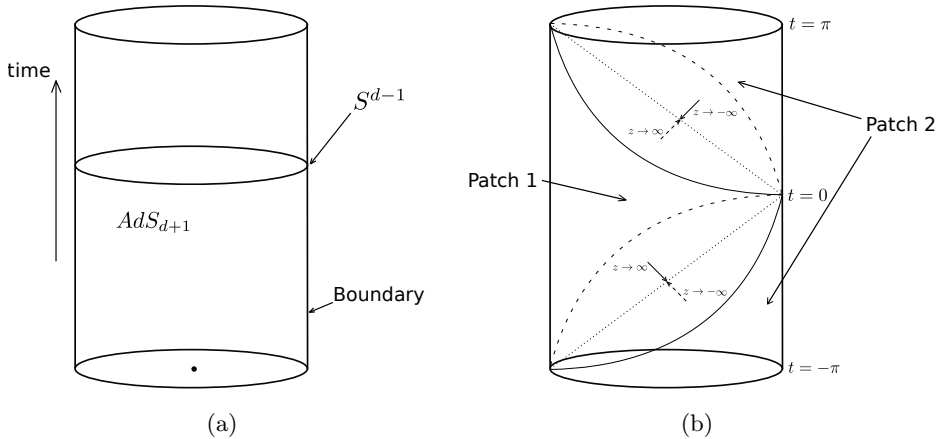


Figure 1.4. (a): Penrose diagram of the universal cover of the anti-de Sitter spacetime. (b): Global (unwrapped!) AdS consists of two Poincaré charts separated from each other by Poincaré horizons $z \rightarrow \pm\infty$. Time is periodic, so time slices $t = -\pi$ and $t = \pi$ are identified.

This set of coordinates is called global, and covers the whole hyperboloid. Note that time is periodic in these coordinates. In order to avoid closed time-like curves, the time axis can be unwrapped to make $t \in (-\infty, \infty)$. We will always consider this universal cover of global AdS .

The topology of the universal cover of AdS is easily recognized as a cylinder (see Fig. 1.4a): the axis of the cylinder ($r = 0$) is codirected with the time axis, the boundary of the cylinder depicts spatial infinity $r = \infty$, and each $t = \text{const}$ slice of the boundary has the topology of a sphere S^{d-1} . The boundary of the cylinder is a visual representation of the so called conformal boundary of AdS - the surface where the quantum field theory that holographically encodes gravity in AdS is defined.

For our future purposes we also introduce a different coordinate system, which is more convenient for many applications - the Poincaré chart

coordinates:

$$X_0 = \frac{z}{2} \left(1 + \frac{1}{z^2} (1 + \vec{x}^2 - t^2) \right), \quad (1.16)$$

$$X_i = \frac{x_i}{z}, \quad (1.17)$$

$$X_{d+1} = \frac{z}{2} \left(1 - \frac{1}{z^2} (1 - \vec{x}^2 - t^2) \right). \quad (1.18)$$

The *AdS* metric in these coordinates has an explicitly conformal form:

$$ds^2 = \frac{1}{z^2} \left(-dt^2 + dz^2 + \sum_{i=1}^{d-1} dx_i^2 \right). \quad (1.19)$$

These coordinates cover only half of the cylinder (as in Fig. 1.4(b)), and describe a case where the conformal boundary is a Minkowski $\mathbb{R}^{1,d-1}$ spacetime (as opposed to $\mathbb{R} \times S^{d-1}$ in the global case) located at $z = 0$.

1.3.2 Holographic interpretation of *AdS* spacetime

According to the holographic principle, the *AdS* gravity should have a dual quantum field theoretical partner on the boundary of *AdS*. We have already announced that the dual theory is a conformal field theory. The reason for this is rooted in the fact that the isometry group $SO(2, d)$ of $(d + 1)$ -dimensional anti-de Sitter spacetime coincides with the conformal group of d -dimensional Minkowski spacetime, which includes $SO(1, d)$ isometry transformations, dilatations and special conformal transformations (radial inversions). Hence it is natural to expect that the symmetries of two sides of the duality should match, and the boundary field theory is actually conformal.

Finally, let us discuss how quantum properties of the boundary theory can be stored in the classical geometry. In the holographic picture we have an extra emergent “radial” coordinate r (or z), which should have some interpretation in the dual boundary terms. To gain some intuition, consider a classical point-like particle in the bulk of AdS_{d+1} . What is it dual to on the boundary? As we will show in the subsequent section, a state of the bulk corresponds to a state of the boundary theory. So, if an empty *AdS* is dual to a ground state, it is natural to expect that this configuration with a point-like particle is dual to an excited state in the corresponding CFT. In conformal field theory, excitations are massless, otherwise

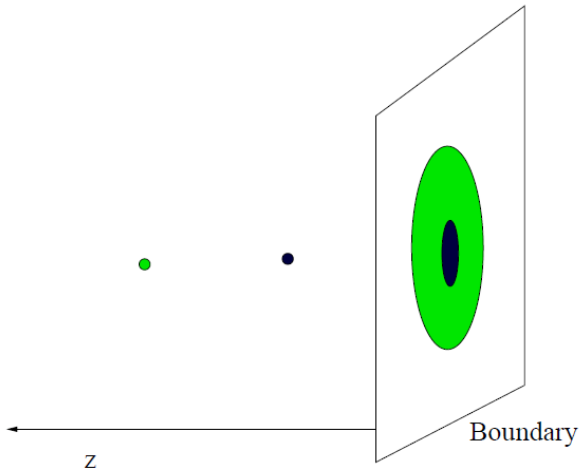


Figure 1.5. The size-to-distance holographic relation.

an explicit scale m would spoil the conformal symmetry. Unlike massive particles, massless conformal excitations are non-local and characterized not only by their position in space, but also by their size [35]. So both the particle in the bulk and the conformal excited state in the boundary can be described by a $(d + 1)$ -vector: the d -vector of the transversal location of the bulk particle encodes for the transversal location of the conformal state, and the extra radial coordinate of the bulk particle encodes for the size of the conformal state (see Fig.1.5). The further the particle is from the boundary, the larger it is. We can see that this interpretation is in perfect agreement with Susskind’s vision laid out in the previous section.

In the momentum representation, the spatial size of the excitation corresponds to its inverse energy. Thus the extra holographic coordinate has meaning of energy scale in the boundary field theory: the boundary $z = 0$ corresponds to the UV limit, while $z \rightarrow \infty$ is the IR. The corresponding variation along this direction ∂_z thus geometrically encodes a renormalization group flow, where the $z = 0$ surface corresponds to the ultraviolet fixed point of the theory.

The boundary field theory can be thought of as defined not only at $z = 0$, but at any $z = \text{const}$ surface. In the case of pure AdS all $z = \text{const}$ slices obviously are equivalent, and the RG flow is trivial as should it be in a completely scale invariant theory. However, as we will see later, the

AdS/CFT correspondence is defined not only for pure *AdS*, but also for any solution of General Relativity that possesses an asymptotically *AdS* form. The strict conformal invariance then may be broken, and we find a non-trivial renormalization flow connecting UV and IR fixed points.

To understand how the spectrum of states of the field theory can be mapped onto the bulk gravity, consider a massive particle evolving in *AdS* with zero transversal momentum. Its Lagrangian has form

$$\mathcal{L} = g_{\mu\nu}\dot{x}^\mu\dot{x}^\nu = -\frac{1}{z^2}\dot{t}^2 + \frac{1}{z^2}\dot{z}^2 = -1. \quad (1.20)$$

The particle has two conserved momenta:

$$E = \frac{\dot{t}}{z^2}, \quad J = \frac{\dot{z}}{z^2}, \quad (1.21)$$

and its radial evolution equation is

$$\dot{z}^2 = -z^2 + E^2 z^4. \quad (1.22)$$

At the boundary, the z^2 -term is leading, and for any value of energy E the r.h.s. is negative. This means that the particle experiences an (infinitely) strong repulsive potential as it approaches the boundary:

$$V(z) \sim \sqrt{-g_{00}} \sim \frac{1}{z}, \quad z \rightarrow 0. \quad (1.23)$$

Thus if instead of a particle we consider a field in the bulk, this repulsive potential will act as an infinitely high quantum well. Posing appropriate boundary conditions at both sides of the well, we obtain a well-defined spectrum of quantized bulk wavefunctions that dualizes to the spectrum in the boundary field theory. In other words, classical boundary conditions in the bulk define the quantization rules in the dual theory.

1.3.3 The Gubser-Klebanov-Polyakov-Witten rule

So far we have discussed only the general ideas of *AdS/CFT* holography. Now we define a precise constructive correspondence that allows for concrete calculations of observables.

We want to be able to calculate correlation functions of gauge invariant operators \mathcal{O}_i in the boundary field theory. On the QFT side, a correlation

function of n operators in Euclidean signature can be defined in terms of a generating functional depending on sources J_i :

$$e^{-W[J_i]} = \langle e^{J_i \mathcal{O}^i} \rangle_{QFT}, \quad (1.24)$$

where the averaging on the r.h.s. means path integral evaluation. The n -point correlation function is then just given by an n -th order functional derivative:

$$\langle \mathcal{O}^{i_1} \dots \mathcal{O}^{i_n} \rangle = \frac{\partial^n}{\partial J_{i_1} \dots \partial J_{i_n}} e^{-W[J_i]} \Big|_{J=0}. \quad (1.25)$$

The holographic correspondence states that these operators should be dual to fields ϕ_i in the bulk. More specifically, the mathematical formalism of the *AdS/CFT* correspondence is based on the formula figured out by S. Gubser, I. Klebanov, and A. Polyakov [10], and E. Witten [11] that resides in the fact that the partition functions of the bulk and boundary theories are identical:

$$e^{-W[J_I]} = Z_{bulk} |_{\phi_I(z=0)=J_I}, \quad (1.26)$$

where the boundary value of the bulk field plays the role of the source in the boundary field theory.

To emphasize the calculational power of this law, let us focus on the original version of the *AdS/CFT* correspondence that equates the $\mathcal{N} = 4$ Super Yang-Mills theory on the boundary and the IIB string theory on $AdS_5 \times S_5$ in the bulk. Super Yang-Mills is a $SU(N)$ gauge theory with the following Lagrangian:

$$L_{SYM} = -\frac{1}{4g_{YM}^2} \text{Tr} \left(F_{\mu\nu} F^{\mu\nu} + D_\mu \Phi^I D^\mu \Phi^I + \bar{\psi}^i \gamma^\mu D_\mu \psi^i + [\Phi^I, \Phi^J]^2 + \dots \right). \quad (1.27)$$

Dots are for interaction terms required by the condition of maximal supersymmetry, and the trace is taken over the gauge indices. $F_{\mu\nu}$ is the gauge field strength. The fields Φ^I ($I = 1, \dots, 6$) are scalars, and ψ^i ($i = 1, \dots, 4$) are fermions, all in the adjoint representation of the gauge group.

This theory is completely defined by two parameters: the rank of the gauge group N , and the coupling constant g_{YM} .¹ On the other hand, the string theory also contains only two defining parameters - the string coupling constant g_s , and the curvature scale L/l_s the theory lives on,

¹In a generic case, the theory also has a θ -term $\frac{\theta}{8\pi^2} \int \text{Tr} F \wedge F$, but this is not relevant for the discussion here.

given in terms of the inverse string length. According to 't Hooft we can redefine the perturbative expansion in terms of $\lambda = g_{YM}^2 N$. Later on, this will allow us to take a smooth limit $N \rightarrow \infty$ while keeping the coupling constant finite.

Without getting into detailed derivations, we just quote that these constants dualize according to the relations:

$$4\pi g_s = \frac{\lambda}{N}, \quad \frac{L}{l_s} = \lambda^{1/4}. \quad (1.28)$$

Here is where the weak/strong nature of the duality manifests itself. If we are interested in the strongly coupled regime of the gauge quantum field theory, $\lambda \gg 1$, we should take $L \gg l_s$. In other words it means that on the string theory side of the duality we consider only large scale dynamics, stringy corrections to the geometry are negligible, and the low energy supergravity limit of the string theory is valid. If we also wish to avoid taking into account quantum gravity effects and keep g_s small, we need to stay at the large N limit of the gauge theory, $\lambda/N \ll 1$. From a field theoretical point of view precisely this $N \rightarrow \infty$ limit with fixed $\lambda \ll 1$ corresponds to the contributions of all planar Feynman diagrams, i.e. those which can be drawn on a topologically trivial surface [36].

In the strongly correlated regime $\lambda \gg 1$ the diagrammatic expansion is not well defined, but on the dual side the supergravity approximation is at work, and in Euclidean signature we have

$$Z_{string} = Z_{gravity} = e^{-S_{gravity}} \Rightarrow W[J_I] = S_{gravity}[\phi_I(z=0) = J_I]. \quad (1.29)$$

When the rank of the boundary gauge group is large, $N \gg 1$, the gravitational action can be evaluated just on the classical solution to the equations of motion. Thus we dualize states in the strongly coupled large N boundary quantum field theory to solutions of the classical supergravity theory.

In this thesis we will be studying physical problems that can not be described by a simple supersymmetric Yang-Mills theory, but these key ingredients will be there. What the large N limit corresponds to in, for instance, condensed matter phenomenology is not completely clear. Roughly speaking, it describes a kind of mean field theory of a many-body system, where a self-consistent approximation of the collective dynamics is governed by the bulk classical action. Of course it would be nice to overcome this limitation, but we might hope that the most interesting properties of the physical systems of interest survive in this limit.

1.3.4 AdS/CFT and thermodynamics

Now we are going to use *AdS/CFT* to study strongly coupled physics and discuss the basic elements of the holographic Glass Bead Game.

All physical processes involve energy dynamics, so the first thing to be shown is how it can be described in holography. The classical supergravity theory includes General Relativity as a universal subsector. So we can ignore the supersymmetric nature of the full *AdS/CFT* construction and stick to the Einstein-Hilbert theory with a negative cosmological constant in the bulk and, in general, some matter:

$$S = \frac{1}{2\kappa^2} \int d^{d+1}x \sqrt{-g} \left(R + \frac{d(d-1)}{L^2} + 2\kappa^2 \mathcal{L}_M \right). \quad (1.30)$$

Following the GKPW rule (1.26) and the large-N limit (1.29) the bulk dynamical field - the metric - gains the following interpretation: fluctuations of the bulk metric sources energy currents on the boundary, and thus *the boundary asymptotics of the metric dualizes to the boundary energy-momentum tensor*. This is not to be confused with the bulk energy-momentum tensor.

Another “bead” to be defined is the notion of thermal matter in holography. It can easily be demonstrated that a black hole metric with *AdS* asymptotics corresponds to a thermal state of the dual field theory with temperature equal to the Hawking temperature of the black hole. Consider the simplest black hole solution - the anti de Sitter-Schwarzschild metric. In Poincare coordinates it takes the form

$$ds^2 = \frac{1}{z^2} \left(-f(z)dt^2 + \frac{dz^2}{f(z)} + dx^i dx^i \right), \quad (1.31)$$

where the emblackening factor

$$f(z) = 1 - \left(\frac{z}{z_H} \right)^d. \quad (1.32)$$

Here, z_H is the location of the horizon. Because in coordinates of the Poincare chart the metric is transversally symmetric along the boundary directions, sometimes it’s called a planar black hole.

We can perform a Euclidean continuation of this metric to imaginary time $t \rightarrow i\tau$:

$$ds_E^2 = \frac{1}{z^2} \left(f(z)d\tau^2 + \frac{dz^2}{f(z)} + dx^i dx^i \right). \quad (1.33)$$

It should be emphasized that the Euclidean continued metric does not solve the Euclidean theory automatically. The imaginary time coordinate is periodic, and it can be shown [37] that (1.33) is a saddle point to the *vacuum* Euclidean version of (1.30), only if we fix the period as²:

$$\tau \sim \tau + \frac{4\pi}{|f'(z_H)|} = \tau + \frac{4\pi z_H}{d}. \quad (1.34)$$

To understand meaning of this fact in the dual field theory language, we can perform a near-boundary expansion of the metric ($z \rightarrow 0$):

$$g_{\mu\nu}(z) = \frac{1}{z^2} g_{(0)\mu\nu} + \dots. \quad (1.35)$$

The expansion coefficient $g_{(0)\mu\nu}$ has a natural interpretation as the background metric the boundary field theory evolves in. Clearly, for any asymptotically AdS spacetime it is

$$g_{(0)\mu\nu} = d\tau^2 + dx^i dx^i, \quad \tau \in [0, 4\pi z_H/d) \quad (1.36)$$

so the dual quantum field theory is also defined on a space with periodic imaginary time. Hence, it is in a thermal state of temperature $T = \frac{d}{4\pi z_H}$ which precisely coincides with the Hawking temperature of the bulk black hole.

Here we have made a standard Wick rotation to periodic imaginary time to make the connection between thermal properties of both sides of the correspondence more clear. However a remarkable property of the *AdS/CFT* holography is that the temperature is now an inherent property of the Lorentzian bulk - it is given by the Hawking temperature. It can be shown by a direct calculation [40] that once we have rotated back to the Lorentzian signature, the field theory still is in a thermal state. Therefore we can work with our bulk objects in real time and at finite temperature simultaneously. This is one of the biggest technical advantages of the holographic language over standard field theory machinery.

The next thermodynamical holographic dictionary entry to be defined is the finite charge density or the chemical potential. Again, the *AdS/CFT* correspondence is capable of including it in a very simple, natural manner. Let's add the electromagnetic Maxwell term to our action:

$$S_M = -\frac{1}{4} \int_0^\infty dz \int d^d x \sqrt{-g} F_{\mu\nu} F^{\mu\nu}, \quad (1.37)$$

²Otherwise the metric would contain an apparent unphysical conical defect [37].

where $F_{\mu\nu}$ is the $U(1)$ gauge field strength tensor in the bulk. Integrating it by parts we get

$$S_M = \int_0^\infty dz \int d^d x \sqrt{-g} A_\nu \partial_\mu F^{\mu\nu} + \frac{1}{2} \int d^d x \sqrt{-g} F_{\mu\nu} A^\mu n^\nu|_{z \rightarrow 0}, \quad (1.38)$$

where n^ν is a unit vector orthogonal to the boundary.

Consider then a solution to the equations of motion of the gauge field A_μ . We can deduce that the radial-directed bulk electric field is

$$\frac{\partial \mathcal{L}_{EM}}{\partial(\partial_z A_0)} = \frac{\partial(F_{\mu\nu} F^{\mu\nu})}{\partial(\partial_z A_0)} = E_z, \quad (1.39)$$

and the field A_μ approaches its boundary value as

$$A_\mu(\vec{x}, z) = A_\mu^{(0)}(\vec{x}) + A_\mu^{(1)}(\vec{x}) z^{d-2} + \dots. \quad (1.40)$$

Substituting this function into the electromagnetic boundary action (second term in (1.38)) we can see that the leading and subleading expansion coefficients are coupled:

$$S_b = - \int d^d x \sqrt{-g_{(0)}} A_\mu^{(0)}(\vec{x}) A^{(1)\mu}(\vec{x}) + \dots, \quad (1.41)$$

thus they should be regarded as holographic dictionary entries for conjugate operators in the boundary field theory. Knowing the asymptotic behaviour (1.40), we can derive that the subleading term $A_0^{(1)}$ is the radial-directed bulk electric field E_z evaluated at the boundary: $A_0^{(1)}(\vec{x}) = E_z(\vec{x})$, which in turn is equal to the surface charge density. So holographically we identify the subleading term with the negative³ boundary charge density, $A_0^{(1)} = \rho$, and its conjugate $A_0^{(0)}$ then can be recognized as the chemical potential, $A_0^{(0)}|_{z \rightarrow 0} = \mu$.

In a similar way we can interpret the spatial transversal components of the gauge field. The spatial subleading expansion coefficients $A_i^{(1)}$ are dual to the current J_i , while their sources $A_i^{(0)}$ are dual to spatial components of the global $U(1)$ boundary field. Note that interestingly the bulk $U(1)$ gauge field dualizes to the global $U(1)$ current on the boundary. That's another basic property of the *AdS/CFT* correspondence: bulk

³Due to the overall minus sign in (1.41)

gauge symmetries holographically encodes for global symmetries in the field theory. That's not only true for the discussed example of $U(1)$, but rather a generic property of the correspondence.

Temperature and chemical potential are two important thermodynamical quantities. But it is trivial to show that the GKPW rule provides a complete description of the thermodynamics of the boundary quantum field theory. By definition the free energy F of a QFT is the logarithm of its partition function:

$$e^{-\beta F} = \langle Z \rangle_{QFT}, \quad (1.42)$$

where $\beta = 1/T$. Through *AdS/CFT*, the right hand side of this identity is equal to the bulk string theory partition function, or, in the large N limit, to the classical exponent evaluated at the gravity saddle point. Thus the free energy is simply

$$F = TS_{grav}, \quad (1.43)$$

where the gravity action also contains a boundary term which fixes the boundary conditions for the bulk fields in accordance with (1.29). All other thermodynamical potentials can be derived from F .

1.3.5 Correlation functions from holography

One of the most important aspects of *AdS/CFT* is that we can also extract much more detailed microscopic information. In principle we can compute the full set of correlation functions of the theory. Let us demonstrate the holographic techniques on the two-point Green's function, one of the most physically interesting and simple to calculate quantities. For simplicity, we firstly reproduce the standard result for a Green's function in a conformal field theory in Euclidean signature. After that we will comment on how to use the power of holography to obtain Green's functions at strong coupling directly in the real time representation.

Consider a massive scalar field action:

$$S = \frac{1}{2} \int dz d^d x \sqrt{g} \left(\partial_\mu \phi \partial^\mu \phi + m^2 \phi \right), \quad (1.44)$$

with the corresponding equations of motion:

$$\frac{1}{\sqrt{g}} \partial_\mu (\sqrt{g} g^{\mu\nu} \partial_\nu \phi) - m^2 \phi = 0. \quad (1.45)$$

A solution to this equation in the Euclidean empty AdS space behaves near the boundary as

$$\phi(z, \vec{x}) \simeq z^{\Delta_-} \phi_{(0)}(\vec{x}) + z^{\Delta_+} \phi_{(1)}(\vec{x}) + \dots, \quad \text{when } z \rightarrow 0, \quad (1.46)$$

where

$$\Delta_{\pm} = \frac{d}{2} \pm \frac{1}{2} \sqrt{d^2 + 4m^2}. \quad (1.47)$$

We already know that the leading term $\phi_{(0)}(\vec{x})$ is a source for a dual boundary operator, $\int d^d x \phi_{(0)}(\vec{x}) \mathcal{O}(\vec{x})$.

The Green's function of the differential operator (1.45) can be found exactly:

$$G(0, \vec{x}; z, \vec{x}') = \frac{z^{\Delta_+}}{(z^2 + |\vec{x} - \vec{x}'|^2)^{\Delta_+}}, \quad (1.48)$$

so the solution (1.46) has a representation:

$$\phi(z, \vec{x}) = \int d^d \vec{x}' \frac{z^{\Delta_+}}{(z^2 + |\vec{x} - \vec{x}'|^2)^{\Delta_+}} \phi_0(\vec{x}'). \quad (1.49)$$

Having the solution, we can substitute it into the action, and evaluate the functional derivative with respect to $\phi_0(\vec{x})$ to apply the GKPW rule. The bulk action variation around the solution is zero by definition, so, as before when we discussed the gauge field, all non-trivial structures are contained in the surface boundary term:

$$\delta S(\phi) = \int d^d \vec{x}' d\Sigma^\mu \partial_\mu \phi \delta \phi, \quad (1.50)$$

where $d\Sigma^\mu$ is the boundary area element. To apply the GKPW rule (1.25), (1.26) we need to express this variation in terms of the boundary data. Varying the boundary action is a subtle procedure that requires accurate treatment of near boundary divergences. Without touching on related technical issues, we just quote the result [38]:

$$\delta \phi = z^{\Delta_-} \delta \phi_0, \quad (1.51)$$

$$\delta S(\phi) = \int d^d \vec{x} d^d \vec{x}' \frac{\phi_0(\vec{x}) \delta \phi_0(\vec{x}')}{|\vec{x} - \vec{x}'|^{2\Delta_+}}. \quad (1.52)$$

Taking the first functional derivative, for the boundary vacuum expectation value sourced by $\phi_0(\vec{x})$ we get

$$\langle \mathcal{O}(\vec{x}) \rangle = \frac{\delta(-S(\phi))}{\delta \phi_0(\vec{x})} = - \int d^d \vec{x}' \frac{\phi_0(\vec{x}')}{|\vec{x} - \vec{x}'|^{2\Delta_+}} \quad (1.53)$$

Repeating the procedure we arrive at the correct result for the Euclidean 2-point conformal Green's function:

$$\langle \mathcal{O}(\vec{x}) \mathcal{O}(\vec{x}') \rangle = \frac{\delta(-S(\phi))}{\delta\phi_0(\vec{x})\delta\phi_0(\vec{x}')} = \frac{\text{const}}{|\vec{x} - \vec{x}'|^{2\Delta_+}}. \quad (1.54)$$

Clearly Δ_+ is the conformal dimension of the operator \mathcal{O} in the boundary field theory. We obtain a new holographic dictionary entry: *the mass of the bulk field corresponds to the conformal dimension of the dual boundary operator.*

In many cases, the Euclidean correlator can be then analytically continued to Lorentzian signature. However sometimes it is really necessary to have the Lorentzian Green's function right away. In particular, we need it when dealing with systems out of equilibrium, like a superconductor quenched by an external pulse, or the quark gluon plasma that exists for a tiny fraction of a second after the moment of a heavy ion collision. In such time dependent cases, Euclideanization usually can not be performed because the state of the theory is different at different time instants, and the notion of global-in-time Wick rotation is ill-defined. Remarkably, the *AdS/CFT* correspondence provides a generic prescription for real-time response functions. But in order to derive it, we need to resolve two issues.

One of the issues with real time QFT is rooted in the fact that unlike the Euclidean case, we can have a multitude of different Green's functions (retarded, advanced, Feynman, Wightman). On the holographic side this is reflected in the fact that there is no unique choice of boundary conditions for the bulk field in the infrared.

For time-like bulk excitations there are two linearly independent solutions to the equations of motion possessing the same near-boundary regular asymptotics. On the other hand, near the Poincare horizon they behave as

$$\phi(z) \sim e^{\pm i q z}, \quad z \rightarrow \infty, \quad \text{where } q = \sqrt{\omega^2 - \vec{k}^2}. \quad (1.55)$$

As proven in [39], for the retarded Green function G_R we have to impose infalling boundary conditions in the IR region:

$$\phi(z) \sim e^{-i q z}. \quad (1.56)$$

This choice is intuitively reasonable. Infallingness means that wave fronts of the bulk field move towards the (black hole or Poincaré) horizon and

disappear behind it. Thus it is in an agreement with the fact that G_R describes causal propagation of an excitation.

The second problem, apart from the ambiguity of the boundary conditions, is that in the Lorentzian signature the two-point Green's function can not be calculated as a second functional derivative of the action. For instance, the boundary action of a 4-dimensional scalar field theory evaluated on the classical solution is

$$S_{bnd} = \int \frac{d^4k}{(2\pi)^4} \phi_0(-k) \mathcal{F}(k, z) \phi_0(k) \Big|_{z=z_B}^{z=z_H}, \quad (1.57)$$

where $\mathcal{F}(k, z)$ is a certain *real* function. Therefore the object naively anticipated to be the retarded Green function is

$$-(\mathcal{F}(k, z) + \mathcal{F}(-k, z)) \Big|_{z=z_B}^{z=z_H}, \quad (1.58)$$

and it is completely real. So this can not be the correct G_R .

In [40] it has been shown that we have to neglect contributions coming from the horizon and contributions of negative momenta, and the proper definition for the retarded propagator in holography is

$$G_R(k) = -2\mathcal{F}(k, z_B). \quad (1.59)$$

This function has both real and imaginary parts, and was proven to reproduce the correct real-time Schwinger-Keldysh formalism in [39].

The prescription (1.59) together with (1.56) works for any spacetime metric with *AdS* asymptotics in an arbitrary dimension, giving us a powerful universal tool for studying real time physics in quantum field theories at finite temperature and charge density, with different field content, in non-trivial external fields, in spatially modulated lattice backgrounds etc.

To summarize the aforementioned technical elements of the *AdS/CFT* correspondence, let us provide the holographic dictionary in the form of a short table.

Bulk AdS gravity	Boundary QFT
Extra dimension	Renormalization group
Hawking temperature of a black hole	Temperature
Maxwell $U(1)$ gauge field	Chemical potential and charge density
Field	Operator
Mass of a field	Conformal dimension of a dual operator
Space-time metric	Energy-momentum tensor
Quantum numbers	Quantum numbers

1.4 The correspondence as a method

In this section we survey several holographic models of real life physical systems. By no means is this exposition exhaustive. The only goal is to demonstrate that the AdS/CFT correspondence is a really universal language that can be applied to a variety of problems in theoretical physics. We start with a brief review of the very first paper on applied holography, dedicated to the minimal shear viscosity of the quark-gluon plasma, and then we focus on condensed matter theory applications of the AdS/CFT correspondence - models of holographic superconductors and non-Fermi liquids.

1.4.1 Minimal viscosity

When dealing with translationally invariant “planar” black hole solutions in AdS , we may ask a question about the physics of small hydrodynamical (long wavelength) fluctuations of the horizon and their boundary field theory interpretation. It turns out that hydrodynamical response functions of the boundary theory can be precisely encoded in the dual long wavelength dynamics of gravity theories with horizons, providing a route to yet another incarnation of applied holography - the fluid/gravity correspondence [25].⁴

A particular system of interest in this context is the quark gluon plasma formed in heavy ion collisions [42]. The QGP is a strongly-coupled

⁴Some subtleties arise if we wish to study high-frequency fluctuations in the boundary field theory [41], but in the low-frequency limit the mapping is unambiguous.

system that exhibits the behaviour of a nearly perfect quantum liquid, and its experimentally measurable properties are defined by the hydrodynamical transport coefficients, especially by the shear viscosity that measures the strength of transversal momentum transport in a liquid. So it is natural to start our discussion of phenomenological applications of the *AdS/CFT* correspondence with the result on minimal shear viscosity obtained in [15, 16].

In a field theory, the shear viscosity can be calculated within the Kubo formalism, which relates it to equilibrium two-point correlation functions:

$$\eta = \lim_{\omega \rightarrow 0} \frac{1}{2\omega} \int dt d^3 \vec{x} e^{i\omega t} \langle [T_{xy}(t, \vec{x}), T_{x,y}(0, \vec{0})] \rangle. \quad (1.60)$$

To compute the correlator in *AdS/CFT*, consider a simple thermal field theory whose dual is the 5-dimensional Schwarzschild black hole in Poincare coordinates:

$$ds^2 = \frac{1}{z^2} \left(- \left(1 - \frac{z^4}{z_H^4} \right) dt^2 + dx^2 + dy^2 + d\xi^2 + \frac{1}{1 - \frac{z^4}{z_H^4}} dz^2 \right). \quad (1.61)$$

As we have discussed in the previous section, according to the *AdS/CFT* correspondence the boundary energy-momentum tensor $T_{\mu\nu}$ is dual to metric perturbations $h_{\mu\nu} = g_{\mu\nu} - g_{\mu\nu}^{(0)}$ in the bulk. From this perspective, the correlator (1.60) corresponds to the graviton absorption rate by the planar black hole:

$$\sigma(\omega) = -\frac{2\kappa^2}{\omega} \text{Im} G^R(\omega) = \frac{\kappa^2}{\omega} \int dt d^3 \vec{x} e^{i\omega t} \langle [T_{xy}(t, \vec{x}), T_{x,y}(0, \vec{0})] \rangle. \quad (1.62)$$

Thus we see that

$$\eta = \frac{\sigma(0)}{2\kappa^2}, \quad (1.63)$$

where $\kappa^2 = 8\pi G$ is the gravitational Newton constant (1.30). Note that the planar black hole has an infinite horizon area, so instead of the absolute Bekenstein entropy we can define the entropy per unit area:

$$s = \frac{a}{4G} = \frac{2\pi a}{\kappa^2}. \quad (1.64)$$

To calculate the quantity (1.63), we can assume that the metric perturbations are orthogonal to the ‘‘holographic’’ direction, and have only

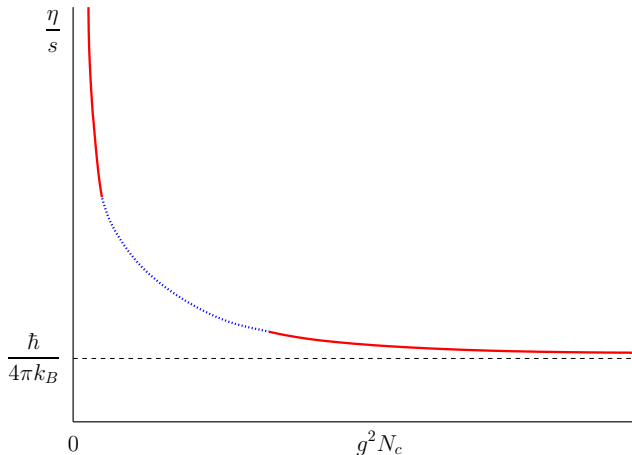


Figure 1.6. Dependence of the η/s ratio on the 't Hooft coupling constant.

transversal xy -polarization. Then on the linearized level, the equation of motion for h_y^x simplifies and takes the form of the Klein-Gordon equation for a massless scalar:

$$\square h_y^x = 0. \quad (1.65)$$

This allows a shortcut to the answer - we can apply the theorem of universality of low frequency scalar field absorption by the black hole [43] and claim

$$\sigma(0) = a = \frac{\kappa^2}{2\pi} s. \quad (1.66)$$

So we arrive at a simple parameter-independent result

$$\frac{\eta}{s} = \frac{\sigma(0)}{2\kappa^2} = \frac{1}{4\pi}, \quad (1.67)$$

or, with restored units:

$$\frac{\eta}{s} = \frac{\hbar}{4\pi k_B}. \quad (1.68)$$

The result is remarkable in at least two fundamental aspects. Here we have sketched the calculation for a simple planar 5-dimensional AdS -Schwarzschild black hole, but this result was also obtained in many different theories within the complete supergravity context, including models dual to various brane configurations [44], and models with non-relativistic Schroedinger symmetry [45]. In this regard it is very universal.

This leads to a conjecture that $\frac{\eta}{s} = \frac{1}{4\pi}$ is the universal minimal bound on the possible values of shear viscosity of quantum liquids, Fig. 1.6. For a long time this conjecture was widely believed to be true, but finally it was figured out that under certain circumstances, e.g. in the presence of matter fields in the fundamental representation, this bound can be violated [46]. Still, the shear viscosity of the quark gluon plasma measured in experiments on high energy ion collisions [42] turned out to be very close to the original $\frac{1}{4\pi}$ value. Historically, this was the first manifestation of the surprising applicability of holographic duality to real life physics. And this ignited the applied holography revolution.

1.4.2 The holographic superconductor

One of the first applications of the *AdS/CFT* correspondence to condensed matter physics was the formulation of a Landau-Ginzburg-like scalar order parameter theory of superconductivity in holographic terms [47].

This set up is particularly elegant. Again, consider a planar Schwarzschild black hole in four dimensions:

$$ds^2 = - \left(r^2 - \frac{M}{r} \right) dt^2 + \frac{dr^2}{r^2 - \frac{M}{r}} + r^2(dx^2 + dy^2). \quad (1.69)$$

The boundary in these coordinates is at $r \rightarrow \infty$. Following the GKPW rule we encode the superconducting order parameter charged under a global $U(1)$ current in a bulk complex charged scalar field coupled to the local gauge $U(1)$ field:

$$S = \int d^4x \sqrt{-g} \left(-\frac{1}{4} F_{\mu\nu} F^{\mu\nu} - \right. \quad (1.70)$$

$$\left. - (\partial_\mu \Psi - i A_\mu \Psi) (\partial^\mu \Psi^* + i A^\mu \Psi^*) \right) + 2\Psi\Psi^*, \quad (1.71)$$

where the mass of the bulk scalar field is taken to be $m^2 = -2$ for simplicity.

The action in the bulk is just the abelian $U(1)$ Higgs model. Higgsing the gauge $U(1)$ symmetry in the bulk corresponds to the spontaneous global $U(1)$ symmetry breaking, opening room for the Landau-Ginzburg phase transition in the boundary field theory.

We now study the system at finite chemical potential, $A_0|_{r \rightarrow \infty} = \mu$. Assuming time independence, homogeneity and isotropy, we impose the

bulk gauge field to have only $A_0 = \Phi$ non-vanishing component, and both $\Psi(r)$ and $\Phi(r)$ to be functions of only the holographic radial coordinate. Then we arrive at the equations of motion:

$$\begin{aligned}\Psi'' + \left(\frac{f'}{f} + \frac{2}{r}\right)\Psi' + \frac{\Phi^2}{f^2}\Psi + \frac{2}{f}\Psi &= 0, \\ \Phi'' + \frac{2}{r}\Phi' - \frac{2\Psi^2}{f}\Phi &= 0.\end{aligned}\tag{1.72}$$

Solving them in the background (1.69), we obtain the near boundary asymptotics:

$$\Psi = \frac{\Psi_1}{r} + \frac{\Psi_2}{r^2} + \dots, \text{ as } r \rightarrow \infty,\tag{1.73}$$

$$\Phi = \mu - \frac{\rho}{r} + \dots.\tag{1.74}$$

As we already know, according to the *AdS/CFT* dictionary the leading coefficient in the near boundary expansion corresponds to the source of a dual operator, and the subleading one corresponds to the expectation value. Thus we can proceed with the following strategy:

- As we are interested in *condensation* of the order parameter, i.e. in formation of the vev in absence of the source, we fix $\Psi_1 = 0$.
- We want to study the thermal phase transition between disordered and superconducting phases, and demonstrate that the system undergoes a second order phase transition as the temperature approaches a critical value T_c . In the holographic setting we can do this by varying the Hawking temperature of the bulk black hole.
- In the superconducting phase we analyze the electric conductivity of the field theory by considering perturbations of spatial components of the gauge field, and explore whether it indeed exhibits the characteristic gap associated with order parameter condensation.

We begin with the analysis of the order parameter condensation. To make our notation consistent with [47], we normalize the order parameter as

$$\langle \mathcal{O}_2 \rangle = \sqrt{2}\Psi_2.\tag{1.75}$$

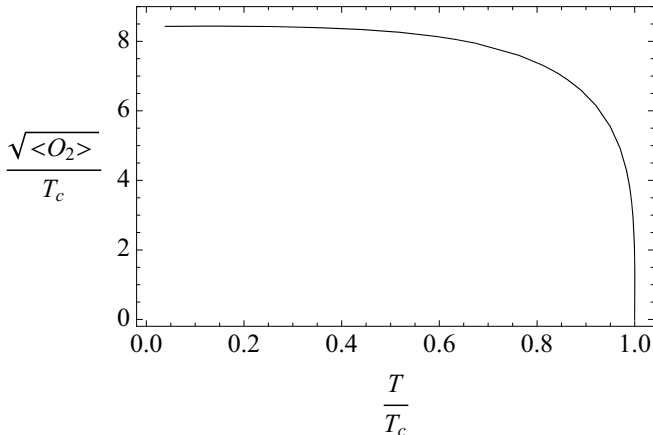


Figure 1.7. Thermal phase transition between superconducting and normal phases of a holographic superconductor.

Its dependence on the temperature can be deduced numerically, and can be perfectly fit with the following law (see also Fig.1.7):

$$\langle \mathcal{O}_2 \rangle = const \cdot T_c \left(1 - \frac{T}{T_c} \right)^{\frac{1}{2}}. \quad (1.76)$$

One can notice that this is completely consistent with the Landau-Ginzburg critical exponent of the second order thermal phase transition in a superconductor.

Next we have to analyze the transport properties of the order parameter and make sure that it really superconducts. Let us recall that in *AdS/CFT*, the boundary electromagnetic current and its source - electric field - are encoded in the near boundary expansion of the spatial bulk gauge field components:

$$A_x = A_x^{(0)} + \frac{A_x^{(1)}}{r} + \dots, \quad (1.77)$$

$$A_x^{bnd} = A_x^{(0)}, \quad \langle J_x \rangle = A_x^{(1)}. \quad (1.78)$$

Consider a small, constant frequency perturbation of the gauge field along the x direction:

$$A_x = A_x(r) e^{-i\omega t}. \quad (1.79)$$

Then we can rewrite the Ohm law as

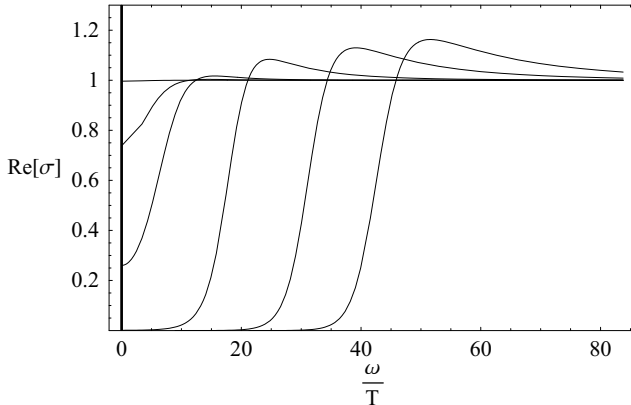


Figure 1.8. Electric conductivity of the holographic superconductor. The D.C. conductivity in the ordered phase is delta function-like, and the A.C. conductivity exhibits a characteristic gap which gradually increases as we lower the temperature .

$$\sigma(\omega) = \frac{\langle J_x \rangle}{E_x} = -\frac{\langle J_x \rangle}{\partial_t A_x} = -\frac{iA_x^{(1)}}{\omega A_x^{(0)}} \quad (1.80)$$

Thus, once we know the solution to the linearized equation of motion for the gauge field, we can read off the conductivity from the near boundary behaviour of A_x .

The e.o.m. is

$$A_x'' + \frac{f'}{f} A_x' + \left(\frac{\omega^2}{f^2} - \frac{2\Psi^2}{f} \right) A_x = 0. \quad (1.81)$$

Solving this equation of motion with infalling boundary conditions near the horizon, we can show that the A.C. conductivity has a gap that gradually increases when the temperature is lowered, and the density of the condensate increases. This gap is qualitatively similar to the gap in a conventional Bardeen-Cooper-Schrieffer superconductor [48], but contra to the standard case, the conductivity is never strictly zero at low frequencies. Rather, we have a soft “algebraic” gap, $\sigma(\omega) \sim \omega^p$, where $p > 0$. The D.C. conductivity in the ordered phase exhibits a delta function-like peak at $\omega = 0$ which persists upon increment of the temperature (Fig. 1.8). The peak might be misinterpreted as yet another signature of superconductivity, but we should be careful here. The considered model is

translationally invariant, so there is no source of momentum dissipation like an atomic lattice or disorder, and the peak is there even in the non-SC phase. Therefore, strictly speaking, we can not judge whether it is a superconductor or a perfect conductor from this consideration. However, in follow-up papers it was shown that the conductivity peak in the condensed phase is not destroyed by translational symmetry breaking [49], so the system actually exhibits superconductivity.

Ideologically, this holographic superconductor is very similar to the superconductor of the Landau-Ginzburg theory. However, it differs in two crucial aspects. First of all, holographically it is possible to describe a scalar order parameter of an arbitrary scaling dimension. Microscopically the scalar is formed of fermionic pairs, so in a weakly interacting system the scaling dimension of the order parameter is just twice that of the fermionic operator dimension, $\Delta_s = 2\Delta_f$. At strong coupling it might be renormalized due to strong non-perturbative interactions, and holography can naturally capture this. Secondly, holographic superconductivity emerges from a critical rather than quasi-particle system. Criticality (in other words, emergent conformal invariance in many-body systems) is commonly believed to underlie the physics of many unconventional phases of strongly correlated systems, like high-Tc superconductors and strange metals [50]. In this regard, *AdS/CFT* is able to explore a whole new range of physical systems, which are inaccessible by perturbative quantum field theory.

1.4.3 AdS/CFT and fermionic matter

In the previous subsection, we have demonstrated how the holographic correspondence can be applied to describe a superconducting phase transition. The next step to be done is to go beyond the order parameter level and take into account the fermionic nature of strongly correlated systems.⁵

The only really well understood phase of fermionic matter is the weakly interacting Fermi liquid [51], and the associated BCS superconductor [52]. The key assumption of the standard Landau theory of the Fermi liquid is the existence of coherent long-living quasiparticle excitations near the Fermi surface. In field theoretical terms, this means that the corresponding fermionic Green function has a sharp pole at a well-defined Fermi-

⁵This will also be an important motivation for Chapter 2 of this thesis.

momentum k_F . However at strong coupling we should not expect the quasi-particle picture to be universal. Strong interactions can cause complicated emergent phenomena that manifest themselves in non-trivial reconstruction (or even destruction) of the Fermi surface, modification of the dispersion relations, exotic transport properties etc.

As we discussed earlier, the conventional analytic and numerical methods fail to provide us with a universal tool to study such systems. Is *AdS/CFT* capable of bringing us a better understanding of strongly coupled fermionic matter at finite charge density, and of providing a mathematical description of phases of quantum matter beyond the conventional Fermi liquid picture? This issue has been addressed independently in Leiden and MIT in 2009 [31, 32], and the result of these studies was a holographic model that clearly exhibits properties of a finite density state of fermionic matter that is not a Fermi liquid; we will call such states non-Fermi liquids.

Consider a 4-dimensional Einstein-Hilbert-Maxwell theory (as in the example of the scalar holographic superconductor), but add to the action a fermionic term⁶:

$$S_\psi = \int d^{d+1}x \sqrt{-g} i \left(\bar{\psi} \Gamma^M D_M \psi - m \bar{\psi} \psi \right), \quad (1.83)$$

where the covariant derivative is

$$D_M = \partial_M + \frac{1}{4} \omega_{abM} \left[\Gamma^a, \Gamma^b \right] - ie A_M. \quad (1.84)$$

Here ω_{abM} is the spin connection, and e is the fermionic electric charge. As we discussed in Sec. 1.3.4, finite charge density at the boundary dualizes to the electric field in the bulk, so in order to account for it we will put the bulk fermion in the background of a charged Reissner-Nordström black hole (and for simplicity treat the fermionic field as a probe):

$$ds^2 = r^2 \left(-f(r) dt^2 + d\vec{x}^2 \right) + \frac{1}{r^2} \frac{dr^2}{f(r)}, \quad f(r) = 1 + \frac{Q^2}{r^4} - \frac{1+Q^2}{r^3}. \quad (1.85)$$

⁶In what follows the capital latin indicies denote coordinates in the bulk, the greek boundary coordinates, and the small latin ones coordinates on a flat tangent bundle. Indices on the gamma matrices always correspond to the tangent space. We choose the gamma matrices basis as

$$\Gamma^r = \begin{pmatrix} 1 & 0 \\ 0 & -1 \end{pmatrix}, \quad \Gamma^r = \begin{pmatrix} 0 & \sigma^\mu \\ \sigma^\mu & 0 \end{pmatrix}, \quad (1.82)$$

where σ^μ are the Pauli matrices.

Here Q is the dimensionless charge of the black hole, and the electric field is

$$A_0 = \mu \left(1 - \frac{1}{r}\right) \quad \mu = g_F Q, \quad (1.86)$$

where g_F is the coupling constant of the Maxwell gauge field.

It is convenient to split the four-component fermionic field into two two-component eigenfunctions of the projector:

$$(1 + \Gamma^r) \psi_{\pm} = \pm \psi_{\pm}, \quad (1.87)$$

Fourier transform it along the boundary directions, and rescale

$$\psi_{\pm} (-gg^{rr})^{-1/4} e^{-i\omega t + \vec{k}\vec{x}} \phi_{\pm}. \quad (1.88)$$

The Dirac equations then become

$$\sqrt{\frac{g_{ii}}{g_{rr}}} (\partial_r \mp m\sqrt{g_{rr}}) \phi_{\pm} = i\sqrt{-\frac{g_{ii}}{g_{tt}}} \left(\omega + eQ \left(1 - \frac{1}{r}\right)\right) \phi_{\pm} - ik_i \sigma^i \phi_{\mp}. \quad (1.89)$$

We are interested in the fermionic Green's function. As shown in [32, 53], in order to derive the Green's function, instead of evaluating the classical action at the saddle point, one just can analyze the near boundary asymptotics of the Dirac bulk wave function:

$$\phi_+ = A(\omega, \vec{k}) r^m + B(\omega, \vec{k}) r^{-m-1} + \dots, \quad r \rightarrow \infty \quad (1.90)$$

$$\phi_- = C(\omega, \vec{k}) r^{m-1} + D(\omega, \vec{k}) r^{-m} + \dots. \quad (1.91)$$

Then

$$G_R = -iD(\omega, \vec{k}) A^{-1}(\omega, \vec{k}). \quad (1.92)$$

As described in [31, 32], imposing infalling boundary conditions at the horizon we can evaluate this function. What has been found is that the theory has a number of remarkable features that distinguish it from the conventional Fermi liquid:

- At zero temperature, the spectral function of the theory has a Fermi surface pole, but the corresponding dispersion relation is not of the linear Landau type $\omega \sim v_F(k - k_F)$, but rather

$$\omega \sim (k - k_F)^z, \quad (1.93)$$

where z can be any value dependent on the parameters of the model.

- As the temperature is raised, the peak is smoothed out. However unlike the Fermi liquid case, its width is not just quadratic in frequency/temperature, but depends non-trivially on frequency and momentum [31]:

$$\Gamma = \tan \gamma |\omega^*(k_F)|, \quad (1.94)$$

where ω^* is the resonant frequency at the Fermi level where the peak is located, and γ is a numerical parameter.

- Another non-FL feature of the model is that, near the Fermi momentum k_F , it has a strong particle-hole asymmetry:

$$G_{ii}(\omega, \vec{k}) \neq G_{ii}(-\omega, \vec{k}). \quad (1.95)$$

- In the limit of small frequencies, the Green function exhibits logarithmic oscillations $G \sim e^{i \log \omega}$.
- The system can have a multitude of Fermi-surfaces.

It remains to be checked experimentally what properties of the holographic non-Fermi liquids can be observed in nature. However, it is already clear that the *AdS/CFT* provides a powerful tool for modeling fermionic systems at finite density beyond the quasi-particle paradigm, and even if this simplest model does not capture all possible physics, the holographic approach has the capacity for constructing more realistic setups [19, 54].

1.5 This thesis

In this thesis we apply the AdS/CFT correspondence to three problems belonging to different areas of theoretical physics.

Chapter 2 is dedicated to the holographic description of superconductivity. While most of the holographic setups describe this phenomenon on the level of the scalar order parameter, a realistic theory should take into account the strong pairing between microscopic fermionic degrees of freedom. Here we make a first step towards filling in the gap and study pairing-induced superconductivity in strongly coupled systems at finite density. The inroad is to study the pairing of quasi-particles. We have just described a holographic model of a non-Fermi liquid, but we can easily change it to a regular Fermi liquid by introducing an IR hard wall cut-off.

This removes gapless critical excitations and allows one to controllably address the dynamics of a single confined Fermi surface. Then, in the weakly coupled dual gravitational theory, the mechanism is that of conventional BCS theory. We study in detail the interplay between the scalar order parameter field and fermion pairing. It is very natural in holography to introduce independent bulk dynamics for the scalar field as well, which corresponds to a non-trivial RG flow of the order parameter. One can then demonstrate that the theory experiences a BCS/BEC crossover controlled by the relative scaling dimensions of the scalar and fermionic operators. A novel technical issue we encounter here is unexpected resonances in the canonical expectation value of the scalar operator at certain values of the scaling dimension, which indicate that in the presence of interacting fields in the bulk, the standard holographic dictionary requires modification.

In chapter 3 we analyze the holographic quark gluon plasma (QGP) formed at a very early stage right after the collision of heavy ions. The $T - \mu$ phase diagram of the QGP is constructed by using a holographic dual model for the heavy ion collision. In this dual model, colliding ions are simulated by charged gravitational shock waves. In accordance with the suggestion in [55], the formation of the deconfined QGP phase is associated in dual terms with the creation of a black hole in the collision of shock waves, which can be detected in the appearance of a trapped surface. Hadronic matter and other confined states correspond to the absence of a trapped surface after the collision.

In addition, we estimate the multiplicity of the ion collision process, i.e. the number of hadrons that forms when the quark gluon plasma has frozen out, which in the dual language is proportional to the area of the trapped surface. We show that a non-zero chemical potential reduces the multiplicity. To plot the phase diagram we use two different dual models of colliding ions, the pointlike and the wall shock waves, and find qualitative agreement of the results.

Finally, in chapter 4 we address a more exotic issue, namely the dynamical evolution of a quantum field in a time machine. Three dimensional gravity in AdS has a very simple eternal time machine solution based on two conical defects moving around their center of mass on a circular orbit. Closed time-like curves in this spacetime extend all the way to the boundary of AdS_3 , violating the causality of the boundary field theory. We apply AdS/CFT to obtain the dual interpretation of this spacetime. By use of the geodesic approximation, we address the “grandfather para-

dox” in the dual $1 + 1$ dimensional field theory and calculate its two-point causal Green’s function. It has a non-trivial analytical structure both at negative and positive times, providing us with constructive intuition on how an interacting quantum field could behave once causality is broken. In particular a clear effect we can see is revivals of the field at certain time moments in the past, preceding the act of the Green’s function sourcing.

We conclude with a discussion of the obtained results and put them into a wider context of the holographic Glass Bead Game.

Bibliography

- [1] E. Y. Loh, Jr., J. E. Gubernatis, R. T. Scalettar, S. R. White, D. J. Scalapino, and R. L. Sugar, “Sign problem in the numerical simulation of many-electron systems”, *Phys. Rev. B* **41**, 9301 (1990).
- [2] M. Troyer and U.-J. Wiese, “Computational Complexity and Fundamental Limitations to Fermionic Quantum Monte Carlo Simulations”, *Phys. Rev. Lett.* **94**, 170201 (2005) [cond-mat/0408370].
- [3] G. 't Hooft, “Dimensional reduction in quantum gravity”, *Salamfest 1993:0284-296* [gr-qc/9310026].
- [4] L. Susskind, “The World as a hologram”, *J. Math. Phys.* **36** (1995) 6377 [hep-th/9409089].
- [5] J. M. Maldacena, “The Large N limit of superconformal field theories and supergravity”, *Adv. Theor. Math. Phys.* **2**, 231 (1998) [hep-th/9711200].
- [6] M. Guica, T. Hartman, W. Song and A. Strominger, “The Kerr/CFT Correspondence”, *Phys. Rev. D* **80** (2009) 124008 [arXiv:0809.4266 [hep-th]].
- [7] A. Strominger, “The dS / CFT correspondence”, *JHEP* **0110** (2001) 034 [hep-th/0106113].
- [8] A. Volovich, “Holography for coset spaces and noncommutative solitons”, UMI-30-51317.
- [9] J. D. Brown and M. Henneaux, “Central Charges in the Canonical Realization of Asymptotic Symmetries: An Example from Three-Dimensional Gravity”, *Commun. Math. Phys.* **104** (1986) 207.
- [10] S. S. Gubser, I. R. Klebanov and A. M. Polyakov, “Gauge theory correlators from noncritical string theory”, *Phys. Lett. B* **428** (1998) 105 [hep-th/9802109].
- [11] E. Witten, “Anti-de Sitter space and holography”, *Adv. Theor. Math. Phys.* **2** (1998) 253 [hep-th/9802150].

- [12] H. A. Kramers and G. H. Wannier, “Statistics of the Two-Dimensional Ferromagnet. Part I”, Phys. Rev. **60**, 252 (1941)
H. A. Kramers and G. H. Wannier, “Statistics of the Two-Dimensional Ferromagnet. Part II”, Phys. Rev. **60**, 263 (1941)
- [13] N. Seiberg and E. Witten, “Electric - magnetic duality, monopole condensation, and confinement in N=2 supersymmetric Yang-Mills theory”, Nucl. Phys. B **426** (1994) 19 [Erratum-ibid. B **430** (1994) 485] [hep-th/9407087].
- [14] A. Beekman, “Vortex duality in higher dimensions”, PhD thesis, Leiden University
- [15] G. Policastro, D. T. Son and A. O. Starinets, “The Shear viscosity of strongly coupled N=4 supersymmetric Yang-Mills plasma”, Phys. Rev. Lett. **87** (2001) 081601 [hep-th/0104066].
- [16] P. Kovtun, D. T. Son and A. O. Starinets, “Viscosity in strongly interacting quantum field theories from black hole physics”, Phys. Rev. Lett. **94** (2005) 111601 [hep-th/0405231].
- [17] W. van der Schee, “Gravitational collisions and the quark-gluon plasma”, PhD thesis, Utrecht University, arXiv:1407.1849 [hep-th].
- [18] T. Sakai and S. Sugimoto, “Low energy hadron physics in holographic QCD”, Prog. Theor. Phys. **113** (2005) 843 [hep-th/0412141].
- [19] G. T. Horowitz, J. E. Santos and D. Tong, “Optical Conductivity with Holographic Lattices”, JHEP **1207** (2012) 168 [arXiv:1204.0519 [hep-th]].
- [20] R. A. Davison, K. Schalm and J. Zaanen, “Holographic duality and the resistivity of strange metals”, Phys. Rev. B **89** (2014) 24, 245116 [arXiv:1311.2451 [hep-th]].
- [21] S. H. Ho, W. Li, F. L. Lin and B. Ning, “Quantum Decoherence with Holography”, JHEP **1401** (2014) 170 [arXiv:1309.5855 [hep-th]].
- [22] Y. Liu, K. Schalm, Y.-W. Sun, J. Zaanen, “Holographic duality for condensed matter physics”, Cambridge University Press, to appear

- [23] N. Brambilla, S. Eidelman, P. Foka, S. Gardner, A. S. Kronfeld, M. G. Alford, R. Alkofer and M. Butenschoen *et al.*, “QCD and Strongly Coupled Gauge Theories: Challenges and Perspectives”, *Eur. Phys. J. C* **74** (2014) 10, 2981 [arXiv:1404.3723 [hep-ph]].
- [24] S. Bhattacharyya, V. E. Hubeny, S. Minwalla and M. Rangamani, “Nonlinear Fluid Dynamics from Gravity,” *JHEP* **0802** (2008) 045 [arXiv:0712.2456 [hep-th]].
- [25] M. Rangamani, “Gravity and Hydrodynamics: Lectures on the fluid-gravity correspondence”, *Class. Quant. Grav.* **26** (2009) 224003 [arXiv:0905.4352 [hep-th]].
- [26] A. Adams, P. M. Chesler and H. Liu, “Holographic Vortex Liquids and Superfluid Turbulence,” *Science* **341** (2013) 368 [arXiv:1212.0281 [hep-th]].
- [27] A. Adams, P. M. Chesler and H. Liu, “Holographic turbulence,” *Phys. Rev. Lett.* **112** (2014) 15, 151602 [arXiv:1307.7267 [hep-th]].
- [28] A. Lucas, S. Sachdev and K. Schalm, “Scale-invariant hyperscaling-violating holographic theories and the resistivity of strange metals with random-field disorder,” *Phys. Rev. D* **89** (2014) 6, 066018 [arXiv:1401.7993 [hep-th]].
- [29] M. Blake and A. Donos, “Quantum Critical Transport and the Hall Angle,” *Phys. Rev. Lett.* **114** (2015) 2, 021601 [arXiv:1406.1659 [hep-th]].
- [30] P. M. Chesler and L. G. Yaffe, “Numerical solution of gravitational dynamics in asymptotically anti-de Sitter spacetimes,” *JHEP* **1407** (2014) 086 [arXiv:1309.1439 [hep-th]].
- [31] H. Liu, J. McGreevy and D. Vegh, “Non-Fermi liquids from holography”, *Phys. Rev. D* **83** (2011) 065029 [arXiv:0903.2477 [hep-th]].
- [32] M. Cubrovic, J. Zaanen and K. Schalm, “String Theory, Quantum Phase Transitions and the Emergent Fermi-Liquid”, *Science* **325** (2009) 439 [arXiv:0904.1993 [hep-th]].
- [33] J. D. Bekenstein, “Black holes and entropy”, *Phys. Rev. D* **7** (1973) 2333.

- [34] S. W. Hawking, “Particle Creation by Black Holes”, *Commun. Math. Phys.* **43** (1975) 199 [Erratum-ibid. **46** (1976) 206].
- [35] J. Maldacena, “The Gauge/gravity duality”, arXiv:1106.6073 [hep-th].
- [36] G. 't Hooft, “A Planar Diagram Theory for Strong Interactions,” *Nucl. Phys. B* **72** (1974) 461.
- [37] S. A. Hartnoll, “Lectures on holographic methods for condensed matter physics”, *Class. Quant. Grav.* **26** (2009) 224002 [arXiv:0903.3246 [hep-th]].
- [38] V. Balasubramanian, P. Kraus, A. E. Lawrence and S. P. Trivedi, “Holographic probes of anti-de Sitter spacetimes”, *Phys. Rev. D* **59** (1999) 104021 [hep-th/9808017].
- [39] C. P. Herzog and D. T. Son, “Schwinger-Keldysh propagators from AdS/CFT correspondence”, *JHEP* **0303** (2003) 046 [hep-th/0212072].
- [40] D. T. Son and A. O. Starinets, “Minkowski space correlators in AdS / CFT correspondence: Recipe and applications”, *JHEP* **0209** (2002) 042 [hep-th/0205051].
- [41] N. Iqbal and H. Liu, “Universality of the hydrodynamic limit in AdS/CFT and the membrane paradigm”, *Phys. Rev. D* **79** (2009) 025023 [arXiv:0809.3808 [hep-th]].
- [42] H. Song, “QGP viscosity at RHIC and the LHC - a 2012 status report,” *Nucl. Phys. A* **904-905** (2013) 114c [arXiv:1210.5778 [nucl-th]].
- [43] S. R. Das, G. W. Gibbons and S. D. Mathur, “Universality of low-energy absorption cross-sections for black holes”, *Phys. Rev. Lett.* **78** (1997) 417 [hep-th/9609052].
R. Emparan, “Absorption of scalars by extended objects”, *Nucl. Phys. B* **516** (1998) 297 [hep-th/9706204].
- [44] C. P. Herzog, “The Hydrodynamics of M theory”, *JHEP* **0212** (2002) 026 [hep-th/0210126].

- [45] J. Maldacena, D. Martelli and Y. Tachikawa, “Comments on string theory backgrounds with non-relativistic conformal symmetry”, *JHEP* **0810** (2008) 072 [arXiv:0807.1100 [hep-th]].
 C. P. Herzog, M. Rangamani and S. F. Ross, “Heating up Galilean holography”, *JHEP* **0811** (2008) 080 [arXiv:0807.1099 [hep-th]].
 C. P. Herzog, M. Rangamani and S. F. Ross, “Heating up Galilean holography”, *JHEP* **0811** (2008) 080 [arXiv:0807.1099 [hep-th]].
- [46] A. Sinha and R. C. Myers, “The Viscosity bound in string theory”, *Nucl. Phys. A* **830** (2009) 295C [arXiv:0907.4798 [hep-th]].
- [47] S. A. Hartnoll, C. P. Herzog and G. T. Horowitz, “Building a Holographic Superconductor”, *Phys. Rev. Lett.* **101** (2008) 031601 [arXiv:0803.3295 [hep-th]].
 S. A. Hartnoll, C. P. Herzog and G. T. Horowitz, “Holographic Superconductors”, *JHEP* **0812** (2008) 015 [arXiv:0810.1563 [hep-th]].
- [48] Mahan G. D., “Many-particle physics”. – Springer Science & Business Media, 2000.
- [49] J. Erdmenger, B. Herwerth, S. Klug, R. Meyer and K. Schalm, “S-Wave Superconductivity in Anisotropic Holographic Insulators”, arXiv:1501.07615 [hep-th].
- [50] Sachdev S., “Quantum phase transitions”. – John Wiley & Sons, Ltd, 2007.
- [51] L. Landau, “The theory of a Fermi liquid”, *Soviet Physics JETP-USSR*, 1957
- [52] J. Bardeen, L. N. Cooper and J. R. Schrieffer, “Theory of superconductivity,” *Phys. Rev.* **108** (1957) 1175.
- [53] N. Iqbal and H. Liu, “Real-time response in AdS/CFT with application to spinors”, *Fortsch. Phys.* **57** (2009) 367 [arXiv:0903.2596 [hep-th]].
- [54] N. Iqbal, H. Liu and M. Mezei, “Lectures on holographic non-Fermi liquids and quantum phase transitions,” arXiv:1110.3814 [hep-th].
- [55] S. S. Gubser, S. S. Pufu and A. Yarom, “Entropy production in collisions of gravitational shock waves and of heavy ions,” *Phys. Rev. D* **78** (2008) 066014 [arXiv:0805.1551 [hep-th]].

Chapter 2

Pairing induced superconductivity in holography

2.1 Introduction

The puzzles posed by strongly correlated electron systems have been considerably illuminated in recent years by the application of gauge-gravity duality. This “holography”, which translates the challenging strongly coupled dynamics to an equivalent weakly coupled gravitational theory in one dimension higher, has given qualitative new insights into quantum critical transport [1, 2], superconductivity beyond the weak coupling Bardeen-Cooper-Schrieffer (BCS) paradigm [3–5], and non-Fermi liquids [6, 7].

A simple way to pose the challenge of strongly coupled systems is that the familiar weakly coupled particles no longer exist as controlled excitations in this regime of the theory. Our microscopic understanding of the observed macroscopics in condensed matter usually rests on the notion of an electron(ic quasi)-particle — a charged spin 1/2 fermion — as the fundamental degree of freedom. The theory of Fermi-liquids and the BCS description of superconductivity are good examples of such weakly coupled systems. Even in strongly correlated phases, parts of this electron quasi-particle picture survive. The transition from such a strongly correlated phase to a superconducting phase is still thought to arise from fundamental electron pairing at the microscopic level. After all, these are the only relevant charge carriers in the system. The open puzzle in strongly correlated electron systems such as high T_c superconductors is the nature of the “glue”: the interaction that allows pairs to form.

In this chapter we take this suggestion that simple pairing mechanisms should survive in strongly coupled systems to heart. While staying ignorant on the glue, it is a very natural step to incorporate the BCS

theory in the holographic framework. A straightforward reason to do so is to use this very well understood standard theory of superconductivity as a benchmark and inroad into a deeper understanding of holographic fermions. Although *AdS/CFT* models of superconductivity that have been constructed up to now are quite successful in capturing the main universal properties of real superconductors, they describe physics on the Landau-Ginzburg level of a scalar order parameter. In doing so it manifestly cannot reveal details of the underlying microscopic mechanisms that drive the superconducting instability, but it also ignores the Cooper pair origin of the order parameter. Our specific question here is whether holographic BCS can fill in the latter gap while being agnostic on the former, and serve as a good foothold for further research on this topic.

The most straightforward implementation of Cooper pairing in holography is to incorporate an attractive four-fermi interaction in the gravitational dual theory. In essence one now has a weakly coupled BCS interaction in the dual description of the strongly coupled theory. Pairing instabilities in this set-up were studied in [8], and the formation of a gap in the fermion spectral functions in a fixed Landau-Ginzburg holographic superconductor background, characteristic of the broken groundstate, was shown in [9]; see also [11].

Both these studies consider the fermions as probes. Since then our understanding of holographic fermions has increased and we now understand that some of the peculiar holographic effects, in particular the non-Fermi-liquid behavior, arise from a coupling to an interacting critical IR [12]. We shall use that improved understanding to go beyond the probe limit and study the full condensation of any paired state, its subsequent groundstate and the self-consistent gap in the fluctuations around it. One way to fully treat the fermion physics is to approximate the fermions in the gravitational dual in a macroscopic fluid limit [13, 14]. In this electron star approximation it is possible to understand the full macroscopic features of the system as it includes gravitational backreaction. A companion article takes this approach [15]. The drawback of the fluid limit is that it essentially describes a system with infinitely many Fermi surfaces — one for each mode in the extra radial AdS direction. This is very unusual from a condensed matter point of view.

Here we pursue an approach that allows us to concentrate on the dynamics of a single Fermi surface. This requires us to consider the fermions quantum-mechanically. In the straightforward holographic set-up this

“quantum electron star” is fraught with subtle issues due to zero-point energy renormalization and its effect on the gravitational background [16, 17]. From the perspective of the field theory side this difficulty is the interaction with the large number of surviving IR degrees in addition to the Fermi-surface quasiparticle. As our first goal is to simply recover the physics of regular BCS in the dual description, the straightforward solution is to lift these extra IR degrees of freedom, and start with a regular confined Fermi-liquid. This can be done by the addition of a hard-wall [12, 16]. This also discretizes the infinite number of Fermi surfaces dual to each radial mode that the AdS theory describes. We then tune the chemical potential such that only a single Fermi surface is occupied. This has the added virtue that the gravitational backreaction will be small, and we are allowed to neglect it. In this straightforward set-up the bulk AdS computation reduces to a standard Hartree BCS calculation but with relativistic fermions in an “effective box” that is spatially curved. This has several technical consequences: working in $d = 3 + 1$ bulk dimensions, there is an effective spin-splitting in that the up and down spin fermions have different Fermi-momenta [18, 19]. Furthermore the non-trivial wavefunctions of the fermions enter into the gap equation. Accounting for this, we shall show that in this hard wall model conventional BCS maps cleanly between the dual gravitational theory and the strongly interacting field theory on the boundary.

To connect this closer to previous study [9] including the standard Landau-Ginzburg holographic superconductor, we next allow the gap-operator to become dynamical: i.e. we introduce a kinetic term for the scalar field in the gravitational bulk. The interpretation of this in the dual field theory is that we have explicitly added an additional charged scalar operator in the theory, that can independently condense. The characteristic quantum number of this new scalar operator in the strongly coupled critical theory is its scaling dimension. Following the well-known AdS/CFT dictionary, this translates into the mass of dual scalar field in the gravitational bulk. For very high mass/dimension the field/operator decouples and we have the conventional BCS scenario constructed earlier. For low masses, the field/operator starts to mix with the Cooper pair operator, and we observe a BCS/BEC crossover. Here we find a novel result. When the operator dimension is strictly degenerate with the that of the Cooper pair, the expectation values of each diverge. Nevertheless their sum — equal to the order parameter — and the gap stay finite. In effect

the extra scalar and the Cooper pair act as a π -Josephson pair in that the relative phase of the condensates is opposite.¹

However, when the operator dimension is degenerate with that of a higher derivative cousin of the Cooper-pair — higher conformal partial wave — there is another resonance where the naive expectation values of each diverge. Arguably the gap should stay finite for any value of the scaling dimension. A direct application of AdS/CFT rules does not extract the gap cleanly and indicates that a clearer definition of the order parameter vev is needed in the AdS/CFT dictionary. We will address this in future work. Here we conclude by showing that one can easily construct an expression that has the right order parameter property in that it stays finite. This postulated gap shows a clean BCS/BEC crossover.

2.2 Review of fermion spectra in the AdS dual: spin splitting

To start we shall recall a lesser known point of spectra of holographic fermions: the spectra depend on the spin [18, 19]. The spectra follow from the simplest AdS model of fermions, Einstein Dirac-Maxwell theory — we shall add the BCS interaction in later. The action is

$$S = \frac{1}{2\kappa^2} \int d^4x \sqrt{-g} \left(R + \frac{6}{L^2} - \frac{1}{4} F_{\mu\nu} F^{\mu\nu} + \bar{\Psi} \Gamma^\mu D_\mu \Psi - m_\Psi \bar{\Psi} \Psi \right), \quad (2.1)$$

Here the covariant derivative equals $D_\mu = \partial_\mu + \frac{1}{4} \omega_\mu^{ab} \Gamma_{ab} - iq A_\mu$, and $\bar{\Psi} = i\Psi^\dagger \Gamma^0$. For the background we choose a pure AdS_4 spacetime with AdS radius L equal to one, and cut-off by a hard wall at a finite value of the holographic direction $z = z_w$.

$$ds^2 = \frac{1}{z^2} \left(-dt^2 + dz^2 + dx^2 + dy^2 \right), \quad z \in [0, z_w], \quad (2.2)$$

We shall consider a large charge $q \gg \kappa$ where it is consistent to ignore gravitational backreaction. The cut off at z_w plays a double role. Together with the AdS potential well, it renders the interval along the holographic coordinate $0 < z < z_w$ effectively finite. This leads to quantization of fermionic energy bands $\omega_n(k)$ (where n is the discrete band number).

¹Recall that the absolute phase of a condensate is unobservable.

Therefore, on the one hand, we have well-defined sharp long living quasi-particles, and on the other hand the removal of the geometry beyond z_w corresponds to a gapping out of normally present low energy deconfined degrees of freedom. This fundamental gap is also present in the fermion spectra itself. See Fig. 2.1(a). In this set-up we can arrive at the dual description of a single Fermi liquid by tuning the chemical potential such that exactly one band is partially occupied [12]. The charge density produced by the occupied fermions backreacts on the gauge field and its profile and the subsequent adjustment in the fermion spectra can be determined in a self-consistent Hartree manner [12]. Changing z_w changes the size of the gap and the level spacing (larger values of z_w correspond to smaller gap), but does not affect the qualitative picture. Only for strictly infinite z_w do we enter a new critical regime which requires a completely different analysis [16, 17]. We will keep z_w finite throughout and therefore set $z_w = 1$ for most of the remainder without loss of generality. Since all our computations will only depend on the combination qA_0 , we also set $q = 1$ in every numerical calculation from hereon.

As we shall review now, due to the spin carried by the relativistic fermions there are actually two Fermi liquids. Moreover, the (background or self-generated) electric field provides a spin-orbit coupling that renders them slightly non-degenerate in the curved background geometry. In addition the lowest energy state is at a non-zero momentum value; this is known as the plasmino mode [18, 19]. This non-degeneracy of the different spin Fermi surfaces will be important in that it leads to a more complex pairing of the fermions.

The spectrum of the fermions is given by normalizable solutions to the Dirac equation. Eliminating the spin connection by rescaling

$$\Psi = (-gg^{zz})^{-1/4} \psi = z^{3/2} \psi, \quad (2.3)$$

Fourier transforming along the boundary directions, and making the assumption that the only non-vanishing component of the vector potential is A_0 , the Dirac equation reduces to the eigenvalue problem

$$\left(i\Gamma^0 \Gamma^z \partial_z + k_i \Gamma^i \Gamma^0 - qA_0 - i \frac{m\Psi}{z} \Gamma^0 \right) \psi = \omega \psi, \quad (2.4)$$

Hereinafter we use tangent-space gamma-matrices, and $i = 1, 2$ refers to the boundary spatial indices.

Due to the impenetrability of the hard wall we choose the canonical momenta to vanish at $z = z_w$:

$$\frac{1}{2}(1 + \Gamma^z)\psi(z_w) = 0, \quad A'_0(z_w) = 0. \quad (2.5)$$

At the boundary $z = 0$ we demand that the fermion and scalar fields are normalizable (i.e. vanish sufficiently fast), and the boundary value of the gauge field sets the chemical potential in dual field theory: $A_0(0) = \mu$.

The fermion spectra are determined together with the gauge field profile self-consistently by (numerical) iteration [12]: solve the Dirac equation for a given gauge field profile (for the initial profile $A_0(z) = \mu$). Then solve Maxwell equations $\nabla_\mu F^{\mu\nu} = -iq\langle\bar{\Psi}\Gamma^\nu\Psi\rangle$ with the source determined from the normalizable wave-functions. This gives a new gauge field profile for A_0 , etc. the result converges to a self-consistent solution after a few iterations (Fig. 2.2).

The interesting feature of the spectrum is that each band has a fine structure. To understand the origin of this splitting we examine profiles of the two spinor modes corresponding to the first band. Fermion spectra are frequently analyzed using rotational invariance to rotate the momentum k_i parallel to the x -axis and choosing an appropriate basis of the gamma matrices one can simplify the problem [6]. It will, however, be useful for us to keep the rotational symmetry manifest. Our objective is to separate the radial evolution of the fermion from its spinorial structure as much as possible. We can solve the Dirac equation (2.4) with the ansatz

$$\psi_\pm(z) = A_\pm(z, |\vec{k}|) u_\pm(\hat{k}_i) + B_\pm(z, |\vec{k}|) \Gamma^0 u_\pm(\hat{k}_i), \quad (2.6)$$

where $A_\pm(z, |\vec{k}|)$ and $B_\pm(z, |\vec{k}|)$ are functions of the radial coordinate and $u_\pm(\hat{k}_i)$ are spinors (with unit norm) independent of z . The latter are defined by the following properties

$$\Gamma^z u_\pm(\hat{k}_i) = u_\pm(\hat{k}_i), \quad \hat{k}_i \Gamma^i \Gamma^0 u_\pm(\hat{k}_i) = \pm u_\pm(\hat{k}_i), \quad (2.7)$$

where \hat{k}_i is a unit (boundary) vector pointing to the direction of the momentum k_i . In the basis (2.15) (which we will use later in this chapter) and with a momentum parallel to the x -axis u_+ (u_-) is the spinor with only fourth (first) nontrivial component.

The Dirac equation implies that

$$\begin{pmatrix} \pm|\vec{k}| - qA_0(z) & i\frac{m_\Psi}{z} + i\partial_z \\ -i\frac{m_\Psi}{z} + i\partial_z & \mp|\vec{k}| - qA_0(z) \end{pmatrix} \begin{pmatrix} A_\pm(z, |\vec{k}|) \\ B_\pm(z, |\vec{k}|) \end{pmatrix} = \omega \begin{pmatrix} A_\pm(z, |\vec{k}|) \\ B_\pm(z, |\vec{k}|) \end{pmatrix}. \quad (2.8)$$

Provided the electrostatic potential is regular near the AdS boundary at $z = 0$, the asymptotic behavior of the solution is

$$\begin{pmatrix} A_\pm(z, |\vec{k}|) \\ B_\pm(z, |\vec{k}|) \end{pmatrix} = a \begin{pmatrix} 0 \\ 1 \end{pmatrix} z^{-m_\Psi} + b \begin{pmatrix} 1 \\ 0 \end{pmatrix} z^{m_\Psi}. \quad (2.9)$$

Normalizable solutions are those with $a = 0$. Note that the scaling dimension of the original fermion is $\Delta_\Psi = m_\Psi + \frac{3}{2}$ and we obtained the powers of z above as a result of the rescaling (2.3). In the IR, the boundary condition (2.5) implies that $A_\pm(z_w, |\vec{k}|) = 0$.

In the absence of an electric field (i.e. $A_0(z)$ is constant), the positive and negative modes have the same energy. In this case we can actually solve our problem exactly in terms of Bessel functions [12]

$$\begin{pmatrix} A_{\pm,n}(z, |\vec{k}|) \\ B_{\pm,n}(z, |\vec{k}|) \end{pmatrix} = N_\pm \sqrt{z} \begin{pmatrix} J_{m_\Psi - \frac{1}{2}}\left(\frac{j_n}{z_w} z\right) \\ i^{\pm|\vec{k}| - \sqrt{(j_n/z_w)^2 + \vec{k}^2}} \frac{J_{m_\Psi + \frac{1}{2}}\left(\frac{j_n}{z_w} z\right)}{j_n/z_w} \end{pmatrix}, \quad (2.10)$$

with the dispersion relation $\omega_n = \sqrt{(j_n/z_w)^2 + \vec{k}^2} - q\mu$. Here j_n is the n -th zero of the Bessel function $J_{m_\Psi - 1/2}$, and N_\pm is the normalization constant.

However, in the presence of an electric field in the bulk ($A'_0(z) \neq 0$) the positive and negative modes no longer have the same energy anymore. The reason is that the densities of the two modes (2.10) have different radial profiles. The “effective chemical potential” $A_0(z)$ felt by each mode is therefore different, if the gauge field has a non-trivial z dependence, and this results in a different energy shift for the two modes (Fig. 2.1(b)).

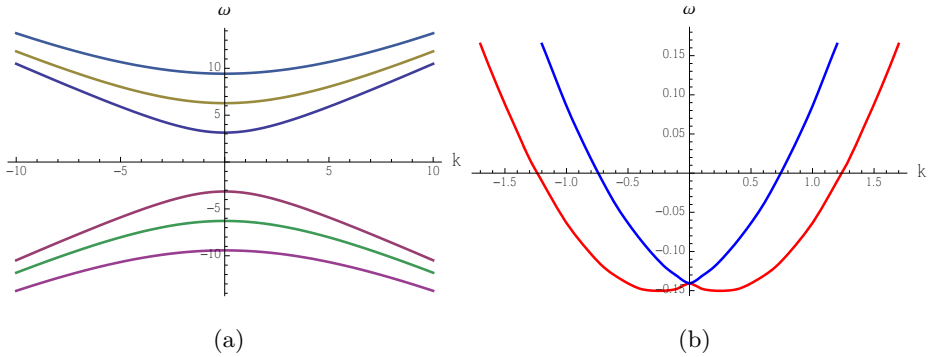


Figure 2.1. (a): Fermionic spectrum in the AdS-hardwall background at zero chemical potential $z_w = 1$ and $m_\Psi = 1$ (b): Spectrum of fermions with unit mass (and $z_w = 1$) in the presence of externally applied electric field $qA_0(z) = 4.5 - 2z$ (without backreaction). We can observe that degeneracy of the two spin states is resolved, and state of a minimal energy is at non-zero momentum. The red and blue curves correspond to positive $u_+(k)$ and negative $u_-(k)$ modes respectively. (When the electric field is self-generated by the fermions the effect is smaller, see Fig. 2.2(a))

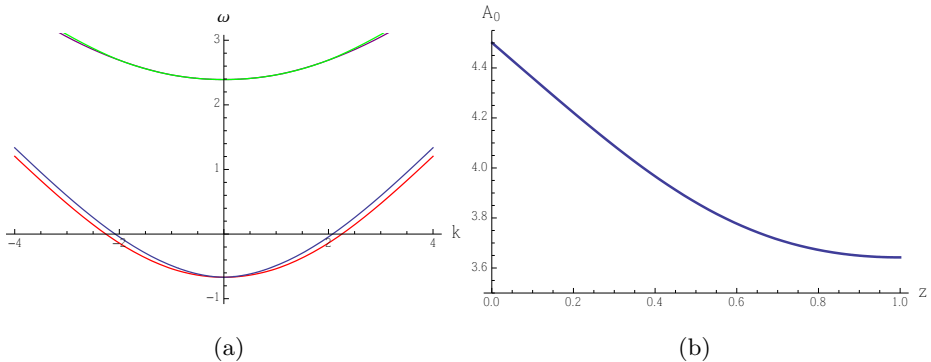


Figure 2.2. (a): Fermionic spectrum in the self-consistent solution of the fermion+gauge field system at $q\mu = 4.5$, $z_w = 1$ and $m_\Psi = 1$. The red and blue curves represent the modes with positive and negative eigenvalues of $\hat{k}_i \Gamma^i \Gamma^0$ respectively. (b): The profile of the gauge field sourced by the fermions.

2.3 Self interacting fermions in AdS and a bulk BCS theory

2.3.1 Majorana interaction

To study pairing driven superconductivity we now add a quartic contact fermionic interaction in the bulk of AdS:

$$\mathcal{L}_{contact} = \frac{\eta_5^2}{m_\phi^2} z^6 \left(\overline{\psi^C} \Gamma^5 \psi \right)^\dagger \left(\overline{\psi} \Gamma^5 \psi^C \right), \quad \overline{\psi} = i\psi^\dagger \Gamma^0, \quad \psi^C = C\Gamma^0 \psi^* \quad (2.11)$$

ψ^C here is a charge conjugated spinor, and the z^6 factor is due to the rescaling (2.3). One can also consider the naive relativistic generalization of the Cooper pair $\overline{\psi^C} \psi$. However to boil down to standard BCS in non-relativistic limit, where the coupling occurs in s-wave channel between states time-reversed to each other, the unique Lorentz invariant term is actually the Majorana coupling $\overline{\psi^C} \Gamma^5 \psi$ (see e.g. [20] for details). We therefore focus only on this term.

As was shown in [18] the direction of the spin of each of the slightly offset modes is perpendicular to the momenta and the two modes have opposite spin. The zero-momentum pairing therefore occurs between opposite spin, without any mixing of the two fermion modes, see Fig. (2.3).

To analyze the interacting theory, we perform the standard Hubbard-Stratonovich transformation with the introduction of an auxiliary the scalar field $\phi(z)$ with charge $q_\phi = 2q$ dual to the superconducting condensate. The scalar part of the action thus takes the form

$$S = \int d^4x \left(i\eta_5^* \phi^* z^3 \overline{\psi^C} \Gamma^5 \psi + \text{h.c.} - m_\phi^2 \phi \phi^* \right) \quad (2.12)$$

This is the theory studied in [9, 8] with the kinetic term for the scalar turned off. We shall reintroduce this kinetic term in section 2.4.3.

2.3.2 Nambu-Gorkov formalism

The resulting system differs from standard BCS in that, as before, we are including the backreaction of the finite density fermions on the gauge field. Assuming translational invariance in the boundary directions, and restrict the scalar and the gauge field to depend only on z -coordinate, the

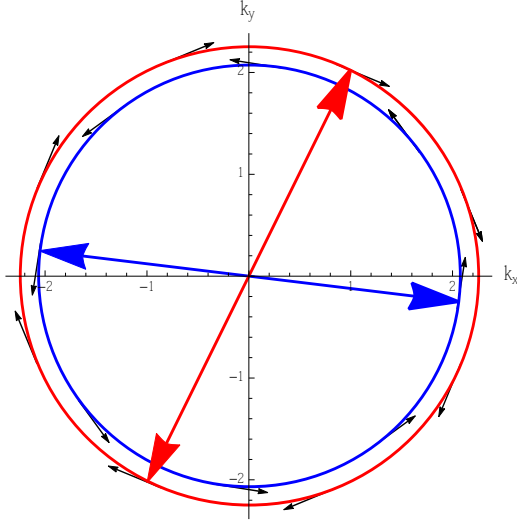


Figure 2.3. The two Fermi surfaces and the *BCS* pairing for the same parameters as in Fig. 2.2. The arrows indicates the direction of the spin of the modes. The pairing happens between opposite spins.

holographic BCS system is formed by

$$\begin{aligned}
 -m_\phi^2 \phi(z) &= -i\eta_5^* z^3 \langle \bar{\psi}^c \Gamma^5 \psi \rangle, \\
 z^2 A_0'' - 2q_\phi^2 A_0 \phi^2 &= qz^2 \langle \psi^+ \psi \rangle.
 \end{aligned}
 \tag{2.13}$$

The fermionic expectation values are assumed to only depend on z as well; they are averaged over all other directions. To compute them, it is convenient to rewrite the action in a quadratic form in terms of the Nambu-Gorkov spinors. We choose the following basis of gamma-matrices

$$\begin{aligned}
 \Gamma^0 &= \begin{pmatrix} i\sigma_2 & 0 \\ 0 & i\sigma_2 \end{pmatrix}, \Gamma^1 = \begin{pmatrix} \sigma_1 & 0 \\ 0 & \sigma_1 \end{pmatrix}, \Gamma^2 = \begin{pmatrix} 0 & \sigma_3 \\ \sigma_3 & 0 \end{pmatrix}, \\
 \Gamma^3 &= \begin{pmatrix} \sigma_3 & 0 \\ 0 & -\sigma_3 \end{pmatrix}, \Gamma^5 = \begin{pmatrix} 0 & -i\sigma_3 \\ i\sigma_3 & 0 \end{pmatrix}.
 \end{aligned}
 \tag{2.14}$$

and rewrite the fermionic part of the action as

$$S_D + S_M = \int d^4x \sqrt{g_{zz}} \left[\bar{\psi} \Gamma^\mu (\partial_\mu - iqA_\mu) \psi - m_\Psi \bar{\psi} \psi - \right. \quad (2.15) \\ \left. - i\eta_5^* \phi^* \bar{\psi} \Gamma^5 \psi + \text{h.c.} \right] = \int d^4x \bar{\chi} K \chi,$$

where the Nambu-Gorkov spinor χ equals

$$\chi = \begin{pmatrix} \psi_1 \\ \psi_2 \\ \psi_3^* \\ \psi_4^* \end{pmatrix}. \quad (2.16)$$

Taking the pure AdS metric (2.2) explicitly, and using rotational invariance of the problem to set $k_y = 0$, the kinetic matrix K equals

$$K = \begin{pmatrix} D_{11} & 2\eta_5 \frac{\phi}{z} \sigma_3 \\ -2\eta_5^* \frac{\phi^*}{z} \sigma_3 & D_{22} \end{pmatrix}, \quad (2.17)$$

with

$$D_{11} = i\sigma_2 (\partial_0 - igA_0) + \sigma_1 \partial_x + \sigma_3 \partial_z - \frac{m_\Psi}{z}, \quad (2.18)$$

$$D_{22} = i\sigma_2 (\partial_0 + igA_0) + \sigma_1 \partial_x - \sigma_3 \partial_z - \frac{m_\Psi}{z}. \quad (2.19)$$

The fermionic expectation values can be written in terms of the Nambu-Gorkov Green's function, which satisfies the equation

$$i\Gamma^0 K G_{\chi_i \chi_j^+} (t, \vec{x}; t', \vec{x}') \equiv (i\partial_0 - H) G_{\chi_i \chi_j^+} (t, \vec{x}; t', \vec{x}') \\ = i\delta(t - t') \delta(\vec{x}_\perp - \vec{x}'_\perp) \delta(z - z'). \quad (2.20)$$

Note the additional factor of $i\Gamma^0$ in our definition.

We determine the Green's function by spectral decomposition. For this we solve the Dirac eigenvalue problem in presence of both the (back-reacted) scalar and gauge field

$$H(i\vec{k}, z) \chi_{\vec{k}, n}^-(z) = \omega_{\vec{k}, n} \chi_{\vec{k}, n}^-(z). \quad (2.21)$$

Note, that the Nambu-Gorkov formalism flips the signs of some pieces of the spectrum. Fig. 2.4(a) shows how the two low-lying energy bands in Fig. 2.2(a) look like in the Nambu-Gorkov formalism.

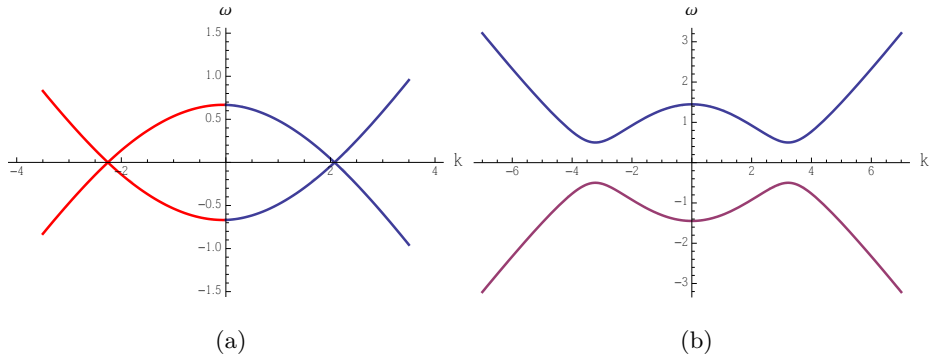


Figure 2.4. (a): The lower two bands from Fig. 2.2 in the Nambu-Gorkov convention (with parameters $q\mu = 4.5$, $z_w = 1$, $m_\Psi = 1$). (b): Energy spectrum for constant gauge field $qA_0 = q\mu = 4.5$ and linear fixed scalar profile $\phi(z) = z$ at $\eta_5 = 0.25$ ($z_w = 1$, $m_\Psi = 1$). The spectrum is gapped at the Fermi surface.

It is convenient to write (2.21) in terms of $(\alpha_1, \alpha_2, \alpha_3, \alpha_4) = (\chi_1, i\chi_2, \chi_3, i\chi_4)$. In this way the redefined “Hamiltonian” H is real (but we will still denote it with H).

We will construct the spectrum numerically, but it is instructive to first consider a toy example. We wish to show that the fermion spectrum becomes gapped in the presence of a condensate for ϕ . Consider the special case when the gauge field is constant $A_0 = \mu$, and the scalar field profile is linear $\phi(z) = z$. Then it is possible to solve the Dirac equation exactly, and the dispersion relation (corresponding to the first band) takes the form (Fig. 2.4(b)):

$$\omega^2 = \left(q\mu - \sqrt{(j_1/z_w)^2 + k^2} \right)^2 + (2\eta_5)^2, \quad (2.22)$$

where j_1 is the first zero of the Bessel-function $J_{m_\Psi-1/2}$. We visibly see the eigenvalue repulsion responsible for the opening of a gap.

2.3.3 Perturbative calculation of the scalar source

In the Nambu-Gorkov formalism it is straightforward to compute the form of fermionic bilinears sourcing the electric and scalar fields (see Appendix

A for details).

$$\langle \psi^+ \psi \rangle = \frac{1}{2\pi} \sum_n \int dk |k| \left(\alpha_{k,n,1}^2 + \alpha_{k,n,2}^2 \right) \Theta(-\omega_{k,n}) \quad (2.23)$$

$$\langle \bar{\psi}^C \Gamma^5 \psi \rangle = \frac{i}{2\pi} \sum_n \int_{-\Lambda(\omega_D)}^{\Lambda(\omega_D)} dk |k| \left[\Theta(\omega_{k,n}) (\alpha_{k,n,1} \alpha_{k,n,4} - \alpha_{k,n,2} \alpha_{k,n,3}) \right] \quad (2.24)$$

where the sum is over the various bands (i.e. radial modes). The sum in the Cooper pair condensate needs to be cut-off at a momentum scale Λ in order to be well-defined. This momentum cut-off corresponds to an energy cut-off ω_D .² From now on we will be using real coupling constant $\eta_5^* = \eta_5$.

A direct discretization of the momentum integral in (2.24) is not the most reliable way to numerically computing the fermionic source for the scalar field because contributions from different momenta are sharply peaked around the Fermi surfaces. For higher numerical accuracy and analytical control we solve (2.21) perturbatively in the scalar field. For this we split the Hamiltonian into an unperturbed piece and an interaction piece $H = H_0 + V$, $H_0 = H|_{\eta_5=0}$. The typical spectrum for the unperturbed operator looks like the one in Fig. 2.4(a). With our choice of Gamma-matrices, the eigenspinor with the unperturbed energy $\omega_k^{(0)}$ and momentum parallel to the x -axis takes the form (we omit the band index)

$$\alpha_{k,+}^{(0)} = \begin{pmatrix} \xi_k \\ 0 \end{pmatrix} \quad (2.25)$$

where ξ_k is a two component spinor. There is also a mode

$$\alpha_{k,-}^{(0)} = \begin{pmatrix} 0 \\ i\sigma_2 \xi_k \end{pmatrix} \quad (2.26)$$

with $-\omega_k^{(0)}$, for which only the lower two components are non-zero. Using nearly degenerate perturbation theory we find the matrix-element controlling the effect of the scalar field:

$$V_k = 2\eta_5 \int_0^{z_w} dz |\xi_k(z)|^2 \frac{\phi}{z}. \quad (2.27)$$

²We use the conventional BCS notation for this cut-off, although there is no explicit connection to any Debye frequency here as the origin of the four-fermion interaction is left in the dark.

The new energy levels are

$$\omega_{\pm} = \pm \sqrt{\left(\omega_k^{(0)}\right)^2 + V_k^2}, \quad (2.28)$$

so the size of the gap is V_{k_F} . We show in the Appendix B that the scalar source has the following form in terms of the unperturbed wave-functions (considering only one fermion mode):

$$\langle \bar{\psi}^C \Gamma^5 \psi \rangle = -\frac{i}{4\pi} \int_{-\Lambda(\omega_D)}^{\Lambda(\omega_D)} dk |k| \frac{V_k}{\sqrt{\left(\omega_k^{(0)}\right)^2 + V_k^2}} |\xi_k(z)|^2. \quad (2.29)$$

2.3.4 Analytical study of the non-dynamical scalar: double gap equation

Eq.(2.29) is very similar to the standard BCS gap equation. The key difference is the way the spatial profiles ξ_k of the fermion wavefunctions modify both the gap V_k and the spatially varying profile of the pairing vev $\langle \bar{\psi}^C \Gamma^5 \psi \rangle$. Since the AdS geometry together with the hard wall confine the wavefunction, what we have essentially done is solve a relativistic BCS in a non-trivial potential.

There is one additional subtlety, in that the Fermi surfaces corresponding to the up-down spin are slightly split. Assuming, as is conventional, that the cut-off frequency is small enough, we are allowed to approximate V_k and ξ_k by their values at the Fermi surfaces. Doing so we can solve the gap equation

$$\phi(z) = \frac{z^3}{4\eta_5} \left[\gamma_1 V_1 \log \left(\frac{\omega_D + \sqrt{\omega_D^2 + V_1^2}}{V_1} \right) \rho_1(z) + \right. \quad (2.30)$$

$$\left. + \gamma_2 V_2 \log \left(\frac{\omega_D + \sqrt{\omega_D^2 + V_2^2}}{V_2} \right) \rho_2(z) \right], \quad (2.31)$$

where $\rho_1(z) = |\xi_{k_{F,1}}|^2$, $\rho_2(z) = |\xi_{k_{F,2}}|^2$ are the fermion wave functions at the two distinct Fermi surfaces, and $\gamma_{1,2} = \frac{\eta_5^2}{m_\phi^2 \pi} \frac{|k_{F1,2}|}{|\omega'(k_{F1,2})|}$. A brief inspection reveals that the gap equation only depends on the dimensionless combinations $\frac{\eta_5}{m_\phi}$ and $\frac{\eta_5}{\omega_D}$.

In Appendix 2.B.2 we show that the solution of the gap equation can be found in a form of linear combination of the two fermionic wave functions (up to an additional z^3 factor)

$$\phi = (C_1\rho_1(z) + C_2\rho_2(z)) z^3. \quad (2.32)$$

For $C_1 \gg C_2$ ($C_2 \gg C_1$) the condensate profile is more similar to the wavefunction at the first (second) Fermi surface. We obtain the coefficients

$$C_1 = (ax + b) \frac{\omega_D}{\eta_5} \exp\left(-\frac{bx + c}{\gamma_2}\right), \quad (2.33)$$

$$C_2 = (bx + c) \frac{\omega_D}{\eta_5} \exp\left(-\frac{bx + c}{\gamma_2}\right), \quad (2.34)$$

where x is the ratio of the two gaps $x = V_1/V_2$, satisfying the following equation

$$x^2 + \left(\frac{I_{22}\gamma_2}{I_{12}\gamma_1} - \frac{I_{11}}{I_{12}}\right)x - \frac{\gamma_2}{\gamma_1} = \frac{\gamma_2}{b}x \log x. \quad (2.35)$$

Here I_{11} , I_{22} , I_{12} , a , b , c are functionals of the fermion profiles ρ_1 , ρ_2 , defined in (2.79), and (2.81) in Appendix B2.

In Fig. 2.5(b) we show the perturbative solutions to the gap equation for $\mu = 4.5$, $q = 1$, $m_\Psi = 1$ and for two different couplings. (In principle there are two solutions but one of these contains a node and is presumably energetically unfavored). We can see a cross-over when we tune the coupling η_5/m_ϕ (see also Fig. 2.6). For small (large) coupling the profile of the condensate is dominated by ρ_2 (ρ_1). Note that the gap at the first Fermi-surface (with fermion wave-function ρ_1) is always smaller than the gap at the second Fermi-surface.

The analysis above is all from the perspective of the bulk AdS physics. All the data of the dual strongly coupled field theory is directly inferred from it. The spectral condition for a normalizable mode is the same [12], hence a gap in the bulk spectra equals a gap in the boundary fermion spectrum. The CFT order parameter is by construction the leading non-zero component of the fermion bilinear vev $\langle \mathcal{O}_{U(1)} \rangle = \lim_{z \rightarrow 0} z^{-2\Delta_\Psi} \langle \overline{\Psi} \Gamma^5 \Psi \rangle$, where Δ_Ψ is the scaling dimension of the single trace fermionic operator \mathcal{O}_Ψ dual to the AdS Dirac field (each normalizable fermion wavefunction behaves as z^{Δ_Ψ}) [21, 22]. We thus neatly see how a bulk BCS coupling holographically encodes standard BCS in the dual CFT.

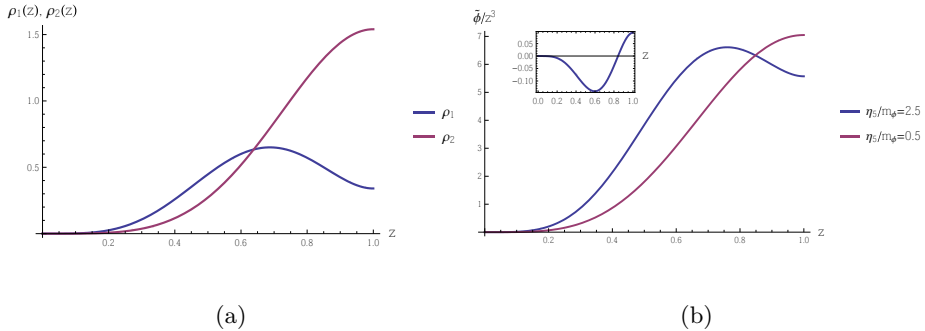


Figure 2.5. (a): wave function profiles of the fermions at the two Fermi surfaces (ρ_1, ρ_2) ($q\mu = 4.5, z_w = 1, m_\psi$). (b) The profiles of the stable solutions of the gap equation $\tilde{\phi} = \phi \exp\left(\frac{bx+c}{\gamma_2}\right)$ (rescaled by z^3) for $\eta_5/\omega_D = 0.5, \eta_5/m_\phi = 0.5$ and $\eta_5/m_\phi = 2.5$. Depending on the coupling the profiles are similar to the fermion wave-functions ρ_1, ρ_2 . In the inset we plot the unstable solution for $\eta_5/m_\phi = 2.5$ (for the other value of the coupling this mode is exponentially small).

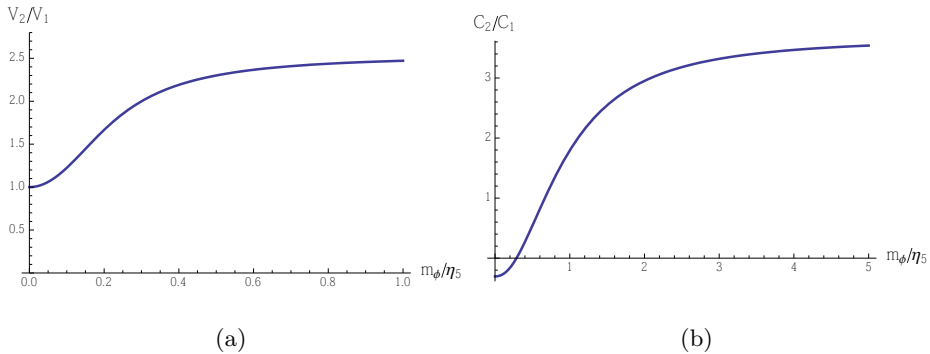


Figure 2.6. (a): The ratio of the gaps (V_2/V_1) as a function of the inverse coupling m_ϕ/η_5 (for fixed $\eta_5/\omega_D = 0.5$). The other parameters are as in Fig. (2.5). For zero boson mass (or infinite coupling) the gaps have the same size but for non-zero mass (smaller coupling) V_2 is bigger and the ratio converges to the value 2.56. (b): The ratio of the coefficients C_2/C_1 as a function of the inverse coupling.

2.4 Fermionic ordering in holography

To establish a closer connection to previous works [9, 10] on fermionic aspects in holographically ordered ground states, we now introduce by hand a kinetic term for the scalar field ϕ . From the bulk perspective this would correspond to a situation where the coherence length (the inverse binding energy) of the Cooper pair is smaller than the relevant cut-off. From the dual boundary field theory perspective this corresponds to the introduction of an explicit scalar operator of scaling dimension

$$\Delta_\phi = \frac{3}{2} + \frac{1}{2}\sqrt{9 + 4m_\phi^2}. \quad (2.36)$$

We reserve the symbol Δ for the scaling dimensions of operators. It is not to be confused with the value of the gap. Again assuming translational invariance in the boundary directions, the bosonic equations now take the form

$$z^2\phi'' - 2z\phi' + z^2q_\phi^2A_0^2\phi - m_\phi^2\phi = -i\eta_5z^3\langle\bar{\psi}^c\Gamma^5\psi\rangle, \quad (2.37)$$

$$z^2A_0'' - 2q_\phi^2A_0\phi^2 = qz^2\langle\psi^+\psi\rangle, \quad (2.38)$$

where $q_\phi = 2q$. In addition one has the Dirac equation

$$K(\phi, A_0)\chi = 0 \quad (2.39)$$

through which one defines the bulk expectation values on the right hand side. Here $K(\phi, A_0)$ is the kinetic matrix in (2.17),

The distinction between the model with a dynamical and non-dynamical scalar field is two-fold:

- (1) Although physically the order parameter in the broken state cannot distinguish between a fermionic Cooper pair origin and a condensed scalar, in this holographic model they mathematically arise at different orders in the $1/N$ expansion. Recall that the coupling constant expansion in AdS/CFT maps to the $1/N$ matrix expansion of the dual field theory, whereas each AdS field is dual to a single trace composite operator. A Cooper pair is thus dual to double trace operator in the dual field theory which are always $1/N$ suppressed. This distinction is the same distinction between classical spontaneous symmetry breaking in a scalar field theory, and “quantum pairing” in BCS.

- (2) Physically, strictly put the scalar is an additional degree of freedom (it will show up in the free energy). If the coherence length of the Cooper pair is smaller than the relevant cut-off, one should indeed introduce this operator separately. In this “strong coupling” (equal to small coherence length) limit, the dynamical scalar field can condense by itself. In the formulation here this is controlled by its mass. For high mass the field should decouple. This is dual to the statement that in the dual field theory the corresponding operator will have a very high scaling dimension and become extremely irrelevant. All the IR dynamics is then controlled by the fermions and we recover the standard BCS of the previous section. For low mass, however, the boson dynamics will start to compete with the fermion pairing and rapidly take over the symmetry breaking dynamics in the IR.

Tuning the scalar mass therefore controls a crossover between pure BCS theory and a classic BEC spontaneous symmetry breaking. Qualitatively one can thus consider the mass/scaling dimension of the scalar operator as a proxy for the coherence length of the Cooper pair. When it is large, the dynamics is pure BCS; as it becomes comparable to and smaller than the relevant cut-off, one should introduce the paired operator independently.

Writing out the spin components explicitly the full system of equations that we are attempting to solve is

$$\begin{aligned}
& z^2 \phi'' - 2z\phi' + 4q^2 z^2 A_0^2 \phi - m_\phi^2 \phi = \tag{2.40} \\
& = \frac{\eta_5 z^3}{2\pi} \sum_n \int_{-\Lambda(\omega_D)}^{\Lambda(\omega_D)} dk |k| \Theta(\omega_{k,n}) (\alpha_{k,n,1} \alpha_{k,n,4} - \alpha_{k,n,2} \alpha_{k,n,3}), \\
& z^2 A_0'' - 8q^2 A_0 = \frac{qz^2}{2\pi} \sum_n \int dk |k| (\alpha_{k,n,1}^2 + \alpha_{k,n,2}^2) \Theta(-\omega_{k,n}), \\
& \begin{pmatrix} \partial_z - \frac{m_\Psi}{z} & -(\omega - k) - qA_0 & 2\eta_5 \frac{\phi}{z} & 0 \\ (\omega + k) + qA_0 & \partial_z + \frac{m_\Psi}{z} & 0 & 2\eta_5 \frac{\phi}{z} \\ 2\eta_5 \frac{\phi}{z} & 0 & \partial_z + \frac{m_\Psi}{z} & (\omega - k) - qA_0 \\ 0 & 2\eta_5 \frac{\phi}{z} & -(\omega + k) + qA_0 & \partial_z - \frac{m_\Psi}{z} \end{pmatrix} \begin{pmatrix} \alpha_1 \\ \alpha_2 \\ \alpha_3 \\ \alpha_4 \end{pmatrix} = 0
\end{aligned}$$

Here all fields depend only on the radial direction z . For completeness we recall boundary conditions for each of the fields. At the impenetrable hard wall all canonical momenta should vanish. For the bosons this means

$$\phi'(z_w) = 0, \quad A_0'(z_w) = 0; \tag{2.41}$$

for the fermions this can be achieved by the choice

$$\alpha_1(z_w) = \alpha_4(z_w) = 0 \tag{2.42}$$

At the AdS boundary, all field should be normalizable: they should vanish as a positive power of z . (For two of the fermion components this is automatic, see eq. (2.9)).

We will approach the fully interacting scalar-fermion system in three steps: we first set all fermions to vanish and construct the purely scalar holographic superconductor. Next we include fermions, but hold the BCS coupling $\eta_5 = 0$; this exhibits bose-fermi competition in the system. Finally we will analyze fully interacting system at $\eta_5 \neq 0$. Details of the numerical calculations are discussed in Appendix C.

2.4.1 Purely scalar holographic superconductor

First, as the scalar field in our system is a fully dynamical degree of freedom, it should condense for small enough mass even in absence of fermions [4, 23, 24]. This hardwall superconductor will be useful for later comparison.

Since we consider a pure hardwall AdS_4 spacetime without a black hole horizon, we study a $T = 0$ groundstate as a function of the mass/conformal dimension of the scalar field/dual scalar operator. Any phase transition is therefore of quantum origin. Note that the hard gap due to the hardwall directly implies that the physics is the same for any temperature $T < 1/z_w$. Only when $T > 1/z_w$ will the the black hole horizon become relevant to the geometry, see e.g. [25].

The numerics of the pure scalar system is particularly simple as there is no need to solve the integro-differential equations iteratively. Varying the scalar conformal dimension we indeed find a condensate value below a critical value (Fig. 2.7). We see a sharp second order phase transition as expected for spontaneous symmetry breaking. Scalar operators with smaller conformal dimensions (dual to lighter bulk scalar fields) are more likely to condense and yield an order parameter with higher density.

2.4.2 Bose-Fermi competition

The next step is to see what happens in a system where both scalar and fermionic fields are present, but interact with each other only via the gauge field A_0 , and not directly (the Majorana coupling $\eta_5 = 0$ vanishes). For

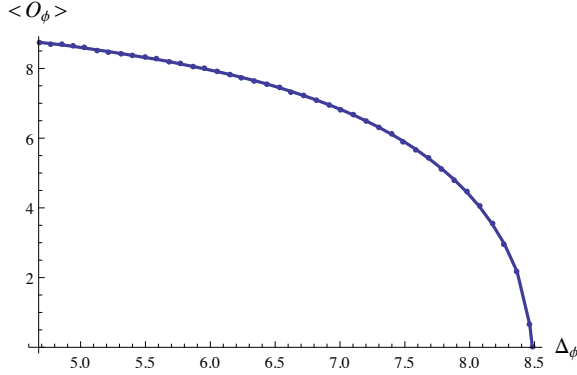


Figure 2.7. Condensate of a scalar order parameter in the boundary theory as a function of scalar conformal dimension at $\mu q = 4.5$, $z_w = 1$, $q_\phi = 2$.

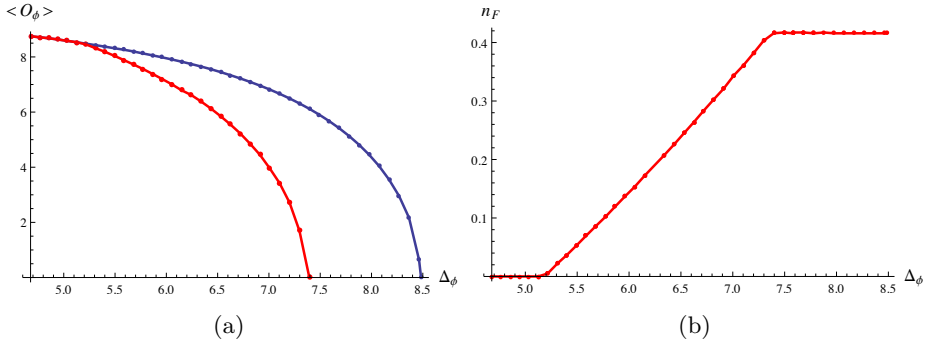


Figure 2.8. (a): Comparison of the superconducting phase transition in a purely scalar system (blue curve) to the one in a system with fermions at $\eta_5 = 0$ (red curve). At small conformal dimension there is no difference between the phase curves at all, while for larger dimension we see effects of Bose-Fermi competition. (b): Total fermionic bulk charge as a function of scalar conformal dimension, $n_F = \int_0^{z_w} qz^2 \langle \psi^\dagger \psi \rangle dz$. Here $\mu q = 4.5$, $z_w = 1$, $q_\phi = 2$, $\omega_D = 0.7$.

the same parameters as in Fig. 2.7 for a scaling dimension of the fermionic operator $\Delta_\Psi = m_\Psi + 3/2 = 5/2$ we obtain a scalar condensate shown on Fig.2.8.

Comparing, the two condensate values become identical with the pure

hardwall superconductor without fermions for low enough Δ_ϕ . For these values the bulk scalar field is so light that it consumes all the energy in the system. *Ceteris paribus* we would need a higher chemical potential to make fermions occupy the first band and backreact on A_0 .

At larger values of Δ_ϕ there is still a scalar condensate, but it is suppressed compared to the pure hardwall superconductor (Fig.2.8(a)). This can be easily understood in terms of canonical ensemble. For fixed total electromagnetic charge of the system, adding new constituents (fermions) would redistribute the available charge (Fig.2.8(b)) and the condensate of the original degrees of freedom would be suppressed. This effect has also been observed in a holographic set-up where the fermions are approximated in the fluid [26, 27]

2.4.3 A dynamical BCS scalar and a BCS/BEC crossover

Now we analyze the most interesting case and include the full dynamics for the scalar field ϕ . Let us give another reason why this is quite natural from the field theory perspective. The evolution in the radial direction in AdS captures the (leading matrix large N contribution to the) RG flow of the corresponding operator in the field theory. The BCS gap, proportional to the vev of the scalar field is certainly sensitive to the RG scale. Hence one expects it to change dynamically as a function of the radial direction. Strictly speaking the double trace pairing operator which sets the value of the gap is a subleading operator in large N and any running that deviates from its semiclassical scaling is therefore a quantum effect in the AdS gravity theory. This is the situation we studied in section 2.3.4. At the $1/N$ level, for small enough coherence length, the pair operator will become dynamical and qualitatively it ought to be given by the dynamical scalar we study here.

We will see a very interesting effect occurs in doing so. Because the scalar is sourced by the Cooper pair condensate, this changes near-boundary fall off of ϕ , and the standard holographic prescription for boundary field theory condensates has to be modified. Without the presence of a Cooper pair condensate, the zero momentum scalar mode equation in AdS_4 is a homogeneous (linear) differential equation

$$z^2\phi''(z) - 2z\phi'(z) + q_\phi^2 z^2 A_0^2(z)\phi(z) - m_\phi^2\phi(z) = 0. \quad (2.43)$$

Near the AdS boundary its solutions have the following form

$$\begin{aligned}\phi(z) &= Az^{3-\Delta_\phi} \cdot (1 + a_1z + a_2z^2 + \dots) + Bz^{\Delta_\phi} \cdot (1 + b_1z + b_2z^2 + \dots), \\ \Delta_\phi &= \frac{3}{2} + \frac{1}{2}\sqrt{9 + 4m_\phi^2},\end{aligned}\tag{2.44}$$

and in the standard quantization scheme the coefficient A of the non-normalizable solution corresponds to the source $J_{\mathcal{O}_\phi}$ for the operator \mathcal{O}_ϕ dual to ϕ , and the coefficient B of the normalizable solution to the vev $\langle \mathcal{O}_\phi \rangle$. Spontaneous symmetry breaking due to a condensation of the operator occurs for a solution in the absence of a source, i.e. with $A = 0$ as a boundary condition.

For the interacting scalar-fermion system this simple one-to-one correspondence between bulk asymptotics and boundary condensates needs modification. We must now consider the inhomogeneous differential equation

$$z^2\phi''(z) - 2z\phi'(z) + q_\phi^2 z^2 A_0^2(z)\phi(z) - m_\phi^2\phi(z) = -i\eta_5 z^3 \langle \bar{\psi}^c \Gamma^5 \psi \rangle.\tag{2.45}$$

The solutions to this equation now include the particular solution responding to the inhomogeneous source in addition to the homogeneous solutions (2.44). For near boundary behavior of the source

$$\lim_{z \rightarrow 0} z^3 \langle \bar{\psi}^c \Gamma^5 \psi \rangle \sim z^{2\Delta_\Psi}\tag{2.46}$$

the particular solution will behave in the same way (assuming $2\Delta_\Psi \neq \Delta_\phi$):

$$\begin{aligned}\phi(z) &= \phi_{hom}(z) + \phi_{part}(z) \\ \phi_{part}(z) &= \mathcal{P}_1 z^{2\Delta_\Psi} + \mathcal{P}_2 z^{2\Delta_\Psi+1} + \mathcal{P}_3 z^{2\Delta_\Psi+2} + \dots\end{aligned}\tag{2.47}$$

This particular solution will control the dominant normalizable near boundary behavior for $\Delta_\phi > 2\Delta_\Psi$. This raises the question what we should use as the vev for the corresponding operator. The canonical AdS/CFT prescription

$$\langle \mathcal{O}_\phi \rangle = \lim_{z \rightarrow 0} z^{-d+1} \partial_z \left(z^{d-\Delta_\phi} \phi(z) \right)\tag{2.48}$$

no longer gives a viable answer. Let us exhibit this in detail. As an aside, note that the near-boundary behavior of the fermions does not change provided the solution for $\phi(z)$ is normalizable.

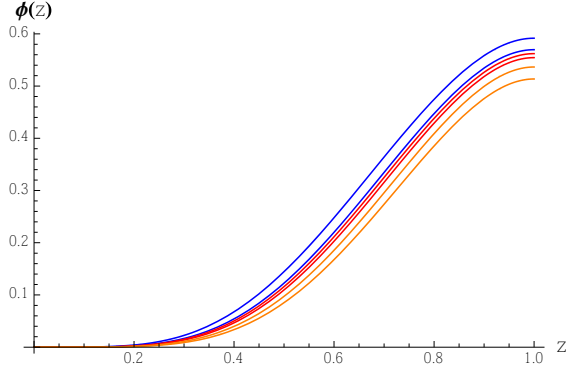


Figure 2.9. Profiles of the bulk scalar wavefunction $\phi(z)$ for $\Delta_\phi = 4.6765$, $\Delta_\phi = 4.8541$ (two blue curves), $\Delta_\phi = 4.9438$, $\Delta_\phi = 5.0341$ (two red curves, - proximity of the critical point), $\Delta_\phi = 5.379$, and $\Delta_\phi = 5.4925$ (two orange curves). Crossing the critical point $\Delta_\phi = 2\Delta_\Psi = 5$ does not lead to any singularities in the bulk wavefunction. The other parameters here are $\eta_5 = 1$, $\mu q = 4.5$, $z_w = 1$, $q_\phi = 2$, $\omega_D = 0.7$.

Denoting the coefficient B of the normalizable homogeneous solution with $B = \mathcal{H}_1$ we extract these coefficients from numerical solutions to the scalar and fermionic equations. (see Fig.2.10, 2.11). Immediately noticeable are the singularities at $\Delta_\phi = 2\Delta_\Psi$ and $\Delta_\phi = 2\Delta_\Psi + 2$. Strictly speaking when $\Delta_\phi = 2\Delta_\Psi + n$ the expansion (2.47) breaks down and the solution has an extra logarithmic term

$$\phi(z) = \mathcal{H}_1 z^{2\Delta_\Psi+n} + \dots + \mathcal{P}_1 z^{2\Delta_\Psi} + \dots + \mathcal{P}_{n+1} z^{2\Delta_\Psi+n} \ln(z) + \dots \quad (2.49)$$

The singular divergence of coefficients is a precursor of this logarithm. There is no singularity at $2\Delta_\Psi + 1$ because \mathcal{P}_2 happens to vanish in our case.³

The indisputable presence of these singularities or resonances can be readily seen by considering a simplified version of the scalar equation.

³This vanishing of \mathcal{P}_2 (due to the vanishing of \mathcal{S}_2) and the structure of the series expansion is determined by the solutions of the Dirac equation. For zero electric field each *even* coefficient would vanish in fact. Since the gauge field profile modifies the higher order coefficients in the series expansion of the Dirac equation, it can be shown that $\mathcal{S}_4 \neq 0$.

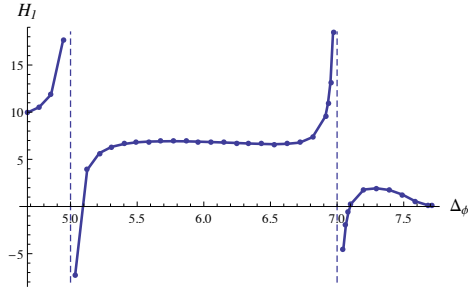


Figure 2.10. Dependence of the leading homogeneous coefficient in the scalar solution expansion on the conformal dimension of the field. Here $\mu q = 4.5$, $\eta_5 = 1$, $z_w = 1$, $q_\phi = 2$, $m_\Psi = 1$ (so $2\Delta_\Psi = 5$), $\omega_D = 0.7$.

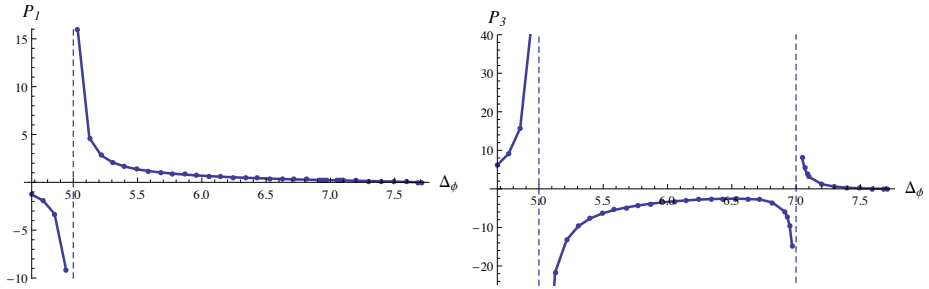


Figure 2.11. Dependence of the two leading particular coefficients in the scalar solution expansion on the conformal dimension of the field. Here $\mu q = 4.5$, $\eta_5 = 1$, $z_w = 1$, $q_\phi = 2$, $m_\Psi = 1$ (so $2\Delta_\Psi = 5$), $\omega_D = 0.7$.

Computing the series solution to the equation

$$z^2 \phi'' - 2z \phi' - m_\phi^2 \phi = \mathcal{S}_1 z^{2\Delta_\Psi} + \mathcal{S}_3 z^{2\Delta_\Psi+2} \quad (2.50)$$

one directly finds the “resonances”

$$\begin{aligned} \mathcal{P}_1 &= \frac{\mathcal{S}_1}{2\Delta_\Psi(2\Delta_\Psi - 3) - \Delta_\phi(\Delta_\phi - 3)}, \\ \mathcal{P}_3 &= \frac{\mathcal{S}_3}{(2\Delta_\Psi + 2)(2\Delta_\Psi - 1) - \Delta_\phi(\Delta_\phi - 3)}. \end{aligned} \quad (2.51)$$

Note that they are Feshbach-like resonances in that the singularity is a single rather than a double pole.

The question is how to extract the information of the strongly coupled dual field theory from this asymptotic behavior of the AdS scalar wavefunction. Despite these singularities in the coefficients, by construction the bulk scalar wavefunction is regular at all points (Fig.2.9). It is therefore physically natural to have regular observables in the boundary field theory as well. There are two obvious points to make here.

- (1) Physically the origin of the order parameter is indistinguishable. One cannot tell whether the broken groundstate is caused by condensation of the Cooper pair or the scalar field.
- (2) Mathematically, the regularity of the bulk solution directly implies that the homogeneous component \mathcal{H}_1 must have a similar resonance but with an opposite sign.

An obvious and physically motivated choice is to postulate that the actual order parameter is the simply the sum of the naive condensates, with the Cooper pair condensate \mathcal{S}_1 renormalized to \mathcal{P}_1 : i.e.

$$\langle \mathcal{O}_\phi \rangle = \mathcal{H}_1 + \mathcal{P}_1. \quad (2.52)$$

Taking this linear combination does in fact lead to a cancelation of “resonances” and a smooth function at $\Delta_\phi = 2\Delta_\Psi$ (see Fig. 2.12). However, the reflection of the next resonance $\Delta_\phi = 2\Delta_\Psi + 2$ in the homogenous solution \mathcal{H}_1 remains. Likewise, a similar partial resolution occurs for the linear combination $\mathcal{H}_1 + \mathcal{P}_3$.

These “resonances” in \mathcal{P}_i and their cancelation by (part of) the homogeneous solution \mathcal{H}_1 will in fact occur at every order of the expansion from

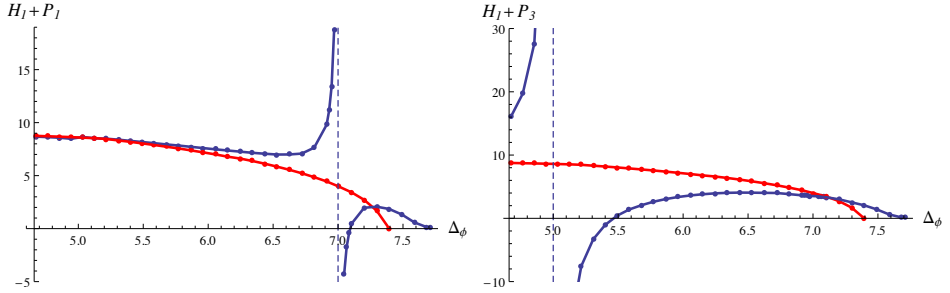


Figure 2.12. Linear combinations of the series expansion coefficients. Red curve represents the boundary scalar operator condensate $\langle \mathcal{O}_\phi \rangle$ as a function of its conformal dimension in presence of fermions at $\eta_5 = 0$ (the same as the red curve on Fig.2.8). The blue curve represent the linear combination $\mathcal{H}_1 + \mathcal{P}_1$ on the left plot, and $\mathcal{H}_1 + \mathcal{P}_3$ on the right one. Resonances in \mathcal{H}_1 and \mathcal{P}_1 precisely cancel each other at $\Delta_\phi = 2\Delta_\Psi$, and so do resonances in \mathcal{H}_1 and \mathcal{P}_3 at $\Delta_\phi = 2\Delta_\Psi + 2$. All parameters are as in Fig.2.10.

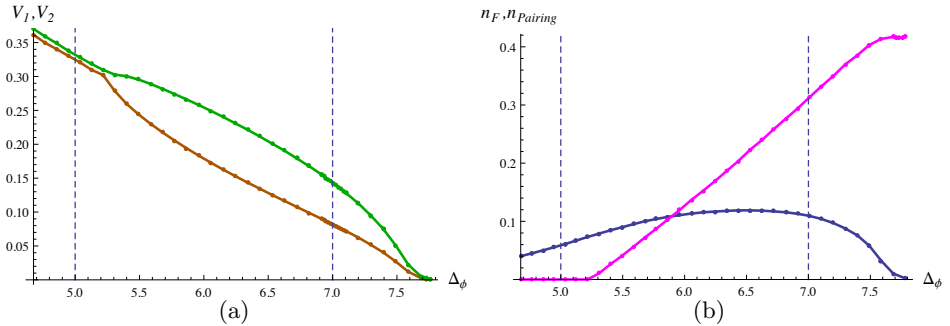


Figure 2.13. (a): Dependence of the two gaps V_1 (orange) and V_2 (green) on Δ_ϕ in the fully interacting case. (b): Dependence of the total fermionic bulk charge $n_F = \int_0^{z_w} qz^2 \langle \psi^\dagger \psi \rangle dz$ (magenta) and the total “number” of pairs $n_{Pairing} = -i\eta_5 \int_0^{z_w} z^3 \langle \overline{\psi} \Gamma^5 \psi \rangle dz$ (blue) on Δ_ϕ . One can see that while at small scalar conformal dimensions the fermionic bulk charge totally vanishes the number of Cooper pairs in the bulk theory stays finite. All parameters are as in Fig.2.10.

the AdS boundary $z = 0$. It hints that the proper definition of the superconducting condensate should be given by a Δ_ϕ -dependent linear combination of the homogeneous \mathcal{H}_1 and particular coefficients $\mathcal{P}_1, \mathcal{P}_3, \mathcal{P}_5, \dots$ that is regular for all Δ_ϕ . One can readily construct such a combination, e.g.

$$\langle \mathcal{O}_\phi \rangle = \mathcal{H}_1 + \frac{1}{2}((2\Delta_\Psi + 2) - \Delta_\phi)\mathcal{P}_1 + \frac{1}{2}(\Delta_\phi - 2\Delta_\Psi)\mathcal{P}_3, \quad (2.53)$$

see Fig. 2.14(a). as a demonstration of the existence of a non-singular combination; though there is no proof at all that this constitutes the actual physical observable.⁴

Normally the strict application of the AdS/CFT dictionary does not assign any role to such higher order coefficients in the bulk wavefunction. It is clear, however, that the singularities arise solely from the extraction of the coefficients, whereas the full AdS wavefunctions at any finite z are regular for $\Delta_\phi = 2\Delta_\Psi + \mathbb{N}$. Let us now give an argument why the coefficient rule can receive modification. The right way to interpret the linear combination $\mathcal{H}_1 + \mathcal{P}_1$ is as a mixing of the two independent operators dual to the fundamental scalar operator and the bilinear (double trace) Cooper pair operator. This suggests that we should think in a similar way about the resonance at $\Delta_\phi = 2\Delta_\Psi + 2$. There should be another Cooper-pair like operator in the theory which mixes with the fundamental scalar, such that the linear combination that constitutes the order parameter is finite.

In AdS/CFT this connection between mixing and resonances is in fact cleanly seen in correlation functions of bilinear operators [28, 29]. These bilinear operators are also known as double trace operators, since in the models where we know the dual CFT, each operator dual to an AdS field is a single trace over an $N \times N$ matrix valued combination of fields. Bilinear operators are thus the normal-ordered product of two single trace operators. Each pair of single trace CFT operators \mathcal{O}_Ψ , however, gives rise

⁴Another putative combination found by chance, $\langle \mathcal{O}_\phi \rangle = \mathcal{H}_1 + \frac{1}{2}e^{-(2\Delta_\Psi - \Delta_\phi)}((2\Delta_\Psi + 2) - \Delta_\phi)\mathcal{P}_1 + \frac{1}{2}e^{-(2\Delta_\Psi + 2 - \Delta_\phi)}(\Delta_\phi - 2\Delta_\Psi)\mathcal{P}_3$ has a remarkable overlap with the scalar condensate in the case $\eta_5 = 0$, see Fig. 2.14(b).

to an infinite tower of independent primary double trace operators:

$$\begin{aligned}
\mathcal{O}_{(0)} &= \mathcal{O}_{\overline{\Psi}C} \mathcal{O}_{\Psi} \\
\mathcal{O}_{(1)} &= \mathcal{O}_{\overline{\Psi}C} (\overleftarrow{\partial}_{\mu} - \overrightarrow{\partial}_{\mu}) (\overleftarrow{\partial}^{\mu} - \overrightarrow{\partial}^{\mu}) \mathcal{O}_{\Psi} - \text{trace} \\
\mathcal{O}_{(2)} &= \mathcal{O}_{\overline{\Psi}C} (\overleftarrow{\partial}_{\mu} - \overrightarrow{\partial}_{\mu}) (\overleftarrow{\partial}^{\mu} - \overrightarrow{\partial}^{\mu}) (\overleftarrow{\partial}_{\nu} - \overrightarrow{\partial}_{\nu}) (\overleftarrow{\partial}^{\nu} - \overrightarrow{\partial}^{\nu}) \mathcal{O}_{\Psi} - \text{traces} \\
&\vdots
\end{aligned} \tag{2.54}$$

These conformal partial waves are all the higher derivative bilinear operators that cannot be written as a descendant (a derivative) of the a lower order primary. All these operators have the same global quantum numbers as the simple pair operator with scaling dimension $2\Delta_{\Psi}$, but increase their dimension by two integer units each time. The correlation function study [28, 29] in particular shows that in the case of an interacting purely scalar bulk theory, all these linearly independent double trace primaries mix in as well and cause single-pole Feshbach resonances in s-wave scattering of single trace operators. The correspondence between the $2n$ difference in scaling dimension⁵ between each successive primary and the location of the resonance in the leading part of the bulk scalar wavefunction supports that this mixing is the right interpretation of the resonance.⁶

We do not yet have a controlled method to extract the quantitative expectation value of these higher order double trace primaries from the constituent single trace fields. The mixing originates in the renormalization of the theory, and this suggests that the proper value of the order parameter results from the introduction of higher order boundary counterterms of the type

$$S_{\text{counter}} \sim \int_{z=\epsilon} d^3x \left(-\phi^2 - \phi \overline{\Psi}_+^C \Psi_- - \phi \overline{\Psi}_+^C \overleftrightarrow{\partial}_{\mu} \overleftrightarrow{\partial}^{\mu} \Psi_- - \dots \right) \tag{2.55}$$

⁵As we mentioned one also expects a resonance at $2\Delta_{\Psi} + 3$ for high enough chemical potential. This is due to the effect of the electric field on the fermion wave functions. From the boundary perspective this could be a result of mixing with $\mathcal{O}_{\psi} J_{\mu} (\overleftarrow{\partial}^{\mu} - \overrightarrow{\partial}^{\mu}) \mathcal{O}_{\psi}$ type operator which has the right scaling dimension ($\Delta_J = 2$).

⁶The conformal partial wave operators share a resemblance with operators relevant for Fulde-Ferrel-Larkin-Ovchinnikov pairing [30, 31]. In the original FFLO set-up one considers the Zeeman splitting of spin-up/spin-down electrons and this causes an offset in their Fermi surfaces of the same form seen here. The discussion about the mixing in of these higher order partial waves does not rely on the split degeneracy of Fermi surfaces. The mixing is therefore not correlated with an FFLO-like phenomenon.

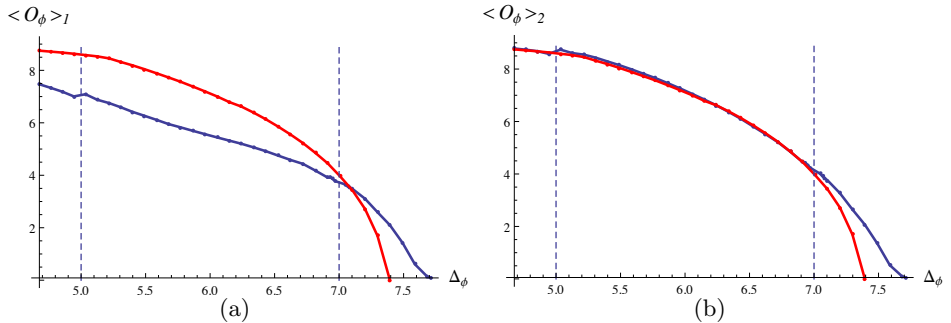


Figure 2.14. (a): The blue curve represents a particular linear combinations of the series expansion coefficients $\langle \mathcal{O}_\phi \rangle_1 = \mathcal{H}_1 + \frac{1}{2}((2\Delta_\Psi + 2) - \Delta_\phi)\mathcal{P}_1 + \frac{1}{2}(\Delta_\phi - 2\Delta_\Psi)\mathcal{P}_3$ such that all the resonances cancel out. The red curve included for comparison represents $\langle \mathcal{O}_\phi \rangle$ at $\eta_5 = 0$. (b): The serendipitous combination $\langle \mathcal{O}_\phi \rangle_2 = \mathcal{H}_1 + \frac{1}{2}e^{-(2\Delta_\Psi - \Delta_\phi)}((2\Delta_\Psi + 2) - \Delta_\phi)\mathcal{P}_1 + \frac{1}{2}e^{-(2\Delta_\Psi + 2 - \Delta_\phi)}(\Delta_\phi - 2\Delta_\Psi)\mathcal{P}_3$ that has a remarkable overlap with the $\eta_5 = 0$ solution at low Δ_ϕ as desired. All parameters are as in Fig.2.10.

where Ψ_\pm are eigenspinors of Γ^5 . To construct this correct set of counterterms and deduce the appropriate extraction of the vev in the boundary field theory is an interesting question to pursue.

The conclusion is that the resulting condensate ought to be of the form in Fig. 2.14. Qualitatively this result shows the BCS/BEC crossover as a function of the scalar scaling dimension Δ_ϕ . Though our set up is rather abstract in that scalar field here is an additional degree of freedom introduced by hand, instead of emerging from microscopic dynamics, it captures the BCS/BEC physics. For small scaling dimension the scalar operator \mathcal{O}_ϕ dominates the Bose-Fermi competition, whereas at large scalar conformal dimensions corresponding to weak coupling regime, $\eta_5/m_\phi \ll 1$, the dynamics of the boson field are suppressed, and its order parameter expectation value is dominated by fermions as shown on Fig. 2.12. The most interesting region is just to the right of the red curve. Here there is no bosonic contribution to the order parameter, but there is an enhanced Cooper pair contribution (due to the proximity effect). This is the most notable region where we have pairing induced superconductivity in holography. At larger scalar conformal dimension the order parameter exponentially decreases with increasing of Δ_ϕ , although it never vanishes.

In the strict $m_\phi \rightarrow \infty$ limit we have the standard BCS scenario of section 2.3.4.

Let us finally briefly comment on the dependence on the UV cut off ω_D . In the previous section we discussed that at very large bulk scalar mass all dynamics depends only on two parameters, η_5/ω_D and η_5/m_ϕ . For a dynamical scalar the dependence is more complicated, but we can still qualitatively infer what will happen. We know that most of the contribution to the pairing operator is located near the Fermi surfaces. Increasing ω_D means taking into account states lying far away from k_F 's. The physical picture will therefore only change minimally; to first approximation it can be compensated by adjusting η_5 such that η_5/ω_D stays constant. A non-trivial effect does happen when ω_D becomes so large that the integral becomes sensitive to fermions in the second band (for instance, see Fig. 2.1), but this is beyond the scope of this chapter.

2.5 Conclusions

We have constructed a holographic model of superconductivity which explicitly takes into account fermionic pairing driving the phase transition. In the simplest holographic models, the microscopic mechanism of superconductivity is not addressed. Specific top-down models may shed light on the strong coupling dynamics and a possible pairing mechanism [32, 33], but generic holographic models operate at a Landau-Ginzburg order parameter level.

Even so, the physics of fermionic pairing and condensation should also be explicitly representable in holographic systems. The most straightforward way to do so is to mimic the classic BCS mechanism. This is what we have done here. By introducing an attractive four-fermion interaction in the *AdS* bulk, we show that this directly reduces to a pairing induced superconducting groundstate both in the bulk and the dual boundary. To cleanly separate the fermion physics, we introduced a hard wall cut-off. This essentially guaranteed this results as the low energy theory in both sides is just a Fermi liquid in the absence of the four-fermion interaction. The one technical difference with textbook BCS is the relativistic nature of the underlying fermion theory.

Next we introduced separately a kinetic term for the *AdS* dual of the order parameter. Physically the paired operator should become dynamical if the coherence length is much shorter than the scales of inter-

est. One should find a BCS/BEC crossover as one tunes between these regimes. Here that control parameter is the scaling dimension of the order parameter field (relative to the scaling dimension of the Cooper pair operator). For large scaling dimension the kinetics of the dual AdS field is suppressed and we have the BCS physics found earlier. For low scaling dimension the scalar dynamics should be energetically favored compared to pairing condensation, and one should find a regular BEC (holographic) superconductor.

In observing this BCS/BEC crossover we encountered a surprise. At specific values $\Delta_\phi = 2\Delta_\Psi$ and $\Delta_\phi = 2\Delta_\Psi + 2$ of the control parameter the independent scalar $\langle \mathcal{O}_\phi \rangle$ and pairing $\langle \mathcal{O}_{\overline{\Psi}C} \mathcal{O}_\Psi \rangle$ vevs diverge. In fact the naive order parameter $\langle \mathcal{O}_\phi \rangle + \langle \mathcal{O}_{\overline{\Psi}C} \mathcal{O}_\Psi \rangle$ remains divergent at $\Delta_\phi = 2\Delta_\Psi + 2$. The mathematics is clear and suggests that these divergences can also occur at higher value of the scaling dimension. Physically, a plausible explanation is that higher order primaries $\mathcal{O}_{\overline{\Psi}C} (\vec{\partial}_\mu - \vec{\partial}_\mu)^n (\vec{\partial}^\mu - \vec{\partial}^\mu)^n \mathcal{O}_\Psi$, that arise in the OPE of the product of two single fermion operators, mix in with the scalar vev and the lowest order primary $\langle \mathcal{O}_\phi \rangle + \langle \mathcal{O}_{\overline{\Psi}C} \mathcal{O}_\Psi \rangle$. To establish this concretely requires a more detailed study of single and double trace operator mixing in AdS/CFT . We aim to address this in a future publication. We can nevertheless readily construct an extraction rule for a finite order parameter that interpolates between the BCS and BEC regimes.

In both aspects the physics that holographic system describes is very conventional. It is again an excellent proving ground for AdS/CFT that it does so, but by construction it does not uncover any unconventional or exotic physics. The main reason it does not do so is the presence of the hard wall. It ensures that the groundstate dynamics closely follows standard Fermi liquid and Landau-Ginzburg theory. It would be very interesting, but technically challenging [16, 17], to try to remove the hard wall. This would reintroduce the low energy dynamics that could yield exotic and novel behaviour. In particular, it might be an important step towards a holographic fermionic theory of unconventional superconductivity.

2.A Green's functions and charge densities

In this Appendix we provide a detailed derivation of the formulas for the fermionic bilinears appearing in the bosonic equations. In principle while calculating these objects one needs to be careful because of the renormal-

ization of these composite operators. However, we are just regularizing these object with a cut off and not attempting to perform the renormalization. We can write the fermionic electric charge density as a limit of Feynman Green's function:

$$\langle \psi^+(x)\psi(x) \rangle = \lim_{t, \vec{x} \rightarrow t', \vec{x}'} \langle T\psi^+(t, \vec{x})\psi(t', \vec{x}') \rangle = \lim_{t, \vec{x} \rightarrow t', \vec{x}'} G_{\psi_i^+\psi_i} \quad (2.56)$$

We would like to express it with the Nambu-Gorkov (NG) Green's function defined as

$$G_{\chi_i\chi_j^+} = \frac{1}{Z} \int D\chi D\chi^+ \chi_i\chi_j^+ \exp\left(i \int d^4x \chi^+ \widetilde{K}\chi\right). \quad (2.57)$$

Using properties of the time ordered product the relations between the original Green's functions and the NG ones are

$$G_{\psi_1^+\psi_1}(t, \vec{x}; t', \vec{x}') = -G_{\chi_1\chi_1^+}(t', \vec{x}'; t, \vec{x}), \quad (2.58)$$

$$G_{\psi_3^+\psi_3}(t, \vec{x}; t', \vec{x}') = G_{\chi_3\chi_3^+}(t, \vec{x}; t', \vec{x}'). \quad (2.59)$$

With these the charge densities can be expressed with the components of the NG Green's function

$$\begin{aligned} \langle \psi^+\psi \rangle &= \lim_{t, \vec{x} \rightarrow t', \vec{x}'} \left(-G_{\chi_1\chi_1^+}(t', \vec{x}'; t, \vec{x}) - G_{\chi_2\chi_2^+}(t', \vec{x}'; t, \vec{x}) \right. \\ &\quad \left. + G_{\chi_3\chi_3^+}(t, \vec{x}; t', \vec{x}') + G_{\chi_4\chi_4^+}(t, \vec{x}; t', \vec{x}') \right), \\ \langle \overline{\psi^c}\Gamma^5\psi \rangle &= \lim_{t, \vec{x} \rightarrow t', \vec{x}'} \left(G_{\chi_1\chi_4^+}(t, \vec{x}; t', \vec{x}') + G_{\chi_2\chi_3^+}(t, \vec{x}; t', \vec{x}') \right. \\ &\quad \left. + G_{\chi_2\chi_3^+}(t', \vec{x}'; t, \vec{x}) + G_{\chi_1\chi_4^+}(t', \vec{x}'; t, \vec{x}) \right). \end{aligned} \quad (2.60)$$

Since the NG Green's function solves (2.20) we can decompose it as

$$G(t, \vec{x}; t', \vec{x}') = \int \frac{d\omega}{2\pi} e^{-i\omega(t-t')} \sum_n \int \frac{d^2k}{4\pi^2} \frac{ie^{i\vec{k}(\vec{x}_\perp - \vec{x}'_\perp)}}{\omega - \omega_{\vec{k},n} + i\text{sgn}(\omega)\epsilon} \chi_{\vec{k},n}(z) \chi_{\vec{k},n}^+(z'), \quad (2.61)$$

where $\chi_{\vec{k},n}(z)$ solves the Dirac equation (2.21) and form an orthonormal basis

$$\int_0^{z_w} dz \chi_{\vec{k},n}^+(z) \chi_{\vec{k},n'}(z) = \delta_{nn'}, \quad (2.62)$$

$$\sum_n \chi_{\vec{k},n}(z) \chi_{\vec{k},n}^+(z') = \delta(z - z'). \quad (2.63)$$

We can immediately perform the ω integral to get (supposing that $t > t'$)

$$G(t, \vec{x}; t', \vec{x}') = \sum_n \int \frac{d^2k}{4\pi^2} e^{-i\omega_{\vec{k},n}(t-t')} e^{i\vec{k}(\vec{x}_\perp - \vec{x}'_\perp)} \chi_{\vec{k},n}^-(z) \chi_{\vec{k},n}^+(z') \Theta(\omega_{\vec{k},n}), \quad (2.64)$$

$$G(t', \vec{x}'; t, \vec{x}) = - \sum_n \int \frac{d^2k}{4\pi^2} e^{-i\omega_{\vec{k},n}(t'-t)} e^{i\vec{k}(\vec{x}'_\perp - \vec{x}_\perp)} \chi_{\vec{k},n}^-(z) \chi_{\vec{k},n}^+(z') \Theta(-\omega_{\vec{k},n}). \quad (2.65)$$

Substituting this into (2.60) we obtain (2.23) and (2.24).

2.B Perturbative solution

2.B.1 Perturbative fermion spectrum, AdS-gap equation

We will solve the fermionic equation of motion (2.21) perturbatively in the scalar interaction and determine the gap equation. It is convenient for this to write the eigenvalue problem in terms of $(\alpha_1, \alpha_2, \alpha_3, \alpha_4) = (\chi_1, i\chi_2, \chi_3, i\chi_4)$. The redefined Hamiltonian is real (but we will still denote it with H).

Our Hamiltonian can be split as $H = H_0 + V$, where $H_0 = H(\eta_5 = 0)$. The perturbation is coming from the Majorana coupling

$$V = 2\eta_5 \frac{\phi}{z} \begin{pmatrix} 0 & -\epsilon \\ \epsilon & 0 \end{pmatrix}, \quad (2.66)$$

where ϵ is the 2x2 matrix $\epsilon = i\sigma_2$

The solution of the unperturbed problem for a given momentum takes the form

$$\alpha_{k,+n}^{(0)} = \begin{pmatrix} \xi_{k,n} \\ 0 \end{pmatrix} \omega_{1,k,n}^{(0)} = \omega_{k,n}^{(0)} > 0, \quad (2.67)$$

$$\alpha_{k,-n}^{(0)} = \begin{pmatrix} 0 \\ \epsilon \xi_{k,n} \end{pmatrix} \omega_{2,k,n}^{(0)} = -\omega_{k,n}^{(0)}. \quad (2.68)$$

We will focus on $n = 1$ and will omit this index.

When doing the perturbation theory we should be careful because near the Fermi-surface different bands are crossing each other. Therefore we start with two modes with unperturbed energy $\omega_k^{(0)}$ and $-\omega_k^{(0)}$ and

approximate the solution as $\alpha_k = a\alpha_{k,+}^{(0)} + b\alpha_{k,-}^{(0)}$. Near the Fermi-surface this is a good approximation.

The perturbed energy and wave-functions can be determined by the off-diagonal matrix element of V (the diagonal elements are zero).

$$V_k = \int_0^{z_w} dz \alpha_{k,+}^{(0)+} V \alpha_{k,-}^{(0)} = 2\eta_5 \int_0^{z_w} dz |\xi_k|^2 \frac{\phi}{z}. \quad (2.69)$$

The new energy levels are

$$\omega_{\pm} = \pm \sqrt{(\omega_k^{(0)})^2 + V_k^2}, \quad (2.70)$$

so the size of the gap is V_{k_F} . The normalized wave-functions are

$$\alpha_{k,+} = \begin{pmatrix} \xi_k \cos \frac{1}{2}\beta_k \\ \epsilon \xi_k \sin \frac{1}{2}\beta_k \end{pmatrix}, \quad \alpha_{k,-} = \begin{pmatrix} -\xi_k \sin \frac{1}{2}\beta_k \\ \epsilon \xi_k \cos \frac{1}{2}\beta_k \end{pmatrix}, \quad (2.71)$$

where

$$\tan \beta_k = \frac{V_k}{\omega_k^{(0)}}. \quad (2.72)$$

Using this perturbative result we can express the scalar source with the unperturbed fermion wave functions:

$$\langle \psi^c \Gamma^5 \psi \rangle = -\frac{i}{4\pi} \int_{-\Lambda(\omega_D)}^{\Lambda(\omega_D)} dk |k| \frac{V_k}{\sqrt{(\omega_k^{(0)})^2 + V_k^2}} |\xi_k(z)|^2. \quad (2.73)$$

Here $\Lambda(\omega_D)$ is a momentum cut-off corresponding to the energy scale ω_D . In our numerics we sample discrete number of momenta and sum over it. In order to capture the contribution around k_F accurately we can use the following discretization

$$\begin{aligned} \int_{-\Lambda(\omega_D)}^{\Lambda(\omega_D)} dk |k| \frac{V_k}{\sqrt{(\omega_k^{(0)})^2 + V_k^2}} |\xi_k|^2 &\approx \sum_{k_i} V_{k_i} k_i \frac{1}{|\omega'(k_i)|} \int_{\omega(k_i)}^{\omega(k_{i+1})} \frac{d\omega}{\sqrt{\omega^2 + V_{k_i}^2}} \\ &= \sum_i |\xi_{k_i}|^2 \frac{V_{k_i} k_i}{\omega'(k_i)} \log \left(\frac{\omega_{i+1}^{(0)} + \sqrt{(\omega_{i+1}^{(0)})^2 + V_{k_i}^2}}{\omega_i^{(0)} + \sqrt{(\omega_i^{(0)})^2 + V_{k_i}^2}} \right) \end{aligned} \quad (2.74)$$

2.B.2 Simplified Gap equation

The dominant contribution for the scalar charge comes from a region near the Fermi surface where the (unperturbed) spectrum is linear. Since the perturbation matrix element V_k is a slowly varying function of k we can approximate its value with $V_{k_{F,1}} = V_1$ and $V_{k_{F,2}} = V_2$.

We have two Fermi surfaces. Hence the gap-equation is (recall that our scalar is an auxiliary field with no dynamics here)

$$\phi(z) = \frac{z^3}{4\eta_5} \left[\gamma_1 V_1 \log \left(\frac{\omega_D + \sqrt{\omega_D^2 + V_1^2}}{V_1} \right) \rho_1(z) + \right. \quad (2.75)$$

$$\left. \gamma_2 V_2 \log \left(\frac{\omega_D + \sqrt{\omega_D^2 + V_2^2}}{V_2} \right) \rho_2(z) \right], \quad (2.76)$$

where $\rho_1(z) = |\xi_{k_{F,1}}|^2$, $\rho_2(z) = |\xi_{k_{F,2}}|^2$ and $\gamma_{1,2} = \frac{\eta_5^2}{m_\phi^2 \pi} \frac{|k_{F1,2}|}{|\omega'(k_{F1,2})|}$. We make the following ansatz

$$\phi = (C_1 \rho_1(z) + C_2 \rho_2(z)) z^3. \quad (2.77)$$

In this case the perturbation matrix element is

$$V_1 = 2\eta_5 (C_1 I_{11} + C_2 I_{12}), \quad V_2 = 2\eta_5 (C_2 I_{22} + C_1 I_{12}), \quad (2.78)$$

where

$$I_{11} = \int_0^{z_w} z^2 \rho_1^2 dz, \quad I_{22} = \int_0^{z_w} z^2 \rho_2^2 dz, \quad I_{12} = \int_0^{z_w} z^2 \rho_2 \rho_1 dz. \quad (2.79)$$

In the limit of $\omega_D \gg \eta_5$ our gap-equations take the following form

$$\begin{aligned} aV_1 + bV_2 &= 2\eta_5 \gamma_1 V_1 \log \left(\frac{\omega_D}{\eta_5 V_1} \right) \\ bV_1 + cV_2 &= 2\eta_5 \gamma_2 V_2 \log \left(\frac{\omega_D}{\eta_5 V_2} \right), \end{aligned} \quad (2.80)$$

with

$$a = \frac{I_{22}}{I_{22}I_{11} - I_{12}^2}, \quad b = \frac{I_{12}}{I_{12}^2 - I_{22}I_{11}}, \quad c = \frac{I_{11}}{I_{22}I_{11} - I_{12}^2}. \quad (2.81)$$

For the ratio $x = V_1/V_2$ we obtain

$$x^2 + \left(\frac{I_{22} \gamma_2}{I_{12} \gamma_1} - \frac{I_{11}}{I_{12}} \right) x - \frac{\gamma_2}{\gamma_1} = \frac{\gamma_2}{b} x \log x. \quad (2.82)$$

We can now solve our equations easily to obtain

$$C_1 = (ax + b) \frac{\omega_D}{\eta_5} \exp\left(-\frac{bx + c}{\gamma_2}\right), \quad C_2 = (bx + c) \frac{\omega_D}{\eta_5} \exp\left(-\frac{bx + c}{\gamma_2}\right). \quad (2.83)$$

2.C Numerical methods

2.C.1 General strategy

To solve the equations (2.41) numerically, we resort to an iterative Hartree resummation:

- At a constant $A_0 = \mu$ and zero scalar field, we find the unperturbed spectrum of fermions. As a result we get a set of fermionic wavefunctions for a discrete array of energies and momenta $(k_i, \omega_{n,i})$.
- With these wavefunctions we construct the source terms on the right hand side of the first two equations in (2.41) and solve for $A_0(z)$ and $\phi(z)$. Both UV cut offs in both k and ω should be imposed to render the sums in the source terms finite.
- Substitute the new $A_0(z)$ and $\phi(z)$ into the Dirac equation and find the new spectrum.
- Repeat steps 2 – 4 till full convergence.

Once the system converges sufficiently, we can extract the information of the dual theory by a fit to the near boundary behavior of the resulting wavefunctions.

We have optimized our numerics in several ways: The most time-consuming part of the algorithm is the repeated calculation of the Dirac fermion spectrum. A significant improvement is obtained using the perturbative prescription described in a previous section. We exclude the $\phi(z)$ field from the Dirac equation, and instead of four coupled ODE we get for fermions two identical decoupled systems of a second order. Then we construct the corrected wavefunctions. In addition, we do not need to

take equally dense sampling in k , because most of the fermionic spectral weight is concentrated around k_F (remember that we have two slightly different Fermi momenta in the theory), and we may take sparser k -sampling away from these points without loss in accuracy.

Empirically we found that different numerical schemes to fermionic and bosonic subsystems was the most efficient. For the fermionic spectrum we use the shooting method: we impose boundary conditions dependent on a free parameter at the boundary cut off $z = \epsilon$, and scan over this parameter to make the resulting solution satisfy physical boundary conditions at the hard wall.

However, the shooting method in the gauge field and scalar sector often leads the system to converge to some higher harmonics instead of the groundstate. The Newton method is much more stable in that case: we impose both AdS-infinity and hardwall boundary conditions at the same time, approximate differential equations by finite differences, and solve the resulting system of linear algebraic equation with a relaxation algorithm. For our purposes a grid of $N_p = 3000$ points in z -direction (for $z_w = 1$) was chosen, in which case the relaxation algorithm converges after 5 – 6 iterations.

Once the bulk wave functions are obtained, it is still not a trivial question how to extract the leading boundary behavior from this data. This is what contains the information of the dual field theory. The analytical puzzles related to this problem were discussed in section 2.A. Here we focus on corresponding numerical issues.

We are interested in coefficients $\mathcal{H}_1, \mathcal{P}_1, \mathcal{P}_3$ defined in (2.51). The function $\phi(z)$ is known in a form of discrete list of values $\{z_i, \phi(z_i)\}$ of the length $N_p = 3000$, therefore our accuracy is limited and naive use of the standard fitting schemes of *Mathematica* leads to large errors.

Instead we first determine the expansion coefficients of the fermionic bilinear sourcing the scalar field

$$-i\eta_5 z^3 \langle \bar{\psi} \Gamma^5 \psi \rangle = \mathcal{S}_1 z^5 + \mathcal{S}_3 z^7 + \dots \quad (2.84)$$

These can be easily found, as contra to the scalar field profile the fermionic bulk wave functions are derived with a great accuracy due to the use of the shooting method.

Then we use the algebraic relations (2.51) to obtain the “particular” coefficients on the base of \mathcal{S}_i .

Knowing \mathcal{P}_1 and \mathcal{P}_3 we can subtract these from the scalar wave function and run the Newton relaxation scheme one more time for

$$\tilde{\phi}(z) = \phi(z) - \mathcal{P}_1 z^5 - \mathcal{P}_3 z^7. \quad (2.85)$$

We now need to fit only for the single coefficient \mathcal{H}_1 . This can be easily done even for moderate number of discretized points N_p .

Bibliography

- [1] C. P. Herzog, P. Kovtun, S. Sachdev and D. T. Son, “Quantum critical transport, duality, and M-theory,” *Phys. Rev. D* **75**, 085020 (2007) [hep-th/0701036].
- [2] S. A. Hartnoll, P. K. Kovtun, M. Muller and S. Sachdev, “Theory of the Nernst effect near quantum phase transitions in condensed matter, and in dyonic black holes,” *Phys. Rev. B* **76**, 144502 (2007) [arXiv:0706.3215 [cond-mat.str-el]].
- [3] S. S. Gubser, “Breaking an Abelian gauge symmetry near a black hole horizon,” *Phys. Rev. D* **78**, 065034 (2008) [arXiv:0801.2977 [hep-th]].
- [4] S. A. Hartnoll, C. P. Herzog and G. T. Horowitz, “Building a Holographic Superconductor,” *Phys. Rev. Lett.* **101**, 031601 (2008) [arXiv:0803.3295 [hep-th]].
- [5] S. A. Hartnoll, C. P. Herzog and G. T. Horowitz, “Holographic Superconductors,” *JHEP* **0812**, 015 (2008) [arXiv:0810.1563 [hep-th]].
- [6] H. Liu, J. McGreevy and D. Vegh, “Non-Fermi liquids from holography,” *Phys. Rev. D* **83**, 065029 (2011) [arXiv:0903.2477 [hep-th]].
- [7] M. Cubrovic, J. Zaanen and K. Schalm, “String Theory, Quantum Phase Transitions and the Emergent Fermi-Liquid,” *Science* **325**, 439 (2009) [arXiv:0904.1993 [hep-th]].
- [8] T. Hartman and S. A. Hartnoll, “Cooper pairing near charged black holes,” *JHEP* **1006**, 005 (2010) [arXiv:1003.1918 [hep-th]].
- [9] T. Faulkner, G. T. Horowitz, J. McGreevy, M. M. Roberts and D. Vegh, “Photoemission ‘experiments’ on holographic superconductors,” *JHEP* **1003**, 121 (2010) [arXiv:0911.3402 [hep-th]].
- [10] S. S. Gubser, F. D. Rocha and P. Talavera, “Normalizable fermion modes in a holographic superconductor,” *JHEP* **1010**, 087 (2010) [arXiv:0911.3632 [hep-th]].

- [11] J. -W. Chen, Y. -J. Kao and W. -Y. Wen, “Peak-Dip-Hump from Holographic Superconductivity,” *Phys. Rev. D* **82**, 026007 (2010) [arXiv:0911.2821 [hep-th]].
- [12] S. Sachdev, “A model of a Fermi liquid using gauge-gravity duality,” *Phys. Rev. D* **84**, 066009 (2011) [arXiv:1107.5321 [hep-th]].
- [13] J. de Boer, K. Papadodimas and E. Verlinde, “Holographic Neutron Stars,” *JHEP* **1010**, 020 (2010) [arXiv:0907.2695 [hep-th]].
- [14] S. A. Hartnoll and A. Tavanfar, “Electron stars for holographic metallic criticality,” *Phys. Rev. D* **83**, 046003 (2011) [arXiv:1008.2828 [hep-th]].
- [15] Y. Liu, K. Schalm, Y. W. Sun and J. Zaanen, “BCS instabilities of electron stars to holographic superconductors,” *JHEP* **1405**, 122 (2014) [arXiv:1404.0571 [hep-th]].
- [16] A. Allais, J. McGreevy and S. J. Suh, “A quantum electron star,” *Phys. Rev. Lett.* **108**, 231602 (2012) [arXiv:1202.5308 [hep-th]].
- [17] A. Allais and J. McGreevy, “How to construct a gravitating quantum electron star,” *Phys. Rev. D* **88**, 066006 (2013) [arXiv:1306.6075 [hep-th]].
- [18] C. P. Herzog and J. Ren, “The Spin of Holographic Electrons at Nonzero Density and Temperature,” *JHEP* **1206**, 078 (2012) [arXiv:1204.0518 [hep-th]].
- [19] Y. Seo, S. -J. Sin and Y. Zhou, “Thermal Mass and Plasmino for Strongly Interacting Fermions,” *JHEP* **1306**, 076 (2013) [arXiv:1305.1446 [hep-th]].
- [20] D. Bertrand, A Relativistic BCS Theory of Superconductivity, PhD Thesis, Louvain 2005. [<http://cp3.irmp.ucl.ac.be/upload/theses/phd/bertrand.pdf>]
- [21] S. Bolognesi and D. Tong, “Magnetic Catalysis in AdS₄,” *Class. Quant. Grav.* **29**, 194003 (2012) [arXiv:1110.5902 [hep-th]].
- [22] S. Bolognesi, J. N. Laia, D. Tong and K. Wong, “A Gapless Hard Wall: Magnetic Catalysis in Bulk and Boundary,” *JHEP* **1207**, 162 (2012) [arXiv:1204.6029 [hep-th]].

- [23] T. Nishioka, S. Ryu and T. Takayanagi, “Holographic Superconductor/Insulator Transition at Zero Temperature,” JHEP **1003**, 131 (2010) [arXiv:0911.0962 [hep-th]].
- [24] G. T. Horowitz and B. Way, “Complete Phase Diagrams for a Holographic Superconductor/Insulator System,” JHEP **1011**, 011 (2010) [arXiv:1007.3714 [hep-th]].
- [25] S. Caron-Huot, P. Kovtun, G. D. Moore, A. Starinets and L. G. Yaffe, “Photon and dilepton production in supersymmetric Yang-Mills plasma,” JHEP **0612**, 015 (2006) [hep-th/0607237].
- [26] Y. Liu, K. Schalm, Y. -W. Sun and J. Zaanen, “Bose-Fermi competition in holographic metals,” JHEP **1310**, 064 (2013) [arXiv:1307.4572 [hep-th]].
- [27] F. Nitti, G. Policastro and T. Vanel, “Dressing the Electron Star in a Holographic Superconductor,” JHEP **1310**, 019 (2013) [arXiv:1307.4558 [hep-th]].
- [28] A. L. Fitzpatrick, E. Katz, D. Poland and D. Simmons-Duffin, “Effective Conformal Theory and the Flat-Space Limit of AdS,” JHEP **1107**, 023 (2011) [arXiv:1007.2412 [hep-th]].
- [29] J. Fan, “Effective AdS/renormalized CFT,” JHEP **1109**, 136 (2011) [arXiv:1105.0678 [hep-th]].
- [30] P. Fulde and R. A. Ferrell, Phys. Rev. **135**, A550 (1964).
- [31] A. I. Larkin and Yu. N. Ovchinnikov, Zh. Eksp. Teor. Fiz. **47**, 1136 (1964); translation: Sov. Phys. JETP, **20**, 762 (1965).
- [32] M. Ammon, J. Erdmenger, M. Kaminski and P. Kerner, “Flavor Superconductivity from Gauge/Gravity Duality,” JHEP **0910**, 067 (2009) [arXiv:0903.1864 [hep-th]].
- [33] M. Ammon, J. Erdmenger, M. Kaminski and A. O’Bannon, “Fermionic Operator Mixing in Holographic p-wave Superfluids,” JHEP **1005**, 053 (2010) [arXiv:1003.1134 [hep-th]].

Chapter 3

Holographic phase diagram of quark-gluon plasma formed in heavy-ions collisions

3.1 Introduction

For the last decade, since the publication of fascinating papers [1–3], it was realized that supersymmetric and non-supersymmetric theories in the strong coupling limit in principle could be pretty close in their properties [4]. The AdS/CFT correspondence, which appeared as a formal duality between the $\mathcal{N} = 4$ super Yang-Mills theory and a quantum gravity in *AdS* background, has become powerful tool for studying various properties of real physical systems in the strong coupling [5].

Important branch of these investigations is the analysis of the Quark Gluon Plasma (QGP) from the point of view of *AdS*-holography, see for example, review [6]. These applications of the AdS/CFT correspondence to strongly coupled QGP have been mostly related to equilibrium properties of the plasma, or to its' kinetics/hydrodynamics near the equilibrium.

A particular application of AdS/CFT to the strongly coupled QGP, is the analysis of thermalization of matter and early entropy production instantly after the collision of relativistic heavy ions. RHIC experiments have shown that a QGP forms at a very early stage just after the heavy ion collision, i.e. a rapid thermalization occurs, and QGP produced in RHIC is believed to be strongly coupled as evidenced by its rapid equilibration. Strong collective flows well reproduced by hydrodynamics, and strong jet quenching [7–9]. This obviously requires a calculation of the strongly coupled field theory in non-equilibrium process.

Not long ago Gubser, Yarom and Pufu [11] have proposed the gravi-

tational shock wave in AdS₅ as a possible holographic dual for the heavy ion and have related the area of the trapped surface formed in a collision of such waves to the entropy of matter formed after collision of heavy ions. Early papers where has been mentioned an analogy between colliding heavy ions and colliding gravitational shock waves in anti-de Sitter space include [12]-[16]. This AdS-holographic model has been also used to find the stress-energy tensor of the QGP formed by ion collision. In accordance with AdS/CFT dictionary this stress-energy tensor is dual to the metric of spacetime after collision of shock waves [16].

The main result of [11, 17], confirmed by numerical calculations performed in [18, 19], is that in the limit of a very large collision energy E the multiplicity (the entropy S) grows as

$$S > \mathcal{C}E^{2/3}, \quad (3.1)$$

\mathcal{C} is a numerical factor (see Sect.3.2.1).

Alvarez-Gaume, Gomez, Sabeo Vera, Tavanfar, and Vazquez-Mozoand [20] have considered central collision of shock waves sourced by a nontrivial matter distribution in the transverse space and they have found critical phenomenon occurring as the shock wave reaches some diluteness limit. This criticality may be related to criticality found in [18]. The numerical results of [18] show the existence of a simple scaling relation between the critical impact parameter and the energy of colliding waves.

The size of colliding nuclei is introduced via the distance of those objects from the boundary along the holographic coordinate z .

The model of infinite homogenous wall has been proposed and analyzed by Shuryak and Lin [18]. The advantage of this model is the essential simplicity of calculations. However, the legitimacy of these calculations requires some additional examinations (see our discussion in Sect. 3.2.2).

In heavy ion collisions not only the energy per nucleus is important variable. One can try to associate different nuclei with different kinds of shock waves. There are several proposal in literature on this subject. For example, in [21] the holographic model with cutting off the UV part of the bulk geometry, has been proposed. Formation of trapped surfaces (TS) in head-on collisions of charged shock waves in the (A)dS background has been considered in [22] and it has been shown that the formation of trapped surfaces on the past light cone is only possible when charge is below certain critical value - situation similar to the collision of two ultrarelativistic charges in Minkowski space-time [23]. This critical value

depends on the energy of colliding particles and the value of a cosmological constant. The formation of trapped surfaces in head-on collisions of shock waves in gravitational theories with more complicated bulk dynamics, in particular with the Einstein-dilaton dynamics, pretended to describe holographic physics that is closer to QCD than the pure AdS theory [24, 21], has been considered recently by Kiritsis and Taliotis [25]¹ and they have found that the multiplicity grows as

$$S \gtrsim E^{0.24}, \quad (3.2)$$

that is rather close to the experimental data.

In this chapter we propose to incorporate the study of collisions of charged shock gravitational waves [22] into the description of colliding nuclei with non-zero baryon chemical potential. In the holographic context, the chemical potential of strongly coupled QGP on the gravity side is related to temporal component A_t of the $U(1)$ gauge field [27]-[34]. The asymptotic value of this gauge field component in the bulk is interpreted as the chemical potential in the gauge theory

$$\mu = A_t|_{\text{boundary}}. \quad (3.3)$$

We use the same identification (3.3) for colliding ions. It would be interesting to perform calculations for the off-center collision of charged gravitational waves or generally smeared charged shock waves. Postponing this problem for further investigations, here we consider the head-on collision of charged point shock waves and charged wall shock waves. This will give us the holographic picture for QGP phase diagram in the first moment after collisions of heavy ions. This phase diagrams, chemical potential (charge) μ versus temperature (energy) T , are displayed in Fig. 5 and Fig. 11. The colored lines separate the TS-phase from the phase free of TS. Let us note that the obtained diagrams differ from the phase diagram for equilibrium QGP (see Fig.3.1 in Sect. 3.2.1).

The chapter is organized as follows. In Sect.2 we present our set up of the problem. In Sect.2.1.1 we describe the role of black holes in AdS/CFT description of strongly coupled QGP. In Sect. 2.1.2. we present the description of the chemical potential of QGP within the AdS/CFT correspondence. In Sect. 2.1.3 we remind the main facts about shock waves in

¹Collision of dilatonic shock waves in the flat background has been considered in [26].

AdS₅ related to the trapped surface formation. In Sect.2.1.4 we describe in details the dual conjecture proposed in [11]. In Sect.2.2 we pay a special attention to the problem of regularization that appears within the wall shock waves approach. In Sect. 3 we present the phase diagram, temperature vs chemical potential, for QGP formed in the heavy-ions collisions by using the holographic approach with the central collision of charged shock waves. In Sect. 4 we present our calculations of the same problem by using the regularized version of the charged wall shock waves. We summarize our calculations in Sect. 5 and present here also further directions related to holographic description of quark-gluon plasma formed in heavy-ions collisions.

3.2 Set up

3.2.1 Dual conjectures

Black holes and AdS/CFT correspondence for strongly coupled QGP

The idea of AdS/CFT applications to description of the QGP is based on the possibility to make an one to one correspondence between phenomenological/thermodynamical parameters of plasma – T, E, P, μ – and parameters that characterize deformations of AdS₅. In the dual gravity setting the source of temperature and entropy are attributed to the gravitational horizons. The relation between energy density and temperature typical for the BH in AdS according [35, 36] is

$$E = \frac{3\pi^3 L^3}{16 G_5} T^4 \tag{3.4}$$

In the phenomenological model of QGP, such as the Landau or Bjorken hydrodynamical models [37, 38], the plasma is characterized by a space-time profile of the energy-momentum tensor $T_{\mu\nu}(x^\rho)$, $\mu, \nu, \rho = 0, \dots, 3$. This state has its counterpart on the gravity side as a modification of the geometry of the original AdS₅ metric. This follows the general AdS/CFT line: operators in the gauge theory correspond to fields in SUGRA. In the case of the energy-momentum tensor, the corresponding field is just the 5D metric. It is convenient to parameterize corresponding 5-dimensional

geometry as

$$ds^2 = L^2 \frac{g_{\mu\nu}(x^\rho, z) dx^\mu dx^\nu + dz^2}{z^2}, \quad (3.5)$$

that is the 5D Fefferman-Graham metric [39]. The flat case $g_{\mu\nu} = \eta_{\mu\nu}$ parametrizes AdS_5 in Poincaré coordinates. The conformal boundary of space-time is at $z=0$ and

$$g_{\mu\nu}(x^\rho, z) = \eta_{\mu\nu} + z^4 g_{\mu\nu}^{(4)}(x^\rho) + \dots \quad (3.6)$$

The AdS/CFT duality leads to the relation

$$g_{\mu\nu}^{(4)}(x^\rho) \sim \langle T_{\mu\nu}(x^\rho) \rangle \quad (3.7)$$

Applications of AdS/CFT correspondence to hydrodynamical description of the QGP is based on the fact that the energy momentum tensor can be read off from the expansion of the BH in AdS_5 metric (3.6) corresponding to simple hydrodynamical model

$$\langle T_{\mu\nu} \rangle \propto g_{\mu\nu}^{(4)} = \text{diag}(3/z_0^4, 1/z_0^4, 1/z_0^4, 1/z_0^4) \quad (3.8)$$

The BH in AdS_5 in the Fefferman-Graham coordinates has the form (3.5) with the following nonzero components of $g_{\mu\nu}(x^\rho, z)$ (see [6] and refs therein)

$$g_{00} = -\frac{\left(1 - \frac{z^4}{z_0^4}\right)^2}{\left(1 + \frac{z^4}{z_0^4}\right)}, \quad g_{ii} = \left(1 + \frac{z^4}{z_0^4}\right) \quad (3.9)$$

A change of coordinates $\tilde{z} = z/(1 + z^4/z_0^4)^{1/2}$ transforms (3.5) to the standard metric form of the AdS-Schwarzschild static black hole

$$\tilde{z}^2 ds^2 = -\left(1 - \frac{\tilde{z}^4}{\tilde{z}_0^4}\right) dt^2 + d\vec{x}^2 + \frac{1}{1 - \frac{\tilde{z}^4}{\tilde{z}_0^4}} d\tilde{z}^2, \quad (3.10)$$

with $\tilde{z}_0 = z_0/\sqrt{2}$ being the location of the horizon.

Chemical potential in QGP via AdS/CFT correspondence

The Reissner-Nordström metric in AdS has the following form:

$$ds^2 = -g(R)dT^2 + g(R)^{-1}dR^2 + R^2 d\Omega_{D-2}^2, \quad (3.11)$$

$$g(R) = 1 - \frac{2M}{R^2} + \frac{Q^2}{R^4} + \frac{\Lambda}{3}R^2, \quad (3.12)$$

where Λ is cosmological constant, $\Lambda/3 \equiv 1/a^2$, M and Q are related to the ADM (Arnowitt-Deser-Misner) mass m and the charge σ

$$M = \frac{4\pi G_5 m}{3\pi^2}, \quad Q^2 = \frac{4\pi G_5 \sigma^2}{3}. \quad (3.13)$$

σ is a charge of the electromagnetic field (pure electric) with only one non-zero component

$$A = A_T dT = \left(-\sqrt{\frac{3}{4}} \frac{Q}{R^2} + \Phi \right) dT, \quad (3.14)$$

here Φ is a constant $\Phi = \frac{\sqrt{3}}{2} \frac{Q}{R_+^2}$, where R_+ is the largest real root of $g(R)$.

Thermodynamics of the charged BH is described by the grand canonical potential (free energy) $W = I/\beta$, the Hawking temperature $T = 1/\beta$, and the chemical potential [40, 41] that are given by

$$I = \frac{\pi\beta}{8G_5 a^2} \left(a^2 R_+^2 + R_+^4 - \frac{Q^2 a^2}{R_+^2} \right), \quad T = \frac{1}{4\pi} g'(R_+), \quad \mu = \frac{\sqrt{3}Q}{2R_+^2}, \quad (3.15)$$

here R_+ is outer horizon, $g(R_+) = 0$, I is given by the value of the action at (3.12) and (3.14). The relation with the first law of thermodynamics, $d\mathcal{E} = Td\mathcal{S} + \mu dQ$ is achieved under identification

$$W = \mathcal{E} - T\mathcal{S} - \Phi Q, \quad \mathcal{E} = m, \quad \mathcal{S} = \frac{S_H}{4G_5}, \quad Q = q, \quad \mu = \Phi \quad (3.16)$$

Note that just the asymptotic value of a single gauge field component gives the chemical potential [27]-[34]

$$\mu = \lim_{r \rightarrow \infty} A_t(r) \quad (3.17)$$

The QGP is characterized at least by two parameters: temperature and chemical potential. Generically speaking, quantum field theories may have non zero chemical potentials for any or all of their Noether charges. Within the AdS/CFT context two different types of chemical potential are considered, namely related to the R charge and to baryon number.

Baryon number charge can only occur when we have a theory containing fundamental flavours. Introduction flavours into the gauge theory

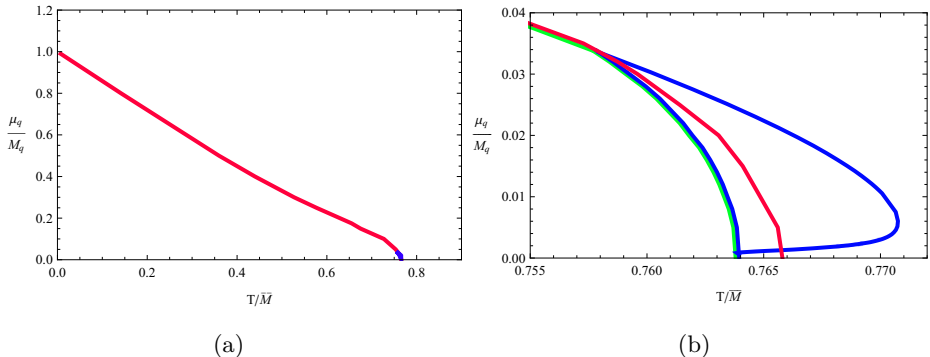


Figure 3.1. Phase diagram from [27]: Quark chemical potential μ_q/M_q , in versus temperature T/\bar{M} . The red line separates the phase of Minkowski embeddings (small temperatures, small μ_q/M_q) from black hole embeddings (see details in [27]). Figure (b) zooms in on the region near the end of this line. Different lines in (b) correspond to different embedding geometries.

by means of a D7 brane leads to appearance of a $U(N_f)$ global flavour symmetry. The flavour group contains a $U(1)_B$, that is a baryon number symmetry, and for this baryon number one adds a chemical potential μ_b [28]. To calculate the free energy one has to calculate the DBI action for a D7 brane. Note that there is a divergence in formal definition, so we must go through the process of renormalization, see for example lectures [42] and for yearly discussion [43].

R charge chemical potential appears for SUSY models [34]. In the $N = 1$ case there is a $U(1)$ R symmetry group. As to extended SUSY, say $N=2$, the quark mass term breaks R symmetry.

The typical phase diagram the chemical potential vs the temperature is presented in Fig. 3.1 (the diagram is taken from [27]). In the phase diagram: $\mu_q = \frac{\mu_b}{N_c}$, μ_q is the quark chemical potential and $\bar{M} \propto m_q$ is a mass scale defined as $\bar{M} = 2M_q/\sqrt{\lambda}$ and $\lambda = g_{YM}^2 N_c$.

Shock waves in AdS_5

Shock waves propagating in AdS have the form

$$ds^2 = L^2 \frac{-dudv + dx_\perp^2 + \phi(x_\perp, z)\delta(u)du^2 + dz^2}{z^2}, \quad (3.18)$$

where u and v are light-cone coordinates, and x_\perp are coordinates transversal to the direction of motion of the shock wave and to z -direction. This metric is sourced by the stress-energy momentum tensor T_{MN} with only one non-zero component T_{uu}^{SW}

$$T_{uu}^{SW} = J_{uu}(z, x_\perp)\delta(u) \quad (3.19)$$

and the Einstein E.O.M. reduces to

$$(\square_{H_3} - \frac{3}{L^2})\Phi(z, x_\perp) = -16\pi G_5 \frac{z}{L} J_{uu}(z, x_\perp) \quad (3.20)$$

where

$$\Phi(z, x_\perp) \equiv \frac{L}{z}\phi(z, x_\perp) \quad (3.21)$$

and

$$\square_{H_3} = \frac{z^3}{L^2} \frac{\partial}{\partial z} z^{-1} \frac{\partial}{\partial z} + \frac{z^2}{L^2} \left(\frac{\partial^2}{\partial x_\perp^2} \right) \quad (3.22)$$

Different forms of the shock waves correspond to different forms of the source $J_{uu}(z, x_\perp)$. The most general $O(3)$ invariant shock wave in AdS located at $u = 0$ corresponds to

$$\Phi^{O(3)}(z, x_\perp) = F(q). \quad (3.23)$$

where q is the chordal distance

$$q = \frac{(x_\perp^1)^2 + (x_\perp^2)^2 + (z - z_0)^2}{4zz_0}, \quad (3.24)$$

In this case ρ , related to J_{uu} as

$$\frac{z}{L} J_{uu}(z, x_\perp) \equiv \rho(z, x_\perp), \quad (3.25)$$

has the form

$$\rho^{O(3)}(z, x_\perp) = \rho(q), \quad (3.26)$$

and the Einstein E.O.M takes the form

$$(\square_{H_3} - \frac{3}{L^2})F = -16\pi G_5 \rho(q) \quad (3.27)$$

or explicitly

$$q(q+1)F''_{qq} + (3/2)(1+2q)F'_q - 3F = -16\pi G_5 L^2 \rho(q), \quad (3.28)$$

The shape of point shock wave F^p is given by the solution to (3.20) with

$$J_{uu} = E\delta(u)\delta(z-L)\delta(x^1)\delta(x^2) \quad (3.29)$$

and has the form is given by

$$F^p(z, x_\perp) = \frac{8L^2G_5Ez^3}{(x_\perp^2 + (z-L)^2)^3} \quad (3.30)$$

This point shock wave shape is in fact equal to $F^p(q)$, $\Phi^{point}(z, x_\perp) = F^p(q)$, that is a solution to (3.28) with

$$\rho^p(q) = \frac{E}{L^3} \frac{\delta(q)}{\sqrt{q(1+q)}}. \quad (3.31)$$

It has the form

$$F^p = \frac{2G_5E}{L} \left(\frac{(8q^2 + 8q + 1) - 4(2q + 1)\sqrt{q(1+q)}}{\sqrt{q(1+q)}} \right) \quad (3.32)$$

The shape of the charged point shock wave is a sum of two components

$$F = F^p + F^Q \quad (3.33)$$

where F^p is given by (3.32) and F^Q is the solution to (3.28) with

$$\rho^{pQ} = \frac{5\bar{Q}^2}{32 \cdot 64 L^5 G_5} \frac{1}{[q(q+1)]^{5/2}} = \frac{5Q_n^2}{\pi 24 \cdot 64 L^5} \frac{1}{[q(q+1)]^{5/2}}, \quad (3.34)$$

explicitly

$$F^Q = \frac{5G_5Q_n^2}{48L^3} \frac{144q^2 + 16q - 1 + 128q^4 + 256q^3 - 64(2q+1)q(q+1)\sqrt{q(1+q)}}{q(1+q)\sqrt{q(1+q)}} \quad (3.35)$$

To establish the connection with [22] let us note the relations of notations

$$\bar{M} = \frac{4G_5E}{3\pi} \quad (3.36)$$

$$\bar{Q}^2 = \frac{4G_5Q_n^2}{3\pi} \quad (3.37)$$

and

$$\frac{3\pi\bar{M}}{2a} = \frac{2G_5E}{L} \quad (3.38)$$

$$\frac{5\pi\bar{Q}^2}{64a^3} = \frac{5G_5Q_n^2}{48L^3} \quad (3.39)$$

More complicated shock waves in AdS and dS have been considered in [44–49].

GYP dual conjecture

Gubser, Yarom and Pufu (GYP) [11] have proposed the following dual to QCD holographic picture for colliding nuclei:

- the bulk dual of the boundary nuclei is the shock waves propagating in AdS of the form (3.18);
- the bulk dual of two colliding nuclei in the bulk is the line element for two identical shock waves propagating towards one another in AdS

$$ds^2 = L^2 \frac{-dudv + dx_\perp^2 + \phi_1(x_\perp, z)\delta(u)du^2 + \phi_2(x_\perp, z)\delta(v)dv^2 + dz^2}{z^2}; \quad (3.40)$$

- when the shock waves collide in the bulk, a black hole should form, signifying the formation of a quark-gluon-plasma.

To estimate the BH formation one usually use the TS technic [50, 51].² A trapped surface is a surface whose null normals all propagate inward [53]. There is no rigorous proof that the TS formation in asymptotically AdS spacetime provides the BH formation, however there is an common belief that trapped surfaces must lie behind an event horizon and that a lower bound on entropy S_{AdS} of the black hole is given by area of the TS, $A_{trapped}$,

$$S_{AdS} \geq S_{trapped} \equiv \frac{A_{trapped}}{4G_5} \quad (3.41)$$

²This estimation can be also performed using so-called capture arguments [52, 26].

To make the proposed duality prescription more precise one has to fix the relations between the bulk parameters, G_5, L, E and the phenomenological parameters of QGP. According to [21], one of these relations is

$$\frac{L^3}{G_5} = \frac{16E \cdot T^4}{3\pi^3} = \frac{11 \cdot 16}{3\pi^3} \approx 1.9 \quad (3.42)$$

The arguments supporting (3.42) are following. Lattice calculations in QGP [57] have shown that ET^4 is a slowly varied quantity and

$$ET^4 \approx 11. \quad (3.43)$$

Just to match the black hole equation of state (3.4) with (3.43), Gubser, Yarom and Pufu [11] have assumed (3.42). It is important to note that here is assumed an identification of the total energy of each nucleus with the energy of the corresponding shock wave. One can modify this identification and assume that only a part of energy of the gravitational shock wave is related to the total energy of nucleus.

To fix the dimensionless parameter EL the AdS/CFT dual relation (3.7) between the expectation value of the gauge theory stress tensor and the AdS_5 metric deformation by the shock wave has been used [11],

$$\langle T_{uu} \rangle = \frac{L^2}{4\pi G_5} \lim_{z \rightarrow 0} \frac{1}{z^3} \Phi(z, x_\perp) \delta(u) \quad (3.44)$$

For the point shock wave Φ^{point} given by (3.30), one gets the following stress tensor in the boundary field theory:

$$\langle T_{uu} \rangle = \frac{2L^4 E}{\pi(L^2 + (x^1)^2 + (x^2)^2)^3} \delta(u) \quad (3.45)$$

The r.h.s. of (3.45) depends on the total energy E and L , and L has a meaning of the root-mean-square radius of the transverse energy distribution. It has been assumed [11] that L is equal to the root-mean-square transverse radius of the nucleons, that is in accordance with a Woods-Saxon profile for the nuclear density [54, 55] is of order of few fm. In particular for Au it is equal to $L \approx 4.3$ fm. For Pb it is $L \approx 4.4$ fm.

The RHIC collides Au nuclei, ($A=197$), at $\sqrt{s_{NN}} = 200$ GeV. This means that each nucleus has energy $E = 100$ GeV per nucleon, for a total of about $E = E_{\text{beam}} = 19.7$ TeV for each nucleus.

LHC will collide Pb nuclei, ($A=208$) at $\sqrt{s_{NN}} = 5.5$ TeV, that means $E = E_{\text{beam}} = 570$ TeV.

Estimations of [11] for dimensionless values EL for Au-Au and Pb-Pb collisions are

$$EL|_{Au-Au, \sqrt{s_{NN}}=200 \text{ GeV}} \approx 4.3 \times 10^5, \quad (3.46)$$

$$EL|_{Au-Au, \sqrt{s_{NN}}=5.5 \text{ TeV}} \approx 1.27 \times 10^7, \quad (3.47)$$

Note, that in [18] has been proposed to tune the scale L or z_0 of the bulk colliding object to the size of the nucleus, or to the “saturation scale” Q_s in the “color glass” models.

Calculations in [11] show that in the limit of a very large collision energy E the entropy grows as $E^{2/3}$,

$$S_{\text{trapped}} \approx \pi \left(\frac{L^3}{G_5} \right)^{1/3} (2EL)^{2/3}, \quad (3.48)$$

Considerations of off-center collisions of gravitational shock waves in AdS do not change the scaling $E^{2/3}$. However, a critical impact parameter, beyond which the trapped surface does not exist has been observed [18] (compare with result of [20]). Experimental indications for similar critical impact parameter in real collisions have been noted [18].

The relation of the total multiplicity, S_{QGP} , given by experimental data, and the entropy produced in the gravitational waves collision in AdS_5 , S_{AdS} has some subtleties [21]. Phenomenological considerations [56, 58, 11], estimate the total multiplicity S_{QGP} by the the number of charged particles N_{ch} times the factor ~ 7.5 .

$$S_{QGP} \approx 7.5 N_{\text{charged}}. \quad (3.49)$$

The trapped surface analysis does not give the produced entropy but it provides a lower bound

$$S_{\text{trapped}} \leq S_{AdS}. \quad (3.50)$$

Taking into account that in calculations [11] the energy of the gravitational shock wave is identified with the energy of colliding ions and L with the nucleus size, one can introduce proportionality constants between these quantities to get

$$\mathcal{M} \cdot S_{\text{trapped}} < N_{\text{charged}} \quad (3.51)$$

where all proportionality factors are included into the overall factor \mathcal{M} . One can take \mathcal{M} to fit the experimental data at some point. But the

scaling $S_{\text{trapped}} \propto s_{NN}^{1/3}$ implied by (3.48) differs from the observed scaling, which is closer to the dependence $S \propto s_{NN}^{1/4}$, that predicted by the Landau model [37], see Fig.3.2. It is obvious, that if $E < E_{max}$ one can avoid a conflict between [11] and experiment, but if E can be arbitrary large the conflict takes place.

In figure 3.2 we plot the dependence of the entropy bound (3.48) on the energy, together with the curve that schematically represents the realistic curve that fits experimental data [59]. We can see that by changing the coefficient \mathcal{M} one can avoid the conflict only for energy up to some E_{max} . The overall coefficient of the numerical plot has been chosen in order to

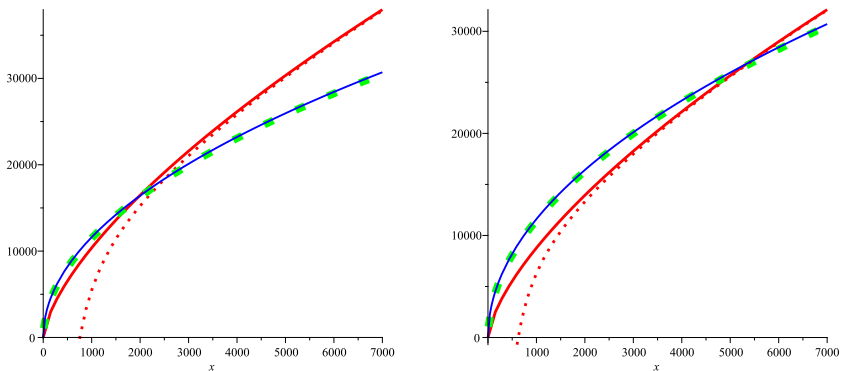


Figure 3.2. (color on-line) Plots of the total number of charged particles vs. energy. The red lines present the estimation (2.45). Plots A and B differ by the overall factor \mathcal{M} . The blue lines correspond to the prediction of the Landau model and the dotted green lines schematically present the curves that fit experimental data. The dashed lines correspond to corrections to the GYP multiplicity via non-zero chemical potential, see Sect.3.

fit the RHIC data [59]. Their are indicated by dots in Fig.3.2.

In the above estimation energy of each shock wave is identified with the energy of colliding beams. As has been noted in [17] one can improve fit to the data by identifying the energy of each shock wave with the fraction of the energy of the nucleus carried by nucleus that participate in the collision. This give an extra parameter to fit data. But still a conflict will arise at large energies. In paper [17] it has been proposed to cure the problem by removing a UV part of AdS bulk. In [25] shock waves corresponding to the BH with non-zero dilaton field [24] were considered and it has been shown that lower bound on N_{charged} scales is rather closer

to $s_{NN}^{1/4}$.

3.2.2 Remarks about the regularization of TS calculations in the case of wall-on-wall collisions

In [18] has been proposed a much simpler dual description of the colliding nuclei that uses a wall-on-wall collision in the bulk. The Einstein equation for the profile of the wall shock wave [18] has the form:

$$(\partial_z^2 - \frac{3}{z}\partial_z)\phi(z) = J_{uu}^{WP}, \quad J_{uu}^{WP} = -16\pi G_5 \frac{E}{L^2} \frac{z_0^3}{L^3} \delta(z - z_0) \quad (3.52)$$

To find a trapped surface that can be formed in the collision of two wall shock waves one needs to find a solution to the Einstein eq.(3.52) that satisfies two conditions. It is convenient to write these conditions in terms of function $\psi(z)$ related to ϕ via

$$\phi(z) = \frac{z}{L}\psi. \quad (3.53)$$

They have the form

$$\psi(z_a) = \psi(z_b) = 0, \quad (3.54)$$

$$\psi'(z_a)\frac{z_a}{L} = 2, \quad \psi'(z_b)\frac{z_b}{L} = -2 \quad (3.55)$$

where z_a, z_b are supposed to be the boundaries of the trapped surface [18]. But as we will see in the moment, strictly speaking, one cannot call the solution to the equation (3.52) with b.c. (3.54) and (3.55) the trapped surface, since by definition this surface supposed to be smooth and compact meanwhile the solution [18] is *non-smooth* and *noncompact*.

By this reason we call the solution found in [18] a quasi-trapped surface. Let us remind the construction presented in [18].

In [60], the solution to the Einstein equation (3.52) is written in such a way that the property (3.54) is satisfied automatically. This solution has the form

$$\psi(z) = \psi_a(z)\Theta(z_0 - z) + \psi_b(z)\Theta(z - z_0) \quad (3.56)$$

$$\psi_a(z) = -\frac{4G\pi E \left(\frac{z_0^4}{z_b^4} - 1\right) z_b^4 z_a^3 \left(\frac{z^3}{z_a^3} - \frac{z_a}{z}\right)}{L^4 (z_b^4 - z_a^4)}$$

$$\psi_b(z) = -\frac{4G\pi E \left(\frac{z_0^4}{z_a^4} - 1 \right) z_a^4 z_b^3 \left(\frac{z^3}{z_b^3} - \frac{z_b}{z} \right)}{L^4 (z_b^4 - z_a^4)}$$

Let us first note that solution (3.56) is not smooth. There is a non-smooth part of the solution (3.56)

$$\Xi = \frac{\mathcal{K}}{z} \left(-\frac{z_b}{z_a^3} (Y_1) - \frac{z_a}{z_b^3} (Y_2) \right), \quad \text{where} \quad (3.57)$$

$$Y_1 = z^4 \Theta(z_0 - z) + z_0^4 \Theta(z - z_0) \quad (3.58)$$

$$Y_2 = z_0^4 \Theta(z_0 - z) + z^4 \Theta(z - z_0) \quad (3.59)$$

where

$$\mathcal{K} = \frac{4G\pi E}{L^4} \frac{z_a^3 z_b^3}{z_b^4 - z_a^4} \quad (3.60)$$

Thus, in order to smooth the solution we have to smooth the function Ξ . We can do it by performing the regularization of the Heaviside step function

$$\Theta(z_0 - z) \approx \Gamma_1 = \frac{\arctan(R(z_0 - z))^3}{\pi} + \frac{1}{2} \quad (3.61)$$

$$\Theta(z - z_0) \approx \Gamma_2 = \frac{\arctan(R(z - z_0))^3}{\pi} + \frac{1}{2} : \quad (3.62)$$

and considering the regularized functions \tilde{Y}_1 and \tilde{Y}_2

$$\tilde{Y}_1 = z^4 \left(\frac{\arctan(R(z_0 - z))^3}{\pi} + \frac{1}{2} \right) + z_0^4 \left(\frac{\arctan(R(z - z_0))^3}{\pi} + \frac{1}{2} \right)$$

$$\tilde{Y}_2 = z_0^4 \left(\frac{\arctan(R(z_0 - z))^3}{\pi} + \frac{1}{2} \right) + z^4 \left(\frac{\arctan(R(z - z_0))^3}{\pi} + \frac{1}{2} \right)$$

For derivatives we have

$$\frac{dY_1}{dz} \approx 4z^3 \Theta(z_0 - z), \quad \frac{d\tilde{Y}_1}{dz} \approx \frac{4z^3 (\arctan(R(z_0 - z))^3 + \pi)}{\pi} \quad (3.63)$$

$$\frac{dY_2}{dz} \approx 4z^3 \Theta(z - z_0), \quad \frac{d\tilde{Y}_2}{dz} \approx \frac{4z^3 (\arctan(R(z - z_0))^3 + \pi)}{\pi} \quad (3.64)$$

In Fig.3.3 we present the derivatives of functions Y_1 , Y_2 as well as derivatives of the smoothed functions \tilde{Y}_1 , \tilde{Y}_2 .

For $R = 10^4$ (see below) the differences between derivatives $\frac{d\tilde{Y}_i}{dz}$ and their approximations given by (3.63) and (3.64)

$$\begin{aligned}\Delta_1(z) &= \frac{d\tilde{Y}_1}{dz} - \left(\frac{d\tilde{Y}_1}{dz}\right)_{appr}, & \Delta_2(z) &= \frac{d\tilde{Y}_2}{dz} - \left(\frac{d\tilde{Y}_2}{dz}\right)_{appr} & (3.65) \\ \Delta_1(z) &= -\Delta_2(z) = -3 \frac{z^4 R^3 (z_0 - z)^2}{(1 + R^6 (z_0 - z)^6) \pi} + 3 \frac{z_0^4 R^3 (z - z_0)^2}{(1 + R^6 (z - z_0)^6) \pi}\end{aligned}$$

are of order $\gtrsim 10^{-3} \text{ fm}^3$ only in the interval $z \in [z'_0, z''_0]$, $z'_0 = 4.293 \text{ fm}$, $z''_0 = 4.307 \text{ fm}$.

Indeed, in our consideration (spread case) the largest value of z_a is 4.260706906 fm and the smallest value of z_b is 4.340400579 fm. At the points $z'_0 = 4.260706906 \text{ fm}$, $z''_0 = 4.340400579 \text{ fm}$ the quantity Δ_1 is less then $\leq 5 \cdot 10^{-6} \text{ fm}^3$.

At the points $z'_0 = 0.6948439783 \text{ fm}$, $z''_0 = 1018.393720 \text{ fm}$ the quantity Δ_1 is less then $\leq 2 \cdot 10^{-12} \text{ fm}^3$.

The schematic picture of locations of roots and a region there $|\Delta_i(z)| \gtrsim 10^{-3}$ are presented in Fig.3.4. We see that the difference Δ_i is not essential in location of the roots and we can use the approximations (3.63) and (3.64).

The regularized version of the the function ψ is

$$\psi_{reg} = \psi_a(z)\Gamma_1 + \psi_b(z)\Gamma_2. \quad (3.66)$$

Now one has to put conditions (3.55) on the regularized functions

$$\frac{z_a}{2L} \frac{d}{dz} \psi_{reg} \Big|_{z=\tilde{z}_a} = 1 \quad (3.67)$$

$$\frac{z_b}{2L} \frac{d}{dz} \psi_{reg} \Big|_{z=\tilde{z}_b} = -1 \quad (3.68)$$

and find \tilde{z}_a and \tilde{z}_b from these conditions. However it is difficult to perform these calculations. Instead of finding \tilde{z}_a from condition (3.109) we propose to use such regularization that does not change z_a found from formal conditions (3.55). We can check that the formal z_a in fact solves also the regularized condition if the regularization is smooth enough. So, we take z_a and substitute it in the LHS of regularized condition (3.109). We define

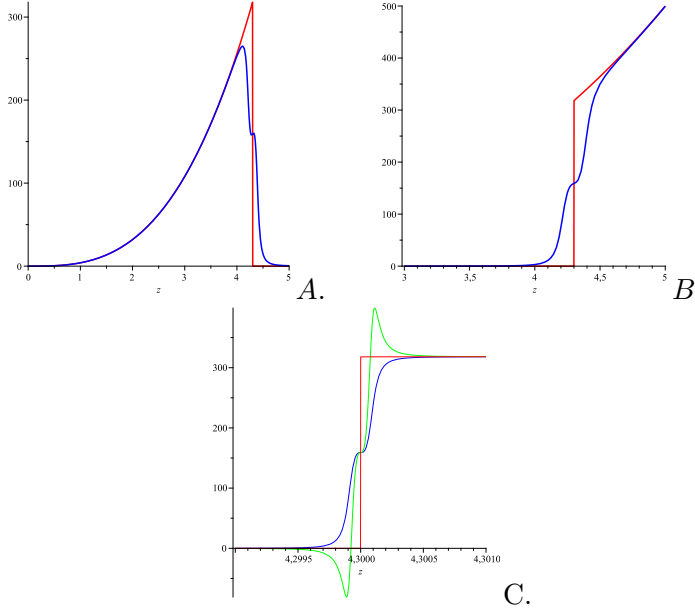


Figure 3.3. A. The functions $\frac{dY_1}{dz}$ (red line), $\frac{d\tilde{Y}_1}{dz} \Big|_{appr}$ (blue line) . B. The functions $\frac{dY_2}{dz}$ (red line), $\frac{d\tilde{Y}_2}{dz} \Big|_{appr}$ (blue line). The regularization parameter $R = 10$ at A and B cases. C. Functions $\frac{dY_2}{dz}$ (red line), $\frac{d\tilde{Y}_2}{dz} \Big|_{appr}$ (blue line) and $\frac{d\tilde{Y}_2}{dz}$ (green line) at the regularization parameter $R = 10^4$.

$$F_{a,reg} \Big|_{z=z_a} = \frac{z_a}{2L} \left(\frac{d\psi_a}{dz} \Gamma_1 + \frac{d\psi_b}{dz} \Gamma_2 \right) \Big|_{z=z_a} = 1 + \delta_1,$$

$$F_{b,reg} \Big|_{z=z_b} = \frac{z_b}{2L} \left(\frac{d\psi_a}{dz} \Gamma_1 + \frac{d\psi_b}{dz} \Gamma_2 \right) \Big|_{z=z_b} = -1 + \delta_2.$$

We can calculate $F_{a,reg}$. The deviation of $F_{a,reg}$ from 1 will show how the regularization changes conditions (3.55). In the following table we present calculations of $F_{a,reg}$ for the wide range of parameter of the theory.

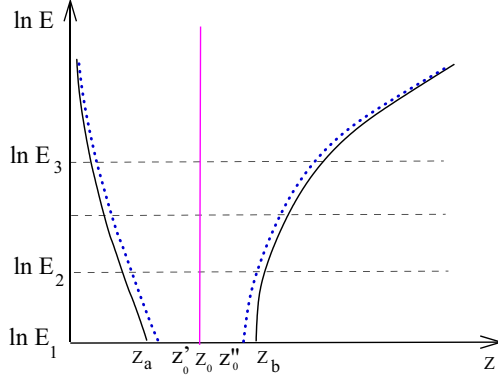


Figure 3.4. (color on-line) The schematic plots of locations of roots (solid black lines) dependent on the energy (in the logarithmic scale) and the location of differences $|\frac{d\tilde{Y}_i}{dz} - (\frac{d\tilde{Y}_i}{dz})_{appr}| \gtrsim 10^{-3}$, $i = 1, 2$ (the magenta shaded region). The magenta solid line shows the location of the wall. The dotted blue lines show location of zeros for the charged wall.

We choose the parameter R as minimally needed to make δ_1 and δ_2 negligible at energies $10^{-4} < E < 10^2$ TeV. Using the direct numerical calculations we choose $R = 10^4$. We perform numerical calculations at $R = 10^4$ and get the following table:

E, TeV	$Q, fm^{1/2}$	z_a, fm	$z_b, fm,$	F_a	F_b
118.2	0	0.044	$4.015 \cdot 10^6$	1.00000	-1.00000
30	0	0.069	$1.019 \cdot 10^6$	1.00000	-1.00000
0.03	0	0.695	1018.394	1.00000	-1.00000
0.00025	0	4.261	4.3404	0.99999	-0.99999

Thus, from the table evidently $F_a \approx 1$, $F_b \approx -1$.

As has been mentioned above, strictly speaking one may not consider infinite surface as a trapped surface of any kind. Nevertheless it is possible

to assume that transversal size of colliding objects is finite but very large, and therefore boundary conditions do not affect the process of gravitational interactions of inner parts of sources. If we are interested only in the specific area of the formed trapped surface in respect to the unit of shock wave area, we may define it as

$$\mathcal{A} \approx \lim_{L \rightarrow \infty} \frac{A_{trap}(L)}{A_{source}(L)}, \quad (3.69)$$

and the approximate equality takes place due to negligibility of boundary effects. As often happens, we can get answers for finite physical systems performing calculations for infinite non-physical objects.

3.3 Holographic QGP phase diagram for the central heavy-ions collisions

In this section we construct the phase diagram for TS formed in the central collision of two identical point-like charged shock waves [22].

The profile of point-like charged shock waves in AdS is given by (3.33) with (3.32) and (3.35). Existence of the trapped surface in the central collision of two point-like charged shock waves means the existence of a real solution, q_0 , to the following equation (see [22] for details)

$$F'(q_0) - \frac{2}{1+2q_0} F(q_0) + \frac{2L}{\sqrt{q_0(1+q_0)}} = 0 \quad (3.70)$$

The left hand side of (3.70) can be written as

$$\mathcal{F}(L, E, \bar{Q}^2, q) = \frac{\mathcal{N}(L, \bar{M}, \bar{Q}^2, q)}{\mathcal{D}(a, q)}. \quad (3.71)$$

The numerator $\mathcal{N}(L, E, \bar{Q}^2, q)$ contains just one term with dependence on \bar{Q}^2 . This dependence is linear with a positive coefficient

$$\mathcal{N}(a, \bar{M}, \bar{Q}^2, q) = \mathcal{N}(a, \bar{M}, q) + 15 \frac{\pi}{a} \bar{Q}^2. \quad (3.72)$$

The denominator in (3.71) does not take infinite values. To find solutions to (3.70) for the shape function given by (3.33) we can draw the function

$$\begin{aligned} - \mathcal{N}(a, \bar{M}, q) &\equiv -(512a^3q^5 + 1280a^3q^4 - \\ &- 96\bar{M}\pi aq^2 + 1024a^3q^3 - 96\bar{M}\pi aq + 256a^3q^2), \end{aligned} \quad (3.73)$$

and see where this function can be equal to a given value $15\bar{Q}^2\frac{\pi}{a}$.

In order to find the maximal allowed \bar{Q}^2 at which solution to (3.70) still exists we find the maximum of function \mathcal{N} for fixed energy,

$$\left. \frac{d\mathcal{N}(a, \bar{M}, q)}{dq} \right|_{q=q_{max}} = 0 \quad (3.74)$$

and the value

$$\frac{a}{15\pi} \mathcal{N}(a, \bar{M}, q)|_{q=q_{max}}$$

defines \bar{Q}_{max}^2 .

Let us remind that we are working in physical units and we use the following notations (3.37) and (3.36): $\bar{M} = \frac{4G_5 E}{3\pi}$ and $\bar{Q}^2 = \frac{4G_5 Q_n^2}{3\pi}$.

Results of calculations are presented in Fig. 3.5.

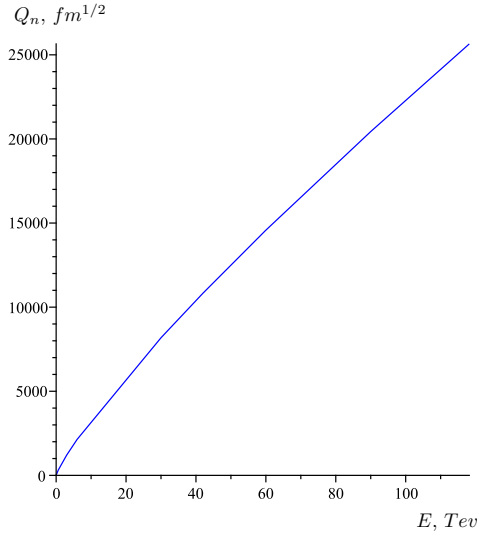


Figure 3.5. The allowed zone for the trapped surface formation is under the line on the diagram. The plot has been constructed by using formulas from [22].

To estimate corrections to GYP multiplicity due to non-zero chemical potential, we use formula (3.17) from [22]. In notations admitted in this paper, (3.32) and (3.35), the formula has the form

$$A_{AdS_5} \approx 4\pi L^3 \left(\frac{G_5 E}{L^2} \right)^{\frac{2}{3}} \left(1 - \frac{1}{24} \left(1 + \frac{5Q_n^2}{EL^2} \right) \left(\frac{2\sqrt{2}L^2}{G_5 E} \right)^{\frac{3}{2}} \right) \quad (3.75)$$

In Fig.3.6 we show the entropy, A_{AdS_5} , for $Q_n = 0$ and $Q_n \neq 0$. The blue line represents $Q_n = 0$. The red line represents $Q_n = 2 \cdot 10^6$. We see that the deviation from the GYP multiplicity is essential for small energies and is almost neglectful for large energies.

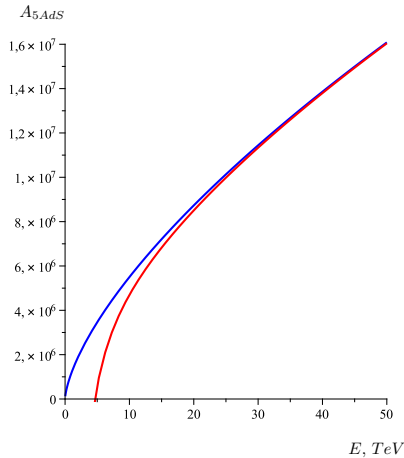


Figure 3.6. The function A_{AdS_5} , at $Q_n = 0$, (blue line) and $Q_n = 2 \cdot 10^6 fm^{1/2}$ (red line).

3.4 Holographic QGP phase diagram in the wall-wall dual model of heavy-ions collisions

3.4.1 Charged wall as a dual model for a heavy-ion

Let us note that the form of the J_{uu}^{WP} in (3.52) can be obtained by spreading out the energy-momentum tensor of an ultrarelativistic point, i.e J_{uu} in the form (3.25) with $\rho(q)$ given by eq.(3.31), over the transversal surface.

The Einstein equation for the charged wall (membrane) has the form

$$(\partial_z^2 - \frac{3}{z}\partial_z)\phi(z) = -16\pi G_5 \left(J_{uu}^{WP} + J_{uu}^{WQ}(Q, z) \right). \quad (3.76)$$

where J_{uu}^{WP} is given by (3.52) and we suppose that $J_{uu}^{WQ}(Q, z)$ can be obtained in the similar way by spreading the energy-momentum tensor of the ultrarelativistic charged point T_{uu}^{pQ} over the transversal surface. In the previous calculations:

$$J_{uu}^{WQ} = \frac{\int_{\mathcal{M}} J_{uu}^{pQ} \mathcal{D}x_{\perp}}{\int_{\mathcal{M}} \mathcal{D}x_{\perp}} \quad (3.77)$$

here the subscript "pQ" means the electromagnetic part of the energy momentum tensor of the charged point particle and " $\mathcal{D}x_{\perp}$ " means that we integrate over the induced metrics on the orthogonal surface \mathcal{M} .

For this purpose we take

$$J_{uu}^{pQ}(z, z_0) = \frac{L}{z} \rho^{pQ} \quad (3.78)$$

where ρ^{pQ} is given by (3.34), and according to our prescription (3.77) we integrate over all transversal coordinates

$$J_{uu}^{pQ,II} = \frac{\frac{L}{z} \int_0^{\infty} \rho^{pQ}(q) \frac{L^2}{z_0^2} \frac{1}{2} dr^2}{\int_0^{\infty} \frac{L^2}{z_0^2} r dr} \quad (3.79)$$

The result is

$$J_{uu}^{pQ} = \mathcal{X} \mathcal{J} \quad (3.80)$$

where

$$\mathcal{J} = \frac{64}{3} z z_0 \left(1 - \frac{z_0^6 - 3 z^2 z_0^4 - 3 z^4 z_0^2 + z^6}{|z_0^2 - z^2|^3} \right) \quad (3.81)$$

$$\mathcal{X} = \frac{5}{256} \frac{Q_n^2}{\pi L^6} = \frac{5}{256} \frac{Q^2}{L^6} \quad (3.82)$$

We see divergency at $z = z_0$, as it should be for the energy-momentum tensor of a charged plane. We introduce regularization by adding the ϵ factor in the denominator.

3.4.2 Charged wall-on-wall collision as a dual model for heavy-ions collisions

To find the TS formation condition in the wall-wall collision one has to solve Einstein equation

$$(\partial_z^2 - \frac{3}{z}\partial_z)\phi(z) = -16\pi G_5 \left(J_{uu}^{pW}(z) + J_{uu}^{QW}(Q, z) \right), \quad (3.83)$$

$$J_{uu}^{pW}(z) = \frac{E}{L^2} \frac{z_0^3}{L^3} \delta(z - z_0), \quad (3.84)$$

$$J_{uu}^{QW}(Q, z) = \frac{128\mathcal{X}}{3} z z_0 \frac{z^4 (-z^2 + 3z_0^2) \theta(z_0 - z) + z_0^4 (-3z^2 + z_0^2) \theta(z - z_0)}{(-z^2 + z_0^2 + \epsilon^2)^3} \quad (3.85)$$

with the following boundary conditions

$$1) \quad \phi(z_a) = \phi(z_b) = 0, \phi_a(z_0) = \phi_b(z_0) \quad (3.86)$$

$$2) \quad \left(\psi'(z_a) \frac{z_a}{L} \right) = 2, \quad \left(\psi'(z_b) \frac{z_b}{L} \right) = -2, \quad (3.87)$$

where z_a and z_b are the boundaries of the TS and ψ is related to

$$\phi(z) = \frac{z}{L} \psi. \quad (3.88)$$

We search for a solution to the Einstein equation with a charged source in the form of the sum of the "neutral" solution and a correction proportional to Q^2

$$\phi = \phi_n + \phi_q \quad (3.89)$$

here ϕ_n denotes the solution of the neutral case.

As in the neutral case it is convenient to consider domains $z < z_0$, $z > z_0$ separately

$$\phi_q = \begin{cases} \phi_{qz_0 > z}, & z_0 > z; \\ \phi_{qz > z_0}, & z > z_0 \end{cases} \quad (3.90)$$

and we have

$$(\partial_z^2 - \frac{3}{z}\partial_z)\phi_q = -16\pi G_5 \mathcal{X} \frac{128}{3} z z_0 \frac{z^4 (-z^2 + 3z_0^2)}{(-z^2 + z_0^2 + \epsilon^2)^3}, \quad z_0 > z \quad (3.91)$$

$$(\partial_z^2 - \frac{3}{z}\partial_z)\phi_q = -16\pi G_5 \mathcal{X} \frac{128}{3} z z_0 \frac{z_0^4 (-3z^2 + z_0^2)}{(-z^2 + z_0^2 - \epsilon^2)^3}, \quad z > z_0 \quad (3.92)$$

Solutions to (3.91) and (3.92) can be presented as :

$$\psi_{qz_0 > z} = z^3 C_1 + \frac{C_2}{z} - \frac{NLz_0 z^3}{4(-z^2 + z_0^2 + \epsilon^2)}, \quad z_0 > z, \quad (3.93)$$

$$\psi_{qz > z_0} = \frac{C_3}{z} + z^3 C_4 + \frac{NLz_0^5}{4z(-z^2 + z_0^2 + \epsilon^2)}, \quad z > z_0 \quad (3.94)$$

Here $N = \frac{40}{3} \frac{\pi G_5 Q^2}{L^6}$. The first two terms in (3.93) and (3.94) are solution to the Lin and Shuryak equation (55) in [18]. If one assumes that they satisfy condition **1**, i.e. $\psi_n(z_a) = \psi_n(z_b) = 0$, $\psi_{na}(z_0) = \psi_{nb}(z_0)$, one gets [60]:

$$\Psi_n = \begin{cases} \psi_{na} = C \left(\frac{z^3}{z_a^3} - \frac{z_a}{z} \right), \quad C = -\frac{4\pi G_5 E \left(\frac{z_0^4}{z_b^4} - 1 \right) z_b}{L^4 \frac{z_b^4 - z_a^4}{z_a^3 z_b^3}}, \quad z < z_0 \\ \psi_{nb} = D \left(\frac{z^3}{z_b^3} - \frac{z_b}{z} \right), \quad D = -\frac{4\pi G_5 E \left(\frac{z_0^4}{z_a^4} - 1 \right) z_a}{L^4 \frac{z_b^4 - z_a^4}{z_a^3 z_b^3}}, \quad z_0 < z \end{cases} \quad (3.95)$$

In the neutral case one find z_a and z_b from the 2-nd condition $\left(\psi'_{na}(z_a) \frac{z_a}{L} \right) = 2$, $\left(\psi'_{nb}(z_b) \frac{z_b}{L} \right) = -2$, here z_a and z_b are the boundaries of the TS.

As to (3.93) and (3.94), choosing

$$C_1 = \frac{NLz_0}{4(z_a^2 - z_0^2)}, \quad C_2 = 0, \quad (3.96)$$

$$C_3 = \frac{NLz_0^5}{4(z_b^2 - z_0^2)}, \quad C_4 = 0, \quad (3.97)$$

we obtain

$$\begin{cases} \psi_{aq} = -\frac{NLz_0 z^3}{4} \frac{-z_a^2 + z^2 - \epsilon^2}{(-z^2 + z_0^2 + \epsilon^2)(-z_a^2 + z_0^2)}, \quad z < z_0 \\ \psi_{bq} = \frac{NLz_0^5}{4z} \frac{-z_b^2 + z^2 + \epsilon^2}{(-z^2 + z_0^2 - \epsilon^2)(-z_b^2 + z_0^2)}, \quad z_0 < z \end{cases} \quad (3.98)$$

Note that for the constructed solution the condition $\psi(z_a) = \psi(z_b) = 0$ is satisfied automatically.

The second requirement (3.87) gives

$$-\frac{8\pi G_5 E (z_0^4 - z_b^4) z_a^3}{L^5 (z_b^4 - z_a^4)} - \frac{N}{4} \frac{z_0 z_a^5}{(-z_a^2 + z_0^2)^2} = 1, \quad (3.99)$$

$$-\frac{8\pi G_5 E (z_0^4 - z_a^4) z_b^3}{L^5 (z_b^4 - z_a^4)} + \frac{N}{4} \frac{z_0^5 z_b}{(-z_b^2 + z_0^2)^2} = -1; \quad (3.100)$$

These equations do not have analytical solutions and we treat them numerically.

Roots of system (3.99),(3.100) could not be found analytically since these equations are equivalent to polynomial equations on z_a and z_b of a high degree (> 4). So we take $z_0 = L$ and analyze the following system numerically

$$F_a \equiv -\frac{8\pi G_5 E (z_0^4 - z_b^4) z_a^3}{z_0^5 (z_b^4 - z_a^4)} - \frac{10}{3} \frac{\pi G_5 Q^2}{z_0^6} \frac{z_0 z_a^5}{(-z_a^2 + z_0^2)^2} = 1, \quad (3.101)$$

$$F_b \equiv -\frac{8\pi G_5 E (z_0^4 - z_a^4) z_b^3}{z_0^5 (z_b^4 - z_a^4)} + \frac{10}{3} \frac{\pi G_5 Q^2}{z_0^6} \frac{z_0^5 z_b}{(-z_b^2 + z_0^2)^2} = -1 \quad (3.102)$$

To show the movement of roots of equations (3.101) and (3.102) we suppose that z_b for given Q is already known and represent function $F_a(z_a, z_b)$ as function of z_a in Fig. 3.7. In the similar way, supposing that z_a is already known we represent function $F_b(z_a, z_b)$ as function of z_b in Fig. 3.8.

In Fig.3.9 we show the charge flows of the roots. Different lines correspond to different energies. We see that the flows go to z_0 and reach the line $z = z_0$ for $Q = Q_{cr}$. In Fig.3.10 we draw the corresponding flow for physical parameters.

3.4.3 Comparison of the results

It is interesting to compare the phase diagrams, the energy (temperature) E vs the charge (chemical potential) Q , corresponding to the pointlike charge and the spread charge. Results of these calculations are collected in the table below and presented in Fig.3.11. We see that this two phase diagrams are qualitatively the same.

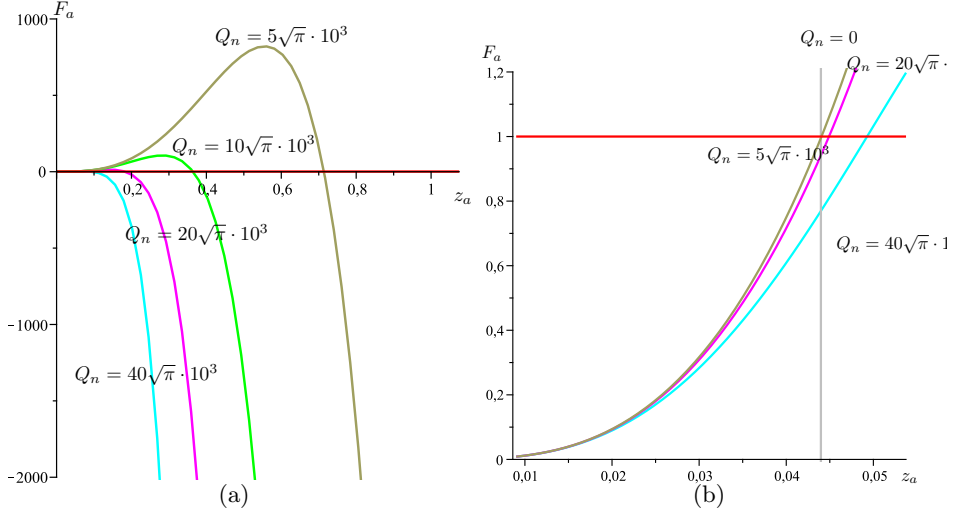


Figure 3.7. (a) The plot of $F_a(z_a, z_b)$ as a function of z_a for fixed z_b near the root $z_a = z_a(E)$ at $E = 118.2$ TeV. (b) Zooming in the region of small F_a and small z_a .

E (TeV)	118.2	60	30	6	3
$Q_{cr, point}$	25649.6	14577.2	8180.6	2138.7	1199.9
$Q_{cr, wall}$	47500	27000	15170	3950	2220
E (TeV)	0.6	0.06	0.03	0.0003	0.00025
$Q_{cr, point}$	313.3	45.6	25.4	0.43	0.37
$Q_{cr, wall}$	570	80	40	0.15	0

From Fig. 3.11 it is evident that the two lines, the red and the blue ones, have a cross point. We represent the cross point in natural and logarithmic scales in Fig. 3.12.

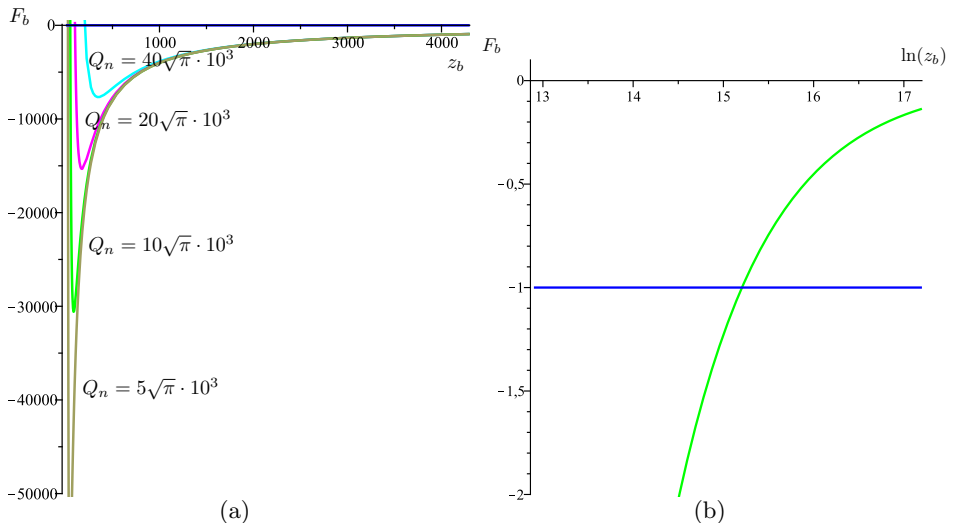


Figure 3.8. (a) The plot of $F_b(z_a, z_b)$ as a function of z_b for fixed z_a near the root $z_b(E)$ at $E = 118.2$ TeV. (b) Zooming in the region of small negative F_b and presenting z_b in the logarithmic scale.

3.4.4 The square trapped surface calculation

Following [18] we calculate entropy lower bound as “the area of the trapped surface” per an unite square of the wall³ using the formula:

$$S = \frac{2A}{4G_5} = \frac{\int \sqrt{g} dz d^2 x_{\perp}}{2G_5}, \quad (3.103)$$

$$s \equiv \frac{S}{\int d^2 x_{\perp}} = \frac{L^3}{4G_5} \left(\frac{1}{z_a^2} - \frac{1}{z_b^2} \right). \quad (3.104)$$

In the absence of transverse dependence one ignores x_{\perp}^2 in (3.103). (3.104) measures entropy per transverse area.

The trapped surface decreases with growth of a charge. The corresponding graphical representations are in Fig. 3.13.

In Fig.3.14 we show the entropy per volume given by (3.104) as function of energy for different Q . This plot is similar to the plot presented

³We put “area” and “trapped surface” in quotation marks since in the strict notions of the trapped surface it has to be smooth and compact. In our case it is not smooth and it does not have finite area, one can only assume this properties after regularization

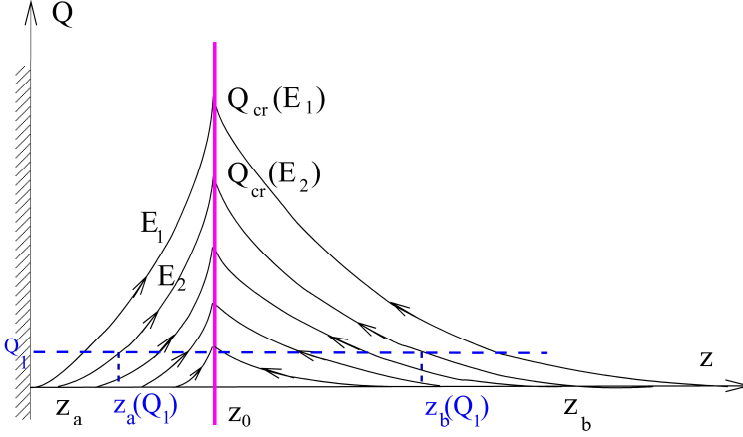


Figure 3.9. The schematic picture of charge flows. The magenta solid line shows the position of the wall. We see that the positions of points $z_a(Q)$ and $z_b(Q)$ move to the point $z = z_0$ when we increase Q . For $Q \rightarrow Q_{cr}(E)$ the segment $[z_a(Q), z_b(Q)]$ shrinks to zero.

in Fig. 3.6. We see that the influence of the chemical potential on the multiplicity is essential for small energies and is almost neglectful for large energies.

3.4.5 Remarks about the regularization

The regularized version of the the function ψ is

$$\psi_{reg} = \psi_a(z)\Gamma_1 + \psi_b(z)\Gamma_2 \quad (3.105)$$

where $\psi_a(z)$ and $\psi_b(z)$ define the function ψ without regularization,

$$\psi = \psi_a(z)\Theta(z_0 - z) + \psi_b(z)\Theta(z - z_0) \quad (3.106)$$

$$\psi_a(z) = -\frac{4G\pi E \left(\frac{z_0^4}{z_b^4} - 1 \right) z_b^4 z_a^3 \left(\frac{z^3}{z_a^3} - \frac{z_a}{z} \right)}{L^4 (z_b^4 - z_a^4)} - \frac{10}{3} \frac{Q^2 G\pi z_0 z^3 (-z_a^2 + z^2)}{L^5 (-z^2 + z_0^2) (-z_a^2 + z_0^2)}$$

$$\psi_b(z) = -\frac{4G\pi E \left(\frac{z_0^4}{z_a^4} - 1 \right) z_a^4 z_b^3 \left(\frac{z^3}{z_b^3} - \frac{z_b}{z} \right)}{L^4 (z_b^4 - z_a^4)} + \frac{10}{3} \frac{Q^2 G\pi z_0^5 (-z_b^2 + z^2)}{L^5 z (-z^2 + z_0^2) (-z_b^2 + z_0^2)}$$

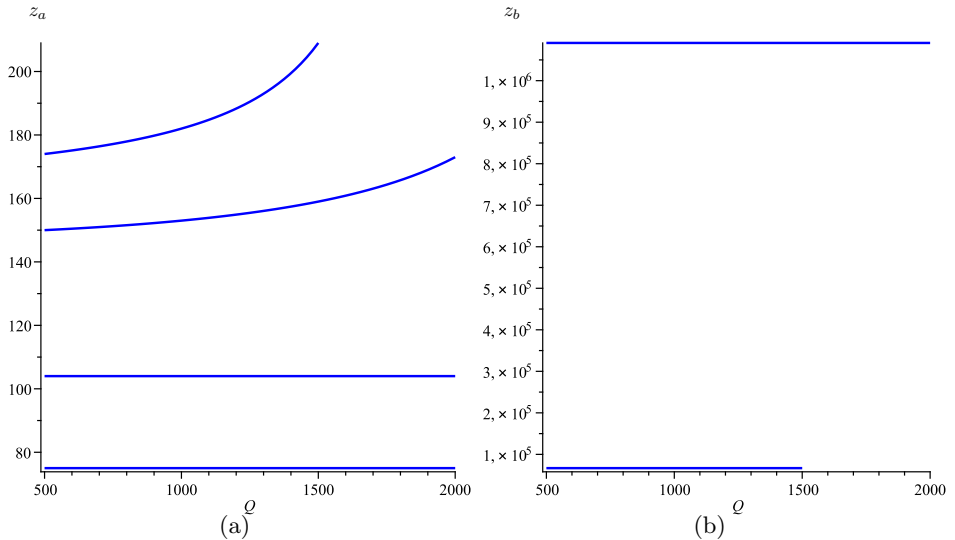


Figure 3.10. (a) The charge flows of the root $z_a(Q)$ for $E = 1.97$ TeV, 3 TeV, 9 TeV, and 24 TeV. (b) The charge flows of the roots $z_b(Q)$ for $E = 1.97$ TeV, 3 TeV.

and

$$\Gamma_1 = \frac{\arctan(R(z_0 - z))^3}{\pi} + \frac{1}{2} \quad (3.107)$$

$$\Gamma_2 = \frac{\arctan(R(z - z_0))^3}{\pi} + \frac{1}{2} \quad (3.108)$$

Now one has to put conditions (3.55) on the regularized functions

$$\frac{z_a}{2L} \frac{d}{dz} \psi_{reg} \Big|_{z=\tilde{z}_a} = 1 \quad (3.109)$$

However it is difficult to find \tilde{z}_a from the condition (3.109). Instead of finding \tilde{z}_a from the condition (3.109) we propose to use such regularization that does not change z_a found from the formal conditions (3.55). We can check that the formal z_a in fact solves also the regularized condition if the regularization is smooth enough. So, we take z_a and substitute it in the LHS of the regularized condition (3.109). We define

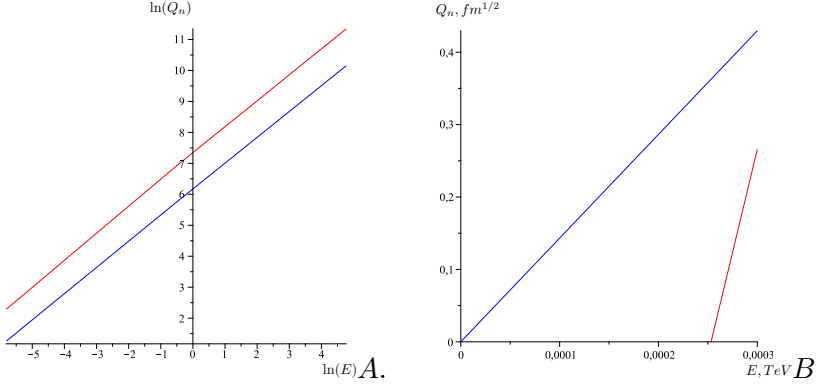


Figure 3.11. A. The phase diagram the logarithm of Q_n vs the logarithm of E at large E . B. The phase diagram E vs Q_n for small E and small Q_n . The blue lines correspond to the pointlike charge and the red lines to the spread charge. The zones above the lines are forbidden for black holes production for corresponding E and Q .

$$F_{a,reg} \Big|_{z=z_a} = \frac{z_a}{2L} \left(\frac{d\psi_a}{dz} \Gamma_1 + \frac{d\psi_b}{dz} \Gamma_2 \right) \Big|_{z=z_a} \approx 1,$$

$$F_{b,reg} \Big|_{z=z_b} = \frac{z_b}{2L} \left(\frac{d\psi_a}{dz} \Gamma_1 + \frac{d\psi_b}{dz} \Gamma_2 \right) \Big|_{z=z_b} \approx -1.$$

We can calculate $F_{a,reg}$ and $F_{b,reg}$. In the following table we present calculations of $F_{a,reg}$ and $F_{b,reg}$ for the wide range of parameter of the theory. Results of calculations at $R = 10^4$ are presented in the following table:

E, TeV	$Q = Q_n/\sqrt{\pi}, fm^{1/2}$	z_a, fm	$z_b, fm,$	F_a	F_b
118.2	40000	0.049	$4.015 \cdot 10^6$	0.99997	-1.00000
3	15000	0.088	$1.019 \cdot 10^6$	1.00000	-1.00000
0.03	40	0.786	1017.792	1.00000	-1.00000

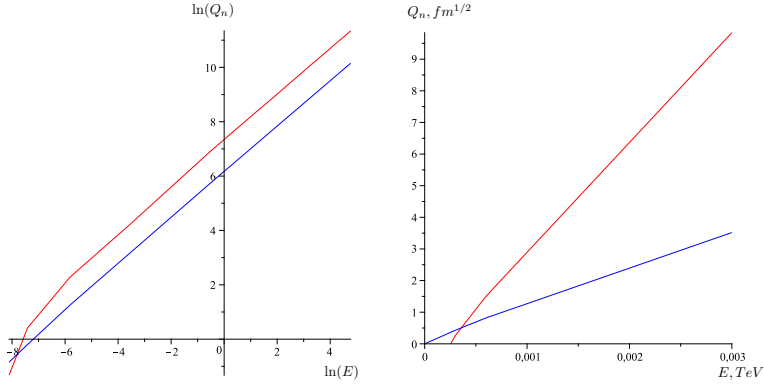


Figure 3.12. The cross point of two diagrams in logarithmic and natural scales.

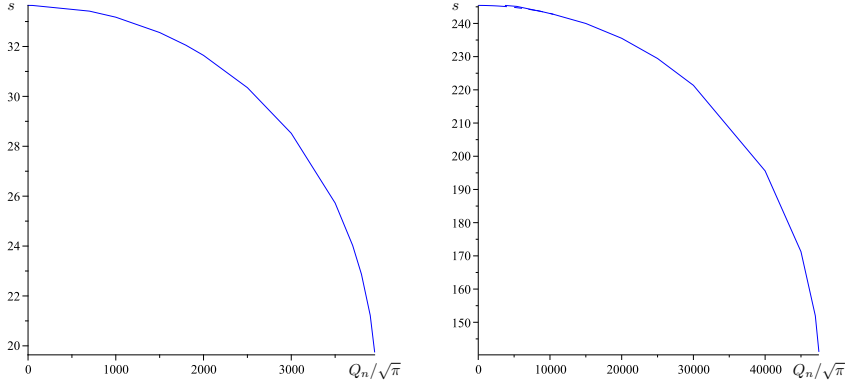


Figure 3.13. The dynamics of the trapped surface area $s(Q_n/\sqrt{\pi})$ at $E = 6 TeV$, $E = 118.2 TeV$.

Thus, from the table it is evident that $F_a \approx 1$, $F_b \approx -1$.

3.5 Conclusion

3.5.1 Summary

In this chapter we have constructed the phase diagram of the quark gluon plasma (QGP) formed at a very early stage just after the heavy ion collision. In this construction we have used a holographic dual model for the heavy ion collision. In this dual model colliding ions are described by the charged shock gravitational waves. Points on the phase diagram

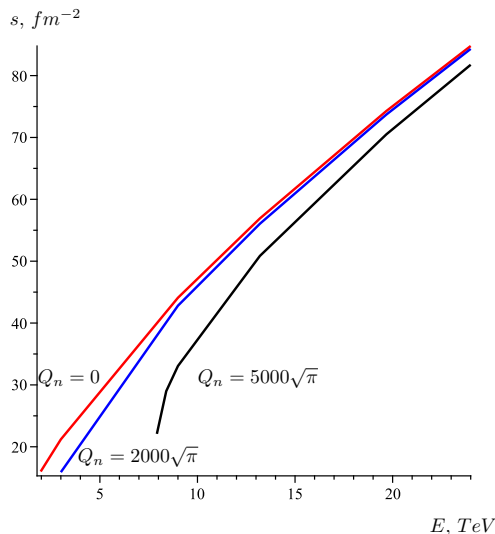


Figure 3.14. The red line corresponds to the case $Q_n = 0 \text{ fm}^{1/2}$, the blue to the case $Q_n = 2000\sqrt{\pi} \text{ fm}^{1/2}$, the black to the case $Q_n = 5000\sqrt{\pi} \text{ fm}^{1/2}$.

correspond to the QGP or hadronic matter with given temperatures and chemical potentials. The phase of QGP in dual terms is related to the case when the collision of shock waves leads to formation of trapped surface. Hadronic matter and other confined states correspond to the absence of trapped surface after collision.

Multiplicity of the ion collision process has been estimated in the dual language as an area of the trapped surface. We have shown that a non-zero chemical potential reduces the multiplicity. To plot the phase diagram we use two different dual models of colliding ions. The first model uses the point shock waves and the second the wall shock waves. We have found qualitative agreement of the results.

A special attention has been devoted to a regularization procedure for calculations performed for wall shock waves. On the one hand technically these calculations are essentially simpler, but on the other hand, this approach, strictly speaking, is incorrect and requires a regularization. We have shown that a natural regularization does exist. Moreover, the proposed regularization does not make calculations to be more complicated as compare with naive (direct) calculations. This opens a new possibility for simple calculations for wall shock waves bearing nontrivial matter charges.

3.5.2 Further directions

Head-on collisions of point charged shock waves have only two parameters. In the dual language they correspond to energy and chemical potential per nucleus. Off-center collisions are also specified by the impact parameter and the change of this parameter can be associated with a dual change from “non-thermal” peripheral to “thermal” central collisions [18]. However, this is still an oversimplification of the problem. The physics of heavy-ion collision in RHIC is richer and as indicated in [18, 60], rapid equilibration and hydrodynamical behavior experimentally observed at RHIC for collisions of two heavy ions such as AuAu, does not have the place for deuteron-Au collisions at the same rapidity. Maybe it is too naive to believe that the simplest shock wave related by a boost to the Schwarzschild black hole in AdS can mimic the nuclear matter in the colliders. However this simple shock wave in fact reproduces the interaction of a relativistic quark with gravity and by this reason, may be considered as a simplest candidate to mimic the nuclear matter within the holographic conjecture. One can try to associate different nuclei with different forms of shock waves. Let us remind in this context that the form of the shock wave follows from the eikonal approximation of the gravity-quark interaction in 5-dimension [61, 26]. The presence of the electromagnetic field or other fields as well as any improvements of the eikonal approximation for sure changes the form of the shock waves and it would be interesting to see holographical consequences of this consideration.

The obtained lower bound on N_{charged} scales as $s_{NN}^{1/3}$, which is a faster energy dependence than the $s_{NN}^{1/4}$ scaling predicted by the Landau model [37] and largely obeyed by the data. If one has a priori a restriction on allowed energy then one can fit constants to guaranty that the experimental data are above the AdS bound. Note that taking into account the chemical potential permits to increase the allowed energy. However one cannot expect too much from the chemical potential corrections. The relevant chemical potential for baryon number is not expected to be large, i.e. $\mu_B \sim 30\text{MeV}$ or $\mu_B/T \sim 0.15$ for recent experiments at RHIC [62] and so any effects will be limited. However, as has been mentioned in the text, the relation between the value of chemical potential and the value of the 5-dimensional charge is in our disposal and we can assume a huge ratio of them.

It would be also interesting to try to use plane gravitational waves in AdS_5 to describe nonperturbative stages in the gauge theories and colli-

sions of these waves to describe the QGP formed in the heavy ions collisions. In the plane case, the Chandrasekhar-Ferrari-Xanthopoulos duality between colliding plane gravitational waves and the Kerr black hole solution, has been used as a model of the BH formation [63]. It would be interesting to generalize this duality to the AdS case. This may get a new insight to a possible dependence of multiplicities on the rapidity.

Bibliography

- [1] J. M. Maldacena, *Adv. Theor. Math. Phys.* 2, 231 (1998) [*Int. J. Theor. Phys.* 38, 1113 (1999)]; arXiv:hep-th/9711200.
- [2] S. S. Gubser, I. R. Klebanov and A. M. Polyakov, *Phys. Lett. B* 428, 105 (1998) ; arXiv:hep-th/9802109.
- [3] E. Witten, *Adv. Theor. Math. Phys.* 2, 253 (1998); arXiv:hep-th/9802150.
- [4] G. Policastro, D. T. Son and A. O. Starinets, “The Shear viscosity of strongly coupled N=4 supersymmetric Yang-Mills plasma,” *Phys. Rev. Lett.* **87**, 081601 (2001); hep-th/0104066.
- [5] J. Casalderrey-Solana, H. Liu, D. Mateos, K. Rajagopal, and U. A. Wiedemann, *Gauge/String Duality, Hot QCD and Heavy Ion Collisions*, arXiv:1101.0618.
- [6] A. Bernamonti and R. Peschanski, *Time-dependent AdS/CFT correspondence and the Quark-Gluon Plasma*, arXiv:1102.0725.
R. A. Janik *The dynamics of quark-gluon plasma and AdS/CFT*, Lectures at the 5th Aegean summer school, “From gravity to thermal gauge theories: the AdS/CFT correspondence”, Adamas, Milos Island, Greece, September 21-26, 2009; arXiv:1003.3291
- [7] E. Shuryak, *Prog. Part. Nucl. Phys.* 53, 273 (2004); arXiv:hep-ph/0312227.
- [8] E. V. Shuryak, *Nucl. Phys. A* 750, 64 (2005); arXiv:hep-ph/0405066.
- [9] U. W. Heinz, *AIP Conf. Proc.* 739, 163 (2004); arXiv:nucl-th/0407067.
- [10] R. A. Janik and R. B. Peschanski, *Phys. Rev. D* 74, 046007 (2006); arXiv:hep-th/0606149.
R. A. Janik and R. Peschanski, *Phys. Rev. D* 73, 045013 (2006); arXiv:hep-th/0512162.

- [11] S.S. Gubser, S.S. Pufu and A. Yarom, *Entropy production in collisions of gravitational shock waves and of heavy ions*, Phys.Rev., D 78 (2008) 066014; arXiv: 0805.1551.
- [12] H. Nastase, “On high energy scattering inside gravitational backgrounds,” hep-th/0410124.
- [13] H. Nastase, “The RHIC fireball as a dual black hole,” hep-th/0501068.
- [14] E. Shuryak, S.-J. Sin, and I. Zahed, “A gravity dual of RHIC collisions,” J. Korean Phys. Soc. 50 (2007) 384–397; hep-th/0511199.
- [15] A. J. Amsel, D. Marolf, and A. Virmani, “Collisions with Black Holes and Deconfined Plasmas,” JHEP **04** (2008) 025; arXiv:0712.2221.
- [16] D. Grumiller and P. Romatschke, “On the collision of two shock waves in AdS5,” arXiv:0803.3226.
- [17] S.S. Gubser, S.S. Pufu and A. Yarom, Off-center collisions in AdS5 with applications to multiplicity estimates in heavy-ion collisions JHEP **11** (2009)050; arXiv:0902.4062.
- [18] S. Lin, E. Shuryak, Grazing Collisions of Gravitational Shock Waves and Entropy Production in Heavy Ion Collision; arXiv:0902.1508.
- [19] A. Duenas-Vidal and M. A. Vazquez-Mozo, “Colliding AdS gravitational shock waves in various dimensions and holography,” JHEP **1007**, 021 (2010); arXiv:hep-th/1004.2609.
- [20] L. Alvarez-Gaume, C. Gomez, A. S. Vera, Al. Tavanfar, M. A. Vazquez-Mozo, *Critical formation of trapped surfaces in the collision of gravitational shock waves*, JHEP **0902**, 009 (2009); arXiv:0811.3969.
- [21] S. S. Gubser, A. Nellore, “Mimicking the QCD equation of state with a dual black hole,” Phys. Rev. **D78** (2008) 086007; arXiv:0804.0434.
- [22] I. Y. Aref’eva, A. A. Bagrov and L. V. Joukovskaya, “Critical Trapped Surfaces Formation in the Collision of Ultrarelativistic Charges in (A)dS,” JHEP **1003** , 002, (2010); arXiv:hep-th/0909.1294.

- [23] H. Yoshino and R. B. Mann, Black hole formation in the head-on collision of ultrarelativistic charges, arXiv:0605131.
- [24] U. Gursoy and E. Kiritsis, “Exploring improved holographic theories for QCD: Part I,” JHEP **0802** (2008) 032; arXiv: 0707.1324.
U. Gursoy, E. Kiritsis and F. Nitti, “*Exploring improved holographic theories for QCD: Part II*,” JHEP **0802** (2008) 019; arXiv: 0707.1349.
- [25] E. Kiritsis, A. Taliotis, “Multiplicities from black-hole formation in heavy-ion collisions”, arxiv:1111.1931.
- [26] I.Ya. Aref’eva, Catalysis of Black Holes/Wormholes Formation in High Energy Collisions, Physics of Particles and Nuclei, 41 (2010), 835, arXiv: 0912.5481.
- [27] D. Mateos, S. Matsuura, R. C. Myers, and R. M. Thomson, “Holographic phase transitions at finite chemical potential”, JHEP **11** (2007) 085,; arXiv:0709.1225
- [28] S. Kobayashi, D. Mateos, S. Matsuura, R.C. Myers and R.M. Thomson, “Holographic phase transitions at finite baryon density,” JHEP **0702**, 016 (2007); arXiv:hep-th/0611099.
- [29] Koji Hashimoto, Norihiro Iizuka, and Takashi Oka, Rapid Thermalization by Baryon Injection in Gauge/Gravity Duality; arXiv:1012.4463
- [30] R. C. Myers, M. F. Paulos, A. Sinha, “Holographic Hydrodynamics with a Chemical Potential,” JHEP **0906**, 006 (2009); arXiv: 0903.1596
- [31] S. Hands, T. J. Hollowood, and J. C. Myers, QCD with Chemical Potential in a Small Hyperspherical Box, JHEP **1007**, 086 (2010); arXiv:1003.5813.
- [32] N. Horigome and Y. Tanii, Holographic chiral phase transition with chemical potential, JHEP **01** (2007) 072,; hep-th/0608198.
- [33] A. Parnachev, Holographic QCD with Isospin Chemical Potential, JHEP **02**, 062 (2008); arXiv:0708.3170.

- [34] J. Erdmenger, M. Haack, M. Kaminski and A. Yarom, “Fluid dynamics of R-charged black holes,” JHEP **0901**, 055 (2009); arXiv:hep-th/0809.2488.
- [35] S. W. Hawking and D. N. Page, Thermodynamics of Black Holes in anti-De Sitter Space, Commun. Math. Phys. **87** (1983) 577.
- [36] S. S. Gubser, I. R. Klebanov, and A. W. Peet, “Entropy and Temperature of Black 3-Branes,” Phys. Rev. D **54** (1996) 3915–3919; hep-th/9602135.
- [37] L. D. Landau, “On the multiparticle production in high-energy collisions,” Izv. Akad. Nauk Ser. Fiz. **17**, 51 (1953) (in Russian). [English translation: *Collected Papers of L. D. Landau, edited by D. ter Haar (Gordon and Breach, New-York, 1968)*].
- [38] J. D. Bjorken, “Highly Relativistic Nucleus-Nucleus Collisions: The Central Rapidity Region,” Phys. Rev. D **27**, 140 (1983).
- [39] C. Fefferman and C.R. Graham, “Conformal Invariants,” in *Elie Cartan et les Mathématiques d’aujourd’hui*, Astérisque (1985) 95.
- [40] A. Chamblin, R. Emparan, C. V. Johnson and R. C. Myers, “Charged AdS black holes and catastrophic holography,” Phys. Rev. D **60**, 064018 (1999); arXiv:hep-th/9902170.
A. Chamblin, R. Emparan, C. V. Johnson and R. C. Myers, “Holography, thermodynamics and fluctuations of charged AdS black holes,” Phys. Rev. D **60**, 104026 (1999); arXiv:hep-th/9904197.
- [41] C. S. Peca and J. P. S. Lemos, “Thermodynamics of Reissner-Nordstroem-anti-de Sitter black holes in the grand canonical ensemble,” Phys. Rev. D **59**, 124007 (1999); arXiv:gr-qc/9805004.
M. Cvetic and S. S. Gubser, “Phases of R-charged black holes, spinning branes and strongly coupled gauge theories,” JHEP **9904**, 024 (1999); arXiv:hep-th/9902195.
- [42] K. Skenderis, Lecture notes on holographic renormalization, Class. Quant. Grav. **19** (2002) 5849; hep-th/0209067.
- [43] I. Y. Aref’eva and I. V. Volovich, “On the breaking of conformal symmetry in the AdS/CFT correspondence,” Phys. Lett. B **433**, 49 (1998); arXiv:hep-th/9804182.

- [44] M. Hotta and M. Tanaka, “Shock wave geometry with nonvanishing cosmological constant,” *Class. Quant. Grav.* **10** (1993) 307–314.
- [45] K. Sfetsos, “On gravitational shock waves in curved space-times,” *Nucl. Phys.* **B436** (1995) 721–746; hep-th/9408169.
- [46] G. T. Horowitz and N. Itzhaki, “Black holes, shock waves, and causality in the AdS/CFT correspondence,” *JHEP* **02** (1999) 010; hep-th/9901012.
- [47] R. Emparan, “Exact gravitational shockwaves and Planckian scattering on branes,” *Phys. Rev.* **D64** (2001) 024025; hep-th/0104009.
- [48] J. Podolsky and J. B. Griffiths, “Impulsive waves in de Sitter and anti-de Sitter space-times generated by null particles with an arbitrary multipole structure,” *Class. Quant. Grav.* **15** (1998) 453–463; gr-qc/9710049.
- [49] I. Y. Arefeva, A. A. Bagrov and E. A. Guseva, “Critical Formation of Trapped Surfaces in the Collision of Non-expanding Gravitational Shock Waves in de Sitter Space-Time,” *JHEP* **0912**, 009 (2009); arXiv:hep-th/0905.1087.
- [50] R. Penrose, unpublished, 1974.
- [51] D. M. Eardley and S. B. Giddings, *Phys. Rev. D* **66**, 044011 (2002); arXiv:gr-qc/0201034.
- [52] N. Kaloper and J. Terning, “How black holes form in high energy collisions,” *Gen. Rel. Grav.* **39**, 1525 (2007) [*Int. J. Mod. Phys. D* **17**, 665 (2008)]; arXiv:hep-th/0705.0408.
- [53] S.W. Hawking and G.R.E Ellis, *The large scale structure of space-time* (Cambridge Univ. Press, Cambridge, 1973).
R.M. Wald, *General relativity* (The University of Chicago Press, Chicago, 1984).
- [54] S. Klein and J. Nystrand, “*Exclusive vector meson production in relativistic heavy ion collisions*,” *Phys. Rev.* **C60** (1999) 014903; hep-ph/9902259.

- [55] **STAR** Collaboration, J. Adams et. al., “*Production of $e^+ e^-$ pairs accompanied by nuclear dissociation in ultra-peripheral heavy ion collision,*” Phys. Rev. **C70** (2004) 031902; nucl-ex/0404012.
- [56] S. Ochs, U. W. Heinz, “Entropy production by resonance decays,” Phys. Rev. **C54**, 3199–3211 (1996); hep-ph/9606458.
- [57] F. Karsch, “Lattice QCD at high temperature and density,” Lect. Notes Phys. **583** (2002) 209–249; hep-lat/0106019.
- [58] B. Muller, A. Schafer, “Entropy Creation in Relativistic Heavy Ion Collisions,” arXiv: 1110.2378
- [59] B. B. Back et. al., “The significance of the fragmentation region in ultrarelativistic heavy ion collisions,” Phys. Rev. Lett. **91** (2003) 052303; nucl-ex/0210015.
- [60] S. Lin, E. Shuryak, Phys.Rev. D, **83**, 045025 (2011); arXiv: 1011.1918.
- [61] G. ’t Hooft, Phys. Lett. B 198 (1987); Nucl. Phys. B 304 (1988) 867.
- [62] S. Ghosh, S. Sarkar and J. Alam, “Observing many body effects on lepton pair production from low mass enhancement and flow at RHIC and LHC energies,” Eur. Phys. J. C **71**, 1760 (2011); arXiv:1009.1260.
- [63] I.Ya. Aref’eva, K.S. Viswanathan, and I.V. Volovich, *Planckian-energy scattering, colliding plane gravitational waves and black hole creation*, Nucl. Phys. B 452 (1995) 346.

Chapter 4

Holographic dual of a time machine

4.1 Introduction

Solutions to the equations of General Relativity that describe space-times containing closed timelike curves (CTC) have attracted significant interest as they revealed at least hypothetical theoretical possibility of travelling in time. Since the renowned publication by Kurt Gödel [1] a number of causality violating solutions in GR as well as in modified theories of gravity have been constructed, among which we can name the Tipler-Van Stockum time machine generated by axially rotating distribution of particles [2], [3], the Morris-Thorne-Yurtsever transversable wormhole [4, 5], the Gott time machine based on moving conical defects [6], the Ori dust solution [7], and the solutions in $f(R)$ theories of gravity [8] and theories with non-minimal matter-curvature coupling [9].

All questions about physics of time machines that could be posed in principle fall into three general categories:

- Is there a physical way to create a time machine?
- Is there any time machine solution that can be stable?
- What dynamical behaviour would a physical system experience evolving in a time machine background?

None of the questions have yet received a definite answer.

The answer to the first question is believed to be negative. Extensive analysis of particular time machine solutions has demonstrated that in order to create a space-time with CTC one needs matter that violates strong, weak or null energy conditions of General Relativity (different solutions require violation of different energy conditions), and only eternal time machines can exist [10, 11]. However we can not be sure that all

matter in the Universe obeys these conditions. For instance, there are a number of models of the dark energy violating the null energy condition [12–15], and this provides a way to by-pass the no-go statement.

The second question was raised by Hawking in [16], where he conjectured that a space-time with CTC can be stable only on classical level, but will be unavoidably destroyed by quantum fluctuations of the metric. The real universal proof or refutation of the conjecture can be obtained only within a framework of a complete theory of quantum gravity. String theory opened a possibility to check the chronology protection condition in specific cases. In [17] authors have shown that appearance of closed timelike curves in a certain (O-plane) orbifold background would cause a Hagedorn transition that restructures the space-time transforming it into a chronologically safe configuration. So this result can be considered as a very accurate and nice supporting evidence in favour of the Hawking conjecture. On the other hand in [18–20], it was demonstrated that the Gödel type solutions can be smoothly embedded in the context of string theory. Closed timelike curves in that case are hidden behind the so called holographic screens and do not violate causality in the rest of the space-time. Thus the chronology is protected, but structure of the CTC remains unbroken by quantum effects. An intriguing observation has been made by authors of [21] and [22], that from the point of view of the AdS/CFT correspondence, the existence of CTC in the bulk can be related to negative or exceeding one fermionic probability in the boundary field theory.

The third category includes various types of the “grandfather paradox”. For a classical wave equation on a non-globally hyperbolic space with CTC the possibility of self-consistent dynamics was demonstrated in [23]. Classical mechanical billiards and their self-consistency conditions have been studied in [24]. A basis of states of a free quantum field theory in the Gott time machine has been constructed in [25], where it was shown that the causality violation leads to an emergence of an effective non-unitary interaction in the theory. Non-unitarity of interacting field theories in time machines was analyzed in [26]. Some authors even argued that evolution of a physical system along closed timelike curves can be studied experimentally by mean of simulation of emergent gravity in metamaterials [27], or a qubit interacting with an older version of itself [28].

However the question about properties of an *interacting* quantum field theory in a time machine background remains open, though the real

“grandfather paradox” can take place only in a self-interacting system. When the notions of time ordering and unitarity are absent from the very beginning, it is unclear how to formulate an interacting field theory. In this chapter we address this problem and by use of the AdS/CFT correspondence provide a constructive solution to it. Here we stand on the position that even if the presence of CTC causes breaking of unitarity in the boundary field theory [22], it should not be regarded as a big problem as long as we can formulate a prescription how to solve the theory. When one is trying to get an insight into physics of paradoxical systems, it is not very useful to rely on the “common sense” intuition and corresponding fundamental principles.

The AdS/CFT correspondence provides an elegant way to address the paradox. In the large N limit it relates quantum field theories to a classical gravity, and thus we can study properties of a quantum theory in the CTC background just by careful analysis of the dual Riemannian geometry, without any need to formulate special quantization rules that would be valid in the case of broken causality.

The chapter is organized as follows. In the next section we introduce a simple set up for the time machine in AdS_3 . In Sec. 4.3 we discuss geodesic structure of the spacetime, and suggest that it could lead to non-trivial effects in the boundary field theory. In Sec. 4.4 we introduce a notion of timelike quasigeodesics that will be then used for connecting timelike separated boundary points. Finally, in Sec. 4.5 we formulate a precise algorithm for the Green function evaluation, provide the results of numerical simulations, and discuss the related phenomenology.

4.2 Time machine in AdS_3

The eternal time machine solution in AdS has been suggested by Gott and DeDeo in [29] (for similar solutions containing CTC but collapsing into a BTZ black hole see [30]). Here we briefly recall its structure closely following the original text.

The three dimensional global anti-de Sitter space-time can be thought of as a hypersurface

$$-X_0^2 - X_3^2 + X_1^2 + X_2^2 = -1, \quad (4.1)$$

embedded in a four-dimensional flat $\mathbb{R}^{2,2}$ space-time with a metric:

$$ds^2 = -dX_0^2 - dX_3^2 + dX_1^2 + dX_2^2. \quad (4.2)$$

In the Schwarzschild coordinates the embedding formulas are

$$\begin{aligned}
X_0 &= \sqrt{1 + R^2} \cos t, \\
X_3 &= \sqrt{1 + R^2} \sin t, \\
X_1 &= R \cos \phi, \\
X_2 &= R \sin \phi,
\end{aligned}
\tag{4.3}$$

where $R \in (0, \infty)$, $t \in (-\infty, \infty)$, $\phi \in [0, 2\pi)$.

The induced metric is then

$$ds^2 = -(1 + R^2)dt^2 + \frac{dR^2}{1 + R^2} + R^2d\phi^2.
\tag{4.4}$$

A massive particle put into a three dimensional space-time removes a wedge with an angle deficit proportional to the mass of the particle, and edges (faces) emerging from this point-like particle. Points on the opposite edges of the wedge are identified, and the resulting space-time contains a conical defect, Fig.4.1(a). When we are looking at the unfolding of the conical defect, coordinate locations of the edges do not have an independent physical meaning, and we are free to rotate them preserving the angular deficit. For our purposes it will be convenient to make the cut out “pizza slice” twist in time with a constant angular velocity in the reference frame of the massive particle, making a full rotation in a period 2π , Fig.4.1(b). Then for the trailing and leading faces of the wedge in the embedding coordinates we get:

$$\begin{aligned}
X_0^t &= \sqrt{1 + R^2} \cos t & X_0^l &= \sqrt{1 + R^2} \cos t, \\
X_3^t &= \sqrt{1 + R^2} \sin t & X_3^l &= \sqrt{1 + R^2} \sin t, \\
X_1^t &= R \cos(t - \alpha/2) & X_1^l &= R \cos(t + \alpha/2), \\
X_2^t &= R \sin(t - \alpha/2) & X_2^l &= R \sin(t + \alpha/2).
\end{aligned}$$

Here α is the angular deficit of the conical spacetime. Integrating the spacetime stress-energy tensor over the angle, we can deduce that the effective mass concentrated in the interior of the bulk is

$$M = -\frac{1}{8G} + \frac{\alpha}{16\pi G}.
\tag{4.5}$$

Here the second term is the mass of the point-like source, and the first one is the contribution from the negative AdS curvature.

For a single static conical defect we can not make its angular deficit α larger than 2π . If the mass of the point-like particle exceeds the limit

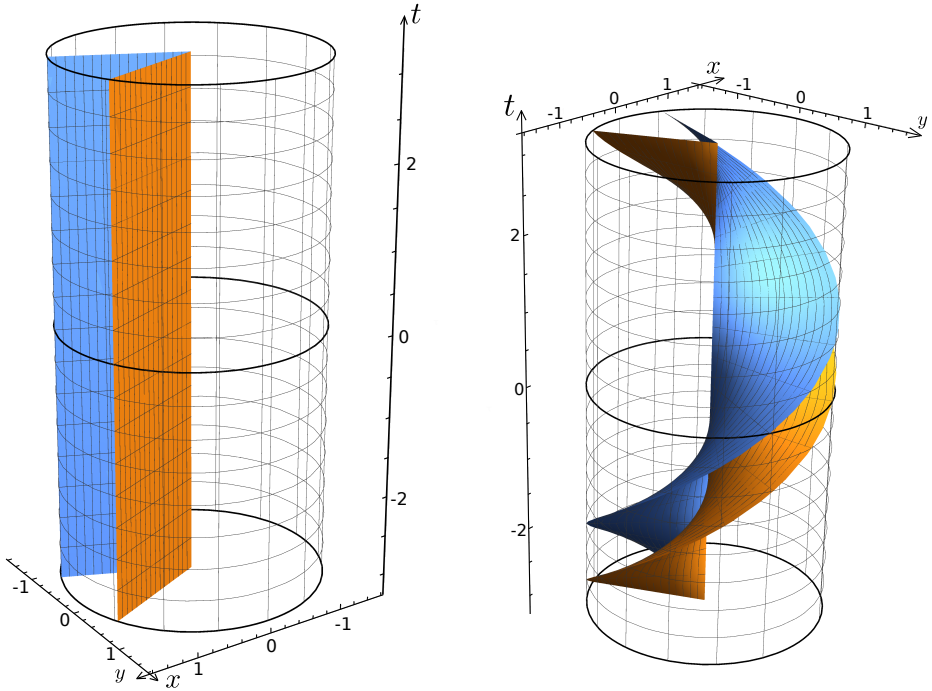


Figure 4.1. Two equivalent unfoldings of the AdS_3 spacetime with a conical defect $\alpha = \sqrt{3}\pi$. The larger part of the spacetime outside of the faces is to be cut out, and the faces are identified. The only physical space is the narrow region between the faces. To construct a time machine the twisted unfolding is more convenient to use.

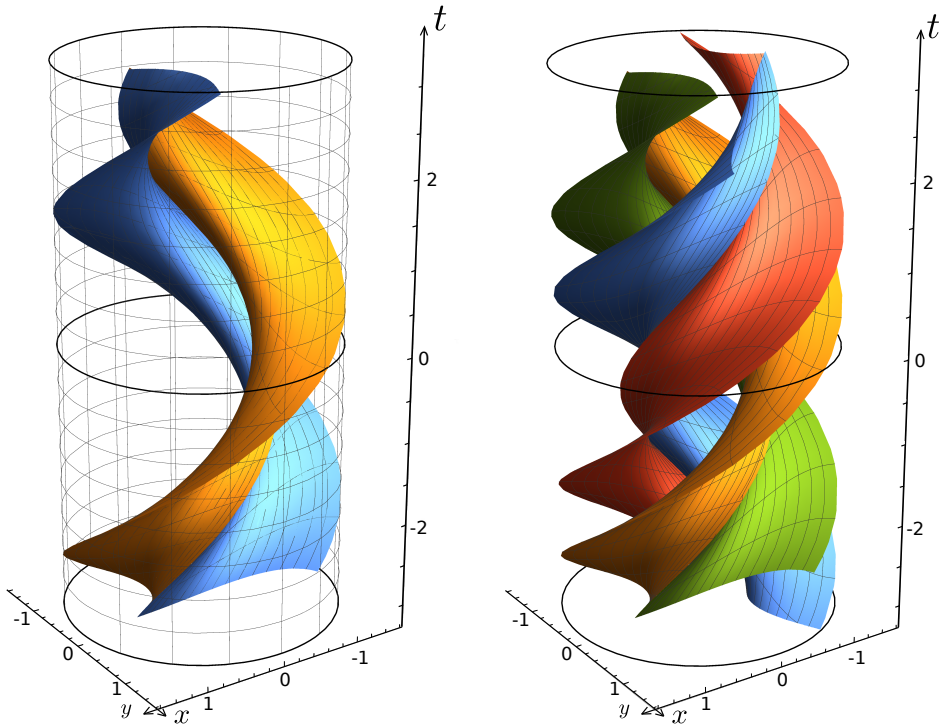


Figure 4.2. Left: a boosted conical defect in AdS_3 . Faces of the wedge are deformed, and the identification occurs between points with different time coordinates (in the centre of mass frame). Here $\alpha = \sqrt{3}\pi$, $\psi = 1$. Right: the DeDeo-Gott time machine.

$\alpha = 2\pi$ ($M \geq 0$), the resulting space-time will be rather a BTZ black hole instead of a naked conical singularity [31].

However, if we boost the massive source, the removed wedge is effectively getting “squeezed” from the point of view of an external observer at rest (see Fig. 4.2(a)). This provides a room for a second conical defect with a deficit angle β such that $\alpha + \beta > 2\pi$. In other words, relative motion can support the system of conical defects, preventing them from collapsing into a black hole. This will be the essence of the DeDeo-Gott construction.

Consider a system of two identical conical defects undergone two opposite Lorentz transformations, in the (X_0, X_1) and (X_3, X_2) planes of the embedding space each:

$$\Lambda_I = \Lambda_{II}^{-1} = \begin{pmatrix} \cosh \psi & 0 & \sinh \psi & 0 \\ 0 & \cosh \psi & 0 & \sinh \psi \\ \sinh \psi & 0 & \cosh \psi & 0 \\ 0 & \sinh \psi & 0 & \cosh \psi \end{pmatrix} \quad (4.6)$$

In the three-dimensional coordinates of the AdS spacetime these Lorentzian transformations correspond to $SO(2, 2)$ isometry transformations.

It can be shown that in the coordinates of global AdS_3 these defects move along the same circular orbit $R = \text{const}$ with a constant velocity, always being at the opposite points of the orbit, Fig.4.2(b). A conical defect sits at $\tilde{R} = 0$ in its rest frame, i.e.

$$\tilde{X}_0 = \cos t, \quad \tilde{X}_1 = 0, \quad \tilde{X}_2 = 0, \quad \tilde{X}_3 = \sin t. \quad (4.7)$$

In the boosted frame

$$X_0 = \cosh \psi \cos t, \quad X_1 = \sinh \psi \cos t, \quad X_2 = \sinh \psi \sin t, \quad X_3 = \cosh \psi \sin t, \quad (4.8)$$

hence

$$R = \sqrt{X_1^2 + X_2^2} = |\sinh \psi|, \quad (4.9)$$

$$\cos \phi = \frac{X_2}{R} = \frac{\sinh \psi \cos t}{|\sinh \psi|} = \text{sgn } \psi \cdot \cos t. \quad (4.10)$$

In the rest frame of a wedge, the points on its edges are identified at equal coordinate times. However if we boost it, from the point of view of an external observer this identification would occur at different

times leading to time jumps for a particle moving around the conical singularity. In the case of a single conical defect its boost can be regarded as a global coordinate transformation of the space-time, which obviously can not cause any new physical effects. However, with two defects moving relative to each other, the relative time jumps become a physical effect that can not be eliminated by a (proper) choice of coordinate system. These time jumps allow for the existence of CTC.

Existence of closed timelike curves in this space-time can be demonstrated by looking at the identification of the edges near the boundary of AdS_3 (at $R \rightarrow \infty$). We refer the reader to [29] for a detailed discussion, here we just quote the result. Speaking in terms of the unfolding of the two-conical space-time, when a timelike particle living on the boundary of the AdS cylinder hits an edge of one of the two wedges, it undergoes a time and an angle jump:

$$\Delta t = 2 \arctan \left(\frac{\sin(\alpha/2) \tanh \psi}{1 + \cos(\alpha/2) \tanh \psi} \right), \quad (4.11)$$

$$\Delta \phi = 2 \arctan \left(\frac{\sin(\alpha/2)}{\tanh \psi + \cos(\alpha/2)} \right). \quad (4.12)$$

It can be shown that $\Delta t + \Delta \phi = \alpha$. If $\alpha \geq \pi$, the world line of the particle becomes a closed timelike curve, and thus the space-time is a time-machine, see Fig.4.3.

In the regime when this limit is not exceeded, and CTC are not present, the space-time has been studied in detail from holographic point of view in [32], but the case of broken causality has not been addressed.

In the next sections we will study geodesic structure of this time machine and explicitly show that in presence of the two orbiting conical defects we deal with a highly-nontrivial lensing of geodesics, and this reflects on the structure of two point Green's functions of the dual boundary theory.

4.3 Entwinement of geodesics and causality violations

When conformal dimension Δ of a boundary operator in AdS/CFT is very high, the corresponding two-point Green function can be derived in the geodesic approximation [31]:

$$G(A, B) = e^{-\Delta \mathcal{L}_{AB}}, \quad (4.13)$$

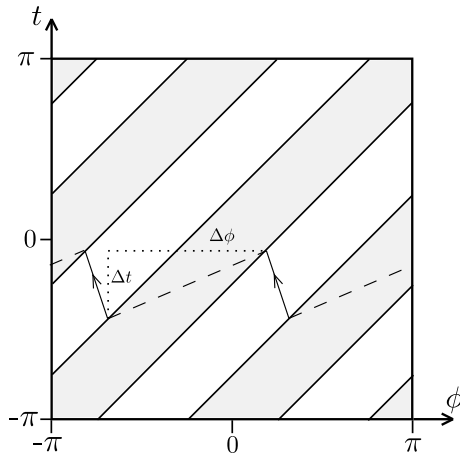


Figure 4.3. A timelike particle moving along the boundary experiences a jump in time and angle when it hits a face of one of the wedges. If $\Delta t + \Delta\phi > \pi$, closed timelike curves become possible. The gray strips are the cut out part of the boundary, and the white strips are the physical part of the boundary.

where \mathcal{L}_{AB} is the length of a geodesic connecting boundary points A and B . If there are more than one geodesic between A and B , they can give additional contributions to the propagator. This is the case for the DeDeo-Gott time machine geometry, and here we address possible outcome of this in details.

Consider two arbitrary points $A(t_1, \phi_1)$ and $B(t_2, \phi_2)$ located in the physical (unremoved) part of the AdS_3 boundary. Having two rotating conical defects in the bulk makes the structure of possible geodesics connecting¹ A and B very nontrivial, so we should find a way to calculate their contributions to the two-point Green's function $G(A, B)$. Let us shoot a geodesic from the boundary point A to the point B . Before it hits the point B it can undergo a number of “refractions” on the faces of wedges, winding around either of two conical defects clockwise (if it hits the leading face of the wedge head on) or counterclockwise (if it overtakes the trailing face of the wedge from behind). For example, schematically a

¹When A and B are timelike separated we encounter some subtleties caused by the fact that in the AdS space-time a timelike geodesic can not reach the boundary. These issues will be commented further on, but the general point of view described in this section remains unchanged.

typical geodesic may have a structure (see also Fig. 4.4)

$$A \rightarrow \mathcal{W}_I^- \rightarrow \mathcal{W}_{II}^+ \rightarrow \mathcal{W}_I^+ \rightarrow \mathcal{W}_{II}^+ \rightarrow B, \quad (4.14)$$

where $\mathcal{W}_{I,II}^{\pm}$ stands for the act of clockwise/counterclockwise winding around the 1-st or the 2-nd wedge respectively.

So, formally the Green's function in the geodesic approximation is given by

$$G(A, B) = \sum_{n=0}^{\infty} \sum_{\{\mathcal{W}_1 \dots \mathcal{W}_n\}} e^{-\Delta \mathcal{L}(A\{\mathcal{W}_1 \dots \mathcal{W}_n\}B)}, \quad (4.15)$$

where the second sum is taken over all different entwinement structures corresponding to the same number of windings, and the first sum is taken over all winding numbers².

It is easy to see that for a given number of windings N the maximal possible number of topologically different geodesics is

$$n_N = 4 \cdot 3^{N-1}. \quad (4.16)$$

The first winding act can be of four different types. But for each of the next steps, if a geodesic wrapped around a conical defect, for example, clockwise, then on the next step it can not go in the opposite direction and wrap around the same conical defect counterclockwise. It means that in the sequence of windings the winding act \mathcal{W}_I^+ can be followed (at least hypothetically) by \mathcal{W}_I^+ , \mathcal{W}_{II}^+ , \mathcal{W}_{II}^- , but not by \mathcal{W}_I^- .

As we will see further, for a given pair of boundary points (A, B) not all sequences of entwinements are physically realistic and can contribute to the sum (4.15).

To find a proper prescription for the lengths of the non-trivial winding geodesics let us discuss in detail a particular example.

Take a look at Fig.4.4. The length of the presented geodesic is a sum of lengths of its' composing arcs:

$$\mathcal{L}(A \rightarrow \mathcal{W}_I^- \mathcal{W}_{II}^+ \mathcal{W}_I^+ \mathcal{W}_{II}^+ \rightarrow B) = \mathcal{L}_{AO_1} + \mathcal{L}_{O_2O_3} + \mathcal{L}_{O_4O_5} + \mathcal{L}_{O_6O_7} + \mathcal{L}_{O_8B}. \quad (4.17)$$

We will refer to points C_i as complementary points, and O_i as refraction points. Coordinates of the refraction points O_i are to be found from coordinates of A and B , and that can be easily done step by step.

²This idea of entwinements in holography has been introduced in [33], but there it was related to a concept of entanglement entropy "shadows" rather than to subleading contributions to the propagator

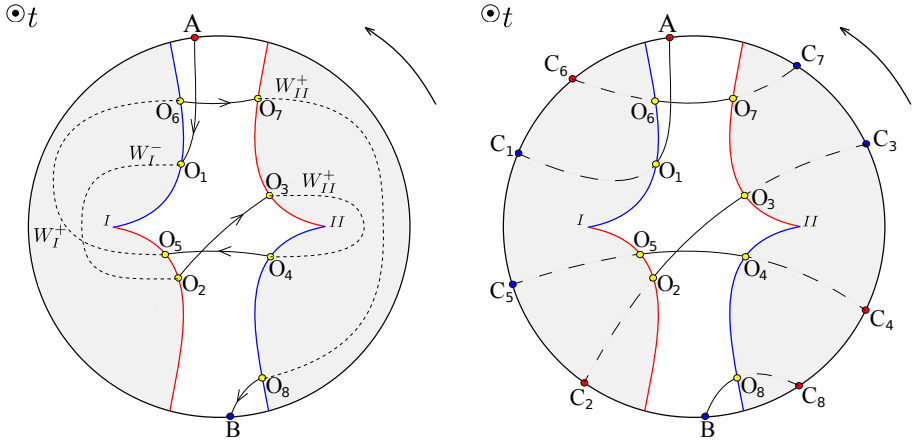


Figure 4.4. Schematic constant time projection of a typical geodesic connecting points A and B in the time machine. Red curves are for leading faces of the rotating wedges, and blue curves - for trailing faces. The entanglement configuration in this particular case is $\mathcal{W}_I^- \mathcal{W}_{II}^+ \mathcal{W}_I^+ \mathcal{W}_{II}^-$ according to the notations introduced in the main text. All shown points in principle can have different time coordinates (here we schematically project them down to a single time section, so the curves the geodesic is made from should be taken only as an approximate artistic representation). On the left picture the acts of entanglement and identifications are shown explicitly. A and B belong to the physical unreduced part of the spacetime, and O_i are the points where the geodesic undergoes “refraction” on the wedges. The right picture demonstrates the idea of complementary points C_i located in the removed part of the spacetime.

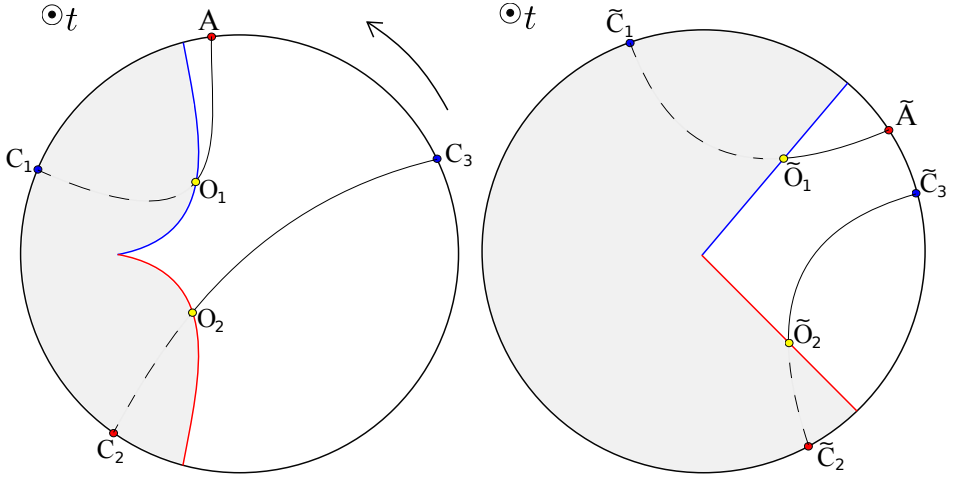


Figure 4.5. The left picture demonstrates \mathcal{W}_I^- refraction of a geodesic on the first conical defect. The right picture demonstrates how it looks like in a reference frame of the conical defect. Again, points generically belong to different time slices, and the representation is purely schematic.

Focus on the first refraction on the wedge, \mathcal{W}_I^- . The points of interest are $\{A, O_1, C_1, C_2, O_2, C_3\}$. Here we neglect for a while the second wedge, so we do not consider the point O_3 at all, and we treat C_3 as a physical point (not just as a point in the complementary “removed” space), see Fig.4.5(a). These six points can be regarded as a result of boost transformation Λ_I applied to the wedge. We can “unboost” the wedge and find static pre-images of these points (see Fig.4.5(b)). For the “unboosted” points the following relations trivially hold

$$\begin{aligned}\tilde{C}_2 &= \Lambda_I^{-1}C_2 = \Lambda_I^{-1}A - (0, \alpha) = \tilde{A} - (0, \alpha), \\ \tilde{C}_3 &= \Lambda_I^{-1}C_3 = \Lambda_I^{-1}C_1 - (0, \alpha) = \tilde{C}_1 - (0, \alpha),\end{aligned}\tag{4.18}$$

where $(0, \alpha)$ is a boundary identification vector proportional to the angular deficit. Here we subtract the identification vector $(0, \alpha)$ because this particular entanglement is counterclockwise. For clockwise \mathcal{W}^+ we should rather add $(0, +\alpha)$. In that case points \tilde{O}_1 and \tilde{O}_2 are intersections of geodesics $\tilde{A}\tilde{C}_1$ and $\tilde{C}_2\tilde{C}_3$ with faces of the static wedge.

Applying the same procedure to the other entanglements, in a generic

case we get a system of recurrent relations

$$\begin{aligned}
C_2 &= \Lambda_1(\Lambda_1^{-1}A \pm (0, \alpha)), \\
C_{2j} &= \Lambda_j(\Lambda_j^{-1}C_{2j-2} \pm (0, \alpha)), \\
C_{2N-1} &= \Lambda_N(\Lambda_N^{-1}B \mp (0, \alpha)), \\
C_{2j-1} &= \Lambda_j(\Lambda_j^{-1}C_{2j+1} \mp (0, \alpha)).
\end{aligned} \tag{4.19}$$

Here $\Lambda_j = \Lambda_I$ if the corresponding winding is \mathcal{W}_I^\pm . $\Lambda_j = \Lambda_{II}$ if the corresponding winding is \mathcal{W}_{II}^\pm . In these formulae we pick up the upper sign if $\mathcal{W}_{I,II}^+$, and the lower sign if $\mathcal{W}_{I,II}^-$.

Note, that the Lorentz boost we have defined in terms of the embedding space coordinates acts non-linearly on the AdS_3 points, therefore we can not simply expand the parentheses in (4.19).

Then for each of the auxiliary arcs $C_{2k}C_{2k+1}$ we can derive coordinates of the refraction points O_{2k} , O_{2k+1} , and write down corresponding lengths of the composing arcs.

Later we will also show that not every formally generated sequence of windings does exist.

4.4 Quasigeodesics connecting boundary points

To discuss causality properties of the dual boundary QFT, we will in particular need to consider boundary points with timelike separation. The conceptual problem we unavoidably encounter here is the absence of timelike geodesics connecting points on the conformal boundary of AdS . The equations for timelike geodesics can be derived from the following Lagrangian for a massive particle in AdS :

$$-(1 + R^2)\dot{t}^2 + \frac{\dot{R}^2}{1 + R^2} + R^2\dot{\phi}^2 = -1. \tag{4.20}$$

Such a particle has two conserved momenta:

$$\mathcal{E} = (1 + R^2)\dot{t}, \tag{4.21}$$

$$\mathcal{J} = R^2\dot{\phi}. \tag{4.22}$$

Substituting them into the Lagrangian we obtain the radial equation of motion:

$$-\frac{\mathcal{E}^2}{1+R^2} + \frac{\dot{R}^2}{1+R^2} + \frac{\mathcal{J}^2}{R^2} = -1, \quad (4.23)$$

$$\dot{R}^2 = -\left(1+R^2\right)\left(1+\frac{\mathcal{J}^2}{R^2}\right) + \mathcal{E}^2. \quad (4.24)$$

Clearly the right hand side of the equation turns negative as $R \rightarrow \infty$, and thus no real solution to this equation can exist.

In the case of a stationary spacetime the obstacle could be easily surmounted by performing the analytic continuation of the metric to the Euclidean signature, calculating the Green function in terms of Euclidean lengths of the geodesics, and making the inverse Wick rotation back to real time. However in our case we deal with a spacetime that is not only non-stationary, but which has no good global notion of time. Hence we are forced to stick to the Lorentzian time.

The way to implement the geodesic approximation for timelike separated boundary points in the single Poincaré patch has been suggested in [34]. Let's turn for a second to the single patch of the AdS_3 spacetime, covered by the Poincaré coordinates:

$$ds^2 = -r^2 dt^2 + \frac{dr^2}{r^2} + r^2 dx^2. \quad (4.25)$$

Again, a massive bulk particle has two kinetic invariants:

$$E = r^2 \dot{t}, \quad (4.26)$$

$$J = r^2 \dot{x}, \quad (4.27)$$

but now we have two different classes of spacelike geodesics.

- For $J^2 > E^2$:

$$\begin{cases} r(\lambda) = \sqrt{J^2 - E^2} \cosh \lambda \\ x(\lambda) = x_0 + \frac{J}{J^2 - E^2} \tanh \lambda \\ t(\lambda) = t_0 + \frac{E}{J^2 - E^2} \tanh \lambda \end{cases} \quad (4.28)$$

- For $E^2 > J^2$:

$$\begin{cases} r(\lambda) = \sqrt{E^2 - J^2} \sinh \lambda \\ x(\lambda) = x_0 - \frac{J}{E^2 - J^2} \coth \lambda \\ t(\lambda) = t_0 - \frac{E}{E^2 - J^2} \coth \lambda \end{cases} \quad (4.29)$$

We will be interested in the geodesics of the second kind. As $\lambda = 0$ these geodesics approach the point $r(0) = 0$, which is the Poincaré horizon of the half- AdS chart. Regarding the horizon as a single infinitely far point (as in the theory of complex functions), we can consider two disconnected spacelike geodesics possessing the same kinetic invariants E and J , but emerging from two different timelike separated boundary points $A(t_A, x_A)$ and $B(t_B, x_B)$, as two branches of a single geodesic reaching the spatial infinity and returning back to the boundary. The length of such a geodesic will be divergent not only as $r \rightarrow \infty$ (the standard holographic UV divergence), but also as $r \rightarrow 0$, but this can be cured by an appropriate renormalization³. The resulting expression for the renormalized length of the geodesic is simply

$$\mathcal{L} = \ln \left((t_B - t_A)^2 - (x_A - x_B)^2 \right), \quad (4.30)$$

which gives the correct answer for the two-point correlation function of $(1+1)$ -dimensional CFT :⁴

$$G(t_A, x_A; t_B, x_B) = e^{-\Delta \mathcal{L}} = \frac{1}{((t_B - t_A)^2 - (x_A - x_B)^2)^\Delta}, \quad \Delta t^2 > \Delta x^2. \quad (4.33)$$

In the global AdS space-time the Poincaré horizon has no special physical meaning, but we can still try to generalize this procedure to this case.

The boundary field theory now is defined on $S^1 \times \mathbb{R}^1$ spacetime, and the two-point Green function that we must be able to reproduce via the geodesic approximation has the form [35]:

$$G(t_A, \phi_A; t_B, \phi_B) = \frac{1}{|\cos(t_B - t_A) - \cos(\phi_B - \phi_A)|^\Delta}. \quad (4.34)$$

Note that this function is periodic both in angle and time. While the angular periodicity is obvious by construction, periodicity in time emerges

³For details see App. B and D of [34]

⁴If $\Delta x^2 > \Delta t^2$, the renormalized length is

$$\mathcal{L} = \ln \left(-(t_B - t_A)^2 + (x_A - x_B)^2 \right), \quad (4.31)$$

and the full Green function is

$$G(t_A, x_A; t_B, x_B) = \frac{1}{|(t_B - t_A)^2 - (x_A - x_B)^2|^\Delta}. \quad (4.32)$$

because of the finite size effects: an excitation created at some point in space and time starts dissipating, but later recollects and revives due to the spatial periodicity.

We will need a function that defines angular separation between boundary points while properly maintaining the rotational invariance of the system. For instance, given two angular coordinates $\phi_2 = \frac{7\pi}{4}$ and $\phi_1 = \frac{\pi}{4}$, the difference between them along the shorter arc is

$$D(\phi_2, \phi_1) = -\frac{\pi}{2} \neq \phi_2 - \phi_1. \quad (4.35)$$

Thus we should use

$$D(\phi_1, \phi_2) = \text{mod}(\phi_2 - \phi_1 + \pi, 2\pi) - \pi. \quad (4.36)$$

Analogously, for the arithmetic average of two angular coordinates (that provides a point exactly at the middle of the shorter arc between ϕ_1 and ϕ_2):

$$\Sigma(\phi_1, \phi_2) = \frac{1}{2} \left(\phi_1 + \phi_2 - 2\pi \theta \left(-\cos \left(\frac{1}{2} (\phi_1 - \phi_2) \right) \right) \right) \quad (4.37)$$

Note that the Green function (4.34) has a symmetry:

$$G(t_A, \phi_A; t_B, \phi_B) = G(t_A, \phi_A; t_B + \pi, \phi_B + \pi), \quad (4.38)$$

where points on the r.h.s. can be spacelike separated while points on the l.h.s. have timelike separation:

$$(t_B - t_A)^2 > D(\phi_B, \phi_A)^2, \quad \text{but} \quad (t_B - t_A + \pi)^2 < D(\phi_B + \pi, \phi_A)^2. \quad (4.39)$$

This symmetry can be used to construct a disjointed spacelike geodesic, with two branches reattached at the Poincaré horizon, connecting timelike separated points.

If we represent the global AdS_3 space-time as a cylinder, the Poincaré horizon consists of two planes cutting the cylinder at 45° . The orientation of the planes (as a rigid construction) can be chosen arbitrarily. Then consider a spacelike geodesic emerging from boundary point A (see Fig.4.6), and terminating at boundary point B^* . Somewhere in the bulk it has a turning point P_1 where its radial coordinate $R^* = R(0)$ is minimal.

Since we are free to choose the location of the Poincaré horizon, we can always orient it in such a way that the AB^* geodesic intersects it at

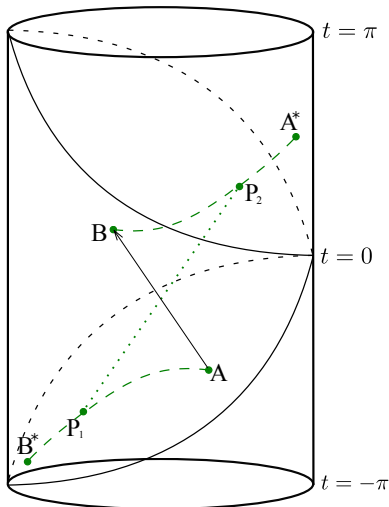


Figure 4.6. A spacelike quasigeodesic connecting two boundary timelike separated points A and B . A spacelike curve emerges from point A and reach the Poincaré horizon at point P_1 . Then it jumps to a mirror point $P_2 = P_1 + (\pi_t, \pi_\phi, 0_R)$ on the second plane of the horizon, and proceeds further to B . The arc P_2B is a rotation of P_1B^* by π .

the turning point P_1 . This point P_1 can be identified with a point $P_2 = P_1 + (\pi_t, \pi_\phi, 0_R)$, located on the other cutting plane. The arc P_1B^* can be then rotationally translated to this point: $P_1 \rightarrow P_2$, and then $B^* \rightarrow B$, where $B = B^* + (\pi, \pi)$. Hereafter we will use disjointed “quasigeodesics” of this AP_1P_2B type to connect timelike separated points.

The explicit analytic expression for the quasigeodesics can be derived in the following way. Let’s take the Poincaré chart geodesics (4.29), and rewrite them in coordinates of the embedding spacetime. The correspond-

ing coordinate transformation is given by:

$$X^0 = \frac{r}{2} \left(\frac{1}{r^2} + 1 + x^2 - t^2 \right), \quad (4.40)$$

$$X^1 = xr, \quad (4.41)$$

$$X^2 = \frac{r}{2} \left(\frac{1}{r^2} - 1 + x^2 - t^2 \right), \quad (4.42)$$

$$X^3 = rt. \quad (4.43)$$

Substituting here (4.29), and recalling the relations between the global and embedding coordinates (4.3), we obtain

$$\sqrt{1 + R^2} \cos t = \frac{(-1 + E^2 - J^2)}{2\sqrt{E^2 - J^2}} \sinh \lambda, \quad (4.44)$$

$$\sqrt{1 + R^2} \sin t = \frac{E}{\sqrt{E^2 - J^2}} \cosh \lambda, \quad (4.45)$$

$$R \cos \phi = \frac{J}{\sqrt{E^2 - J^2}} \cosh \lambda, \quad (4.46)$$

$$R \sin \phi = \frac{(-1 - E^2 + J^2)}{2\sqrt{E^2 - J^2}} \sinh \lambda. \quad (4.47)$$

These can be solved to give us the embedding of the Poincaré chart space-like geodesic into the global AdS :

$$t(\lambda) = \arctan \left(\frac{2E}{-1 + E^2 - J^2} \coth \lambda \right) + t_0, \quad (4.48)$$

$$\phi(\lambda) = \arctan \left(\frac{-1 - E^2 + J^2}{2J} \tanh \lambda \right) + \phi_0, \quad (4.49)$$

$$R(\lambda) = \sqrt{\frac{J^2}{E^2 - J^2} \cosh^2 \lambda + \frac{(-1 - E^2 + J^2)^2}{4(E^2 - J^2)} \sinh^2 \lambda}. \quad (4.50)$$

This quasigeodesic already has a π -jump in time at the turning point $\lambda = 0$, and as explained before we also need to adjust the discontinuity in angle:

$$\tilde{\phi}(\lambda) = \phi(\lambda) + \pi\theta(\lambda) = \arctan \left(\frac{-1 - E^2 + J^2}{2J} \tanh \lambda \right) + \pi\theta(\lambda) + \phi_0. \quad (4.51)$$

From now on we will omit the tilde.

The kinetic invariants can then be expressed in terms of the boundary coordinates:

$$E = \frac{\sin \frac{t_2 - t_1}{2}}{\sin \frac{D(\phi_2 - \pi, \phi_1)}{2} - \cos \frac{t_2 - t_1}{2}}, \quad (4.52)$$

$$J = \frac{\cos \frac{D(\phi_2 - \pi, \phi_1)}{2}}{\sin \frac{D(\phi_2 - \pi, \phi_1)}{2} - \cos \frac{t_2 - t_1}{2}}. \quad (4.53)$$

The integration constants t_0 and ϕ_0 in (4.49) can be represented as:

$$t_0 = \frac{1}{2} (t_1 + t_2), \quad \phi_0 = \Sigma(\phi_1, \phi_2 - \pi). \quad (4.54)$$

Inverting equation (4.50) we obtain dependence of the affine parameter on the radial coordinate:

$$\lambda(R) = \pm \operatorname{arcsinh} \sqrt{\frac{4(E^2 - J^2)R^2 - 4J^2}{(-1 - E^2 + J^2)^2 + 4J^2}}, \quad (4.55)$$

where the minus sign is taken on the first branch of the geodesic or quasi-geodesic (i.e. before the turning point, - when particle moves away from the boundary), and the plus sign is taken on the second branch (when particle moves towards the boundary). This function can be used to define the geodesic length, which is simply

$$\mathcal{L}(R_1, R_2) = \lambda_{\pm}(R_2) - \lambda_{\pm}(R_1), \quad (4.56)$$

for two points with radial coordinates R_1 and R_2 .

Note that for a geodesic connecting two boundary points the length is divergent:

$$\mathcal{L} = \lim_{R \rightarrow \infty} (\lambda_+(R) - \lambda_-(R)) = 2 \lim_{R \rightarrow \infty} \sqrt{\frac{4(E^2 - J^2)R^2 - 4J^2}{(-1 - E^2 + J^2)^2 + 4J^2}} = \infty, \quad (4.57)$$

and needs to be renormalized. The natural way to do it is to subtract the parameter independent divergent part, and define the geodesic length as

$$\begin{aligned} \mathcal{L}_{ren} &= \lim_{R \rightarrow \infty} (\lambda_+(R) - \lambda_-(R) - 2 \ln R) = \\ &= \ln \left(\frac{16(E^2 - J^2)}{E^4 - 2E^2(-1 + J^2) + (1 + J^2)^2} \right). \end{aligned} \quad (4.58)$$

The argument of the logarithm is always positive for quasigeodesics connecting timelike separated points, but can be less than 1. It means that the geodesic length after the renormalization in principle can be negative. Using (4.58) along with (4.52) we obtain the correct result for the retarded Green function:

$$G_c(t_1, \phi_1; t_2, \phi_2) = e^{-\Delta\mathcal{L}_{ren}} = \frac{1}{(\cos(t_2 - t_1) - \cos(\phi_2 - \phi_1))^\Delta} \quad (4.59)$$

where $(t_2 - t_1)^2 > D(\phi_1, \phi_2)^2$,

where $D(\phi_1, \phi_2)$ is the function introduced in (4.36). The possible negativity of the renormalized geodesic length is the reason why singularities of the correlator can be captured in the geodesic approximation.

Here we must pause for a second and stress Lorentz non-invariance of (4.59). We define $SO(2, 2)$ isometries of AdS_3 in terms of the Lorentz boosts of the embedding $\mathbb{R}^{(2,2)}$ space (4.6). If we take two boundary points A and B , and act on them with a bulk isometry transformation Λ of this type, we will observe that it does not preserve the Green's function (4.59):

$$G_c(\Lambda A, \Lambda B) \neq G_c(A, B). \quad (4.60)$$

It is the fundamental difference between holography of a Poincaré chart and holography of global AdS . In the first case the bulk isometries induce Lorentzian boosts on the boundary, so the Green function of a dual boundary field theory is a relativistic invariant object (4.33). In the second case the isometries rather act as conformal transformations leaving the Green function *covariant*, i.e. invariant up to some coordinate dependent scaling prefactors.

In the holographic language this is encoded in the fact that the renormalized lengths connecting boundary points are dependent on the choice of the reference frame. Below when we consider the DeDeo-Gott time machine geometry, we should be especially careful about this, since the geodesics there are combinations of Lorentz invariant and non-invariant terms as, for example, in (4.17). The proper way to deal with it is explained in the first subsection of Sec. 4.5.

In the next section we will analyze lensing of the quasigeodesics on the conical defects and calculate the Green function of the dual field theory in presence of the closed timelike curves in the bulk.

4.5 The two point Green's function

4.5.1 The algorithm

In Sec. 4.3 we have discussed the general idea of using the geodesic approximation to compute the boundary Green's function for the DeDeo-Gott geometry. Now we will formulate an exact algorithm for that.

- Introduce coordinate system on the unfolding of the double-cone space in such a way, that the physical (unremoved) part of the boundary consists of two stripes covered by coordinate intervals:

$$\begin{aligned}
 t &\in (-\infty, \infty), \\
 \phi &\in \left(-\frac{\pi}{2} - \frac{\Delta\phi}{2} + t, -\frac{\pi}{2} + \frac{\Delta\phi}{2} + t\right) \cup \left(\frac{\pi}{2} - \frac{\Delta\phi}{2} + t, \frac{\pi}{2} + \frac{\Delta\phi}{2} + t\right).
 \end{aligned}
 \tag{4.61}$$

- Fix two boundary points A and B . For simplicity we can choose $A = (0, -\frac{\pi}{2})$.
- Fix the total number of windings N that a geodesic of interest undergoes on the way from A to B . In our simulations we will not go beyond $N = 4$, because the higher-order contributions to the Green's function are highly suppressed.
- For the given A, B , and the number N , generate all possible $4 \cdot 3^{N-1}$ sets of the complementary points $\{C_1, \dots, C_{2N}\}$ corresponding to different sequences of windings $\{\mathcal{W}_1, \dots, \mathcal{W}_N\}$. The (quasi)geodesics then consist of $N + 1$ arcs $AC_1, C_2C_3, \dots, C_{2N}B$, each of which is just a (quasi)geodesic curve in empty AdS_3 .
- Impose that each of the “odd” complementary points C_{2i+1} belongs to the causal future of the previous “even point”: $C_{2i+1} \succ C_{2i}$.

Let us elaborate on what the reason to do so is. The most clear question we can ask is whether *causal* propagation of a signal from the future to the past is possible. To define the dual retarded Green function in presence of the CTC in the bulk, we should recall that evolution of a particle moving in the bulk of AdS can be split in two parts: “physical” continuous motion along a timelike or a spacelike geodesic, and “topological” time jumps caused by entwinement around the conical defects. In the holographic language

geodesic branches $C_{2i}C_{2i+1}$ correspond to the continuous evolution, and $C_{2i+1} \rightarrow C_{2i+2}$ identifications - to the time jumps. In absence of the closed timelike curves a signal could causally propagate from A to B if B belongs to the future light cone of A : $B \succ A$. A natural generalization of this prescription for the time machine case is to impose that this should hold true for all “physical” segments, i.e. $C_{2i+1} \succ C_{2i} \forall i$.

- For each of the causal quasigeodesics, solve for the intersection points $\{O_1, \dots, O_{2N}\}$. The easiest way to do this is to transform for each winding back to the rest frame of the corresponding wedge. For example, if branch $C_{2i}C_{2i+1}$ intersects first the trailing face of the 2nd wedge, and then the leading face of the 1st wedge, we perform a Lorentz transformation of the branch to the 2nd rest frame, then untwist the wedge by a simple coordinate transformation $\phi' = \phi - t$, such that angular location of the face remains still in these co-rotating coordinates, and solve the equation

$$(\phi_{C_{2i}C_{2i+1}}^{II}(\lambda_{2i}) - t_{C_{2i}C_{2i+1}}^{II}(\lambda_{2i})) \bmod 2\pi = \phi'_{T_{II}} \bmod 2\pi. \quad (4.62)$$

Then we repeat the procedure in the 1-st rest frame:

$$(\phi_{C_{2i}C_{2i+1}}^I(\lambda_{2i+1}) - t_{C_{2i}C_{2i+1}}^I(\lambda_{2i+1})) \bmod 2\pi = \phi'_{L_I} \bmod 2\pi. \quad (4.63)$$

- Make sure that all these equations have real solutions (otherwise discard the geodesic).
- Make sure that if a branch is not expected to intersect other faces within the physical region of the space, it actually does not (fake intersections within the removed part of the unfolding are allowed). In other words, if an arc $O_{2i}O_{2i}$ emerges from the face L_I and terminates at the face T_{II} , it should not have intersections with L_{II} and T_I .
- Calculate the lengths of all inner segments of the geodesic ($O_{2i}O_{2i+1}$). They are finite by construction and equal to

$$L_{O_{2i}O_{2i+1}} = \lambda_{2i+1} - \lambda_{2i}. \quad (4.64)$$

- Renormalize the lengths of the boundary segments AO_1 and $O_{2N}B$ as they are divergent:

$$L_{AO_1} = \frac{1}{2}L_{AC_1}^{ren} + \lambda_1, \quad (4.65)$$

$$L_{O_{2N}B} = \frac{1}{2}L_{C_{2N}B}^{ren} - \lambda_{2N}. \quad (4.66)$$

- Calculate the renormalized lengths of L_{AO_1} and $L_{O_{2N}B}$ in the *original frame*. As mentioned in the previous section, the renormalized lengths are not Lorentz-invariant. So, while we are free to constantly switch between different reference frames in order to calculate lengths of the finite inner segments $O_{2i}O_{2i+1}$, the renormalized lengths of the two boundary segments must be calculated in the original frame where we define the Green's function. In our case it is the “centre-of-mass frame”, where the two conical defects are symmetrically boosted.
- Finally calculate contribution of the geodesics to the Green function:

$$G(A, B) = \sum_k e^{-\Delta L_k}, \quad (4.67)$$

where the index k runs over the set of geodesics that satisfy aforementioned conditions.

In accordance with the described algorithm we subsequently account for contributions from higher winding numbers starting with $N = 2^5$. In other words, we formulate a kind of “perturbation theory” with the number of entwinements as a control parameter.

One property of this series expansion must be comment on. Each geodesic contributes to the Green function exponentially:

$$e^{-\Delta L_{ren}}. \quad (4.68)$$

For higher windings the number of internal segments $C_{2i}C_{2i+1}$ of the geodesic grows linearly in N , and so does its renormalized length L_{ren} .

⁵For negative times $N = 1$ windings do not contribute as they are due to the lensing on a single conical defect, that obviously can not lead to time travelling. But for positive times we take them into account.

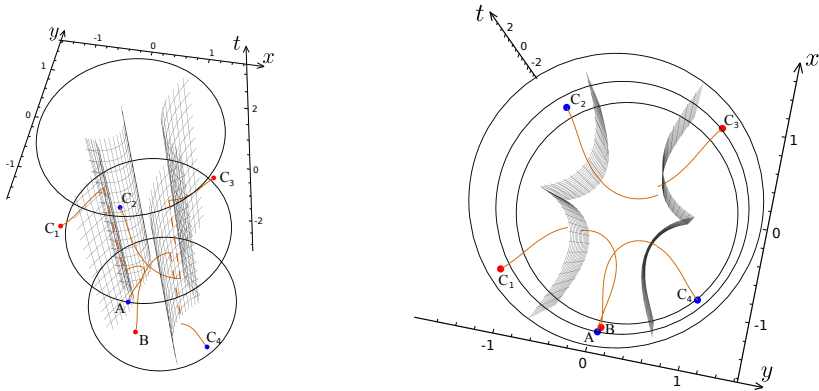


Figure 4.7. A quasigeodesic with winding number $N = 2$ connecting boundary points A and B .

Therefore the corresponding contribution to the Green function is exponentially small⁶. On the other hand the total number of possible topologically different geodesics scales as

$$n \sim 3^{N-1}, \quad (4.69)$$

i.e. grows exponentially. Therefore in principle these two effects can compete and we can not say a priori that the higher order contributions to the Green function are suppressed, and the sum over entanglements is convergent. If not, this could mean that our setup is unstable and undergoes a Hagedorn like transition.

However there are three different reasons for it not to happen. Firstly, by no means all of these $4 \cdot 3^{N-1}$ winding configurations satisfy the causality condition: $C_{2i+1} \succ C_{2i}$. Secondly, even if the causality condition for the set of complementary points is satisfied, the geometric structure of the geodesics becomes more and more complicated as the number of windings increases, and it becomes hard to force a geodesic curve to undergo the concrete sequence of windings (it is easy to see on Fig.4.8(b)). Finally, the “decaying” exponent has a conformal dimension as a knob, so at large enough Δ it dominates over the “growing” exponent.

Another way to understand convergence of the series expansion in all orders relies on a simple and general argument. Consider a germ of

⁶In a generic case when $L_{ren} > 0$.

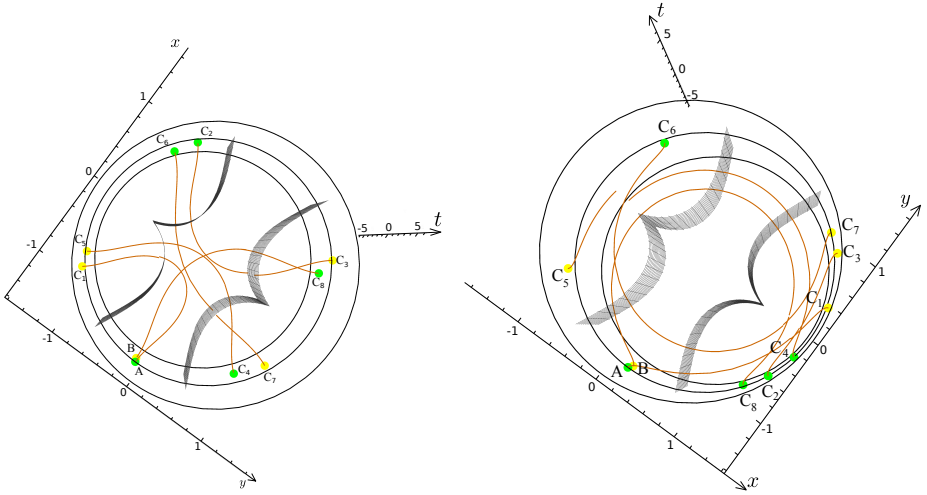


Figure 4.8. Left: an example of a physical $N = 4$ geodesic contributing to the Green function. Right: an example of physically impossible winding: for a given sequence of entanglements a geodesic can not be fit in the unremoved part of the spacetime.

all possible quasigeodesics emerging from point A . The first segment of a generic quasigeodesic curve hits the boundary at some point C_1 , first in the sequence of complementary points $\{C_i\}$. If we go along the curve further, we will obviously see that it is defined uniquely up to the final moment when it reaches the physical part of the boundary at point B . Thus, for a fixed initial point A , for each of the “first-in-the-sequence” complementary points C_1 the final point B is defined unambiguously. Now, as we have already emphasized, the singular contributions to the Green function come at the points where the renormalized geodesic length is infinitely negative, $\mathcal{L}^{ren} = -\infty$. It is possible if and only if C_1 is located exactly on a generatrix of the light cone emerging from point A , or C_2N is located on the generatrix of the light cone of point B . Quasigeodesics having the complementary points C_1 and C_2N right on the corresponding light cones form a zero measure subset among all possible quasigeodesics. Thus the set of boundary points where the Green function is infinite is also a zero measure subset of the boundary spacetime. Everywhere else the Green function is finite and well-defined.

4.5.2 Phenomenology and discussion

We are now ready to implement our computational algorithm for the DeDeo-Gott geometry. As shown in Sec. 4.2, closed timelike curves in the spacetime are present when the total angular deficit is more than 2π . For concreteness we impose $\alpha_{I,II} = \sqrt{3}\pi$, and the boost rapidities $\psi_{I,II} = \pm 1$. In their corresponding rest frames (in the co-rotating coordinates) the locations of the edges are taken to be

$$\begin{aligned}\phi'_{L_1} &= \alpha/2 & \phi'_{T_1} &= -\alpha/2, \\ \phi'_{L_2} &= \alpha/2 + \pi & \phi'_{T_2} &= -\alpha/2 + \pi.\end{aligned}\tag{4.70}$$

It is more convenient to calculate the Green function also in the co-rotating coordinates:

$$G^{cr}(t_1, \phi'_1; t_2, \phi'_2) = G(t_1, \phi_1 - t_1; t_2, \phi_2 - t_2).\tag{4.71}$$

For simplicity we will mostly study the Green function on a one-dimensional

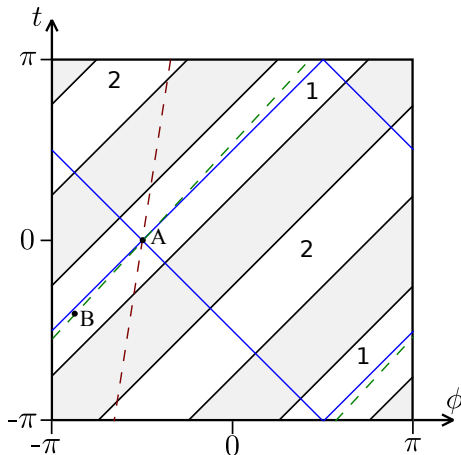


Figure 4.9. The Green function is sourced at point A with coordinates $(0, -\pi/2)$. Blue lines depict the light cone emerging from this point. Any timelike line would cross the removed region and enter another strip (red dashed line). In order to avoid formulating the boundary field theory on both strips simultaneously we calculate the Green function on a timelike line very close to the light cone generatrix.

timelike line passing through the point A . We should be careful here. Any

timelike line originated in one physical strip crosses the cut out region and enters the second strip. To formulate a quantum field theory on both strips simultaneously is possible yet tricky due to the fact that on the unification of two parts of the boundary time can not be globally defined. To avoid this difficulty we will consider the Green function on a timelike line in a close vicinity of the generatrix of the light cone. Then in a large range of times we will stay within one strip of the boundary.

In other words, the object we will attempt to evaluate is (in the co-rotating frame)

$$G^{cr}(0, -\pi/2; t, -\pi/2 + \epsilon t), \quad \epsilon \ll 1. \quad (4.72)$$

We have performed the numerical calculation of the retarded Green function for negative times $t < 0$ up to $N = 4$ order, and for positive times $t > 0$ up to $N = 2$.

Let's discuss firstly the analytic behaviour of the Green function at negative times, - how the quantum particle behaves travelling back in time. A naive expectation would be to think that the Green function decays as $t \rightarrow -\infty$, and it is partially true. However as we can see at not very large negative times the function develops a number of non-trivial features, - peaks which we can interpret as the "most probable" regions of times the particle can reach using the time machine. The corresponding results are present on Fig.4.10. As an illustration we also provide a two dimensional plot for the leading $N = 2$ winding at negative times, Fig4.11.

The origin of these peaks can be traced back to the fact that renormalized length of a geodesic can be negative. Generically at small conformal weights $N = 2$, $N = 3$ and $N = 4$ contributions are commensurate, but already at $\Delta \gtrsim 2$, higher entwinement terms are getting suppressed as compared to $N = 2$. However at specific points, where $\mathcal{L}_{ren} < 0$, the corresponding contributions to the Green function are getting enhanced in the large Δ limit⁷, forming a sharp peak. For instance, $N = 2$ set of geodesics contains such a curve around $t_2 = -1.9$, and $N = 4$ set has a special point at $t_2 \simeq -1.45$, Fig.4.10.

We have not performed numerical simulations for $N > 4$, but we can not exclude that such negative length curves can appear also at large N . The geodesic length is defined by lengths of internal segments (always positive) and lengths of the two boundary segments (that in principle can

⁷Strictly speaking, the geodesic approximation is reliable only in this limit.

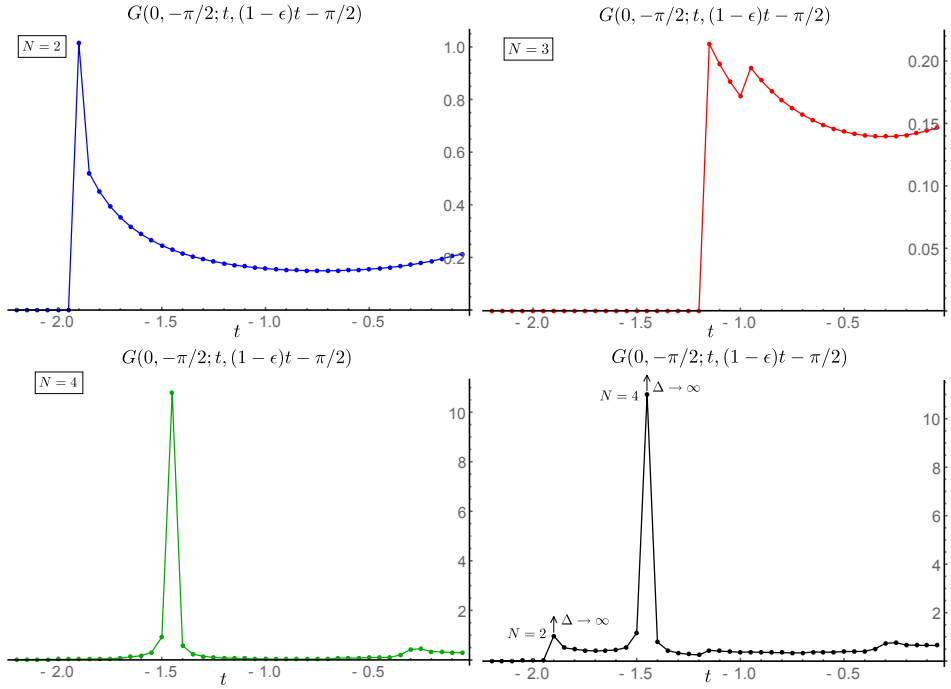


Figure 4.10. $N = 2$, $N = 3$, and $N = 4$ contributions to the retarded Green function at negative times at $\Delta = 1.5$. Discontinuities of the curves are artifacts of the geodesic approximation. The bottom right angle: the retarded Green function at $\Delta = 1.5$ ($N = 2$, $N = 3$ and $N = 4$ contributions are added up). For the large conformal dimensions peaks are enhanced, not suppresses, and we can see revival of the particle at moments preceding the excitation of the Green function. A not very large conformal dimension is chosen for convenience of presentation. Here $\epsilon = 0.1$.

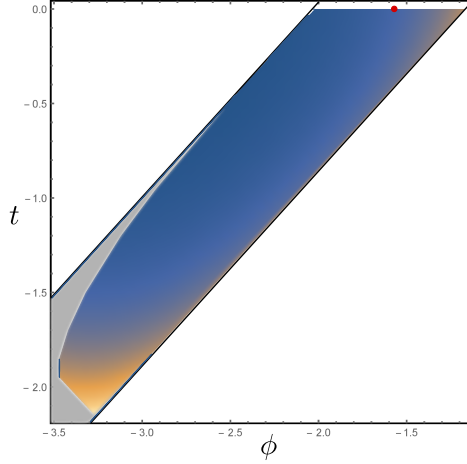


Figure 4.11. $N = 2$ contribution to the retarded Green function at $\Delta = 1.5$ at negative times in two dimensions. The Green function is sourced at the red point $(0, -\pi/2)$. We construct the theory only within one of the two strips of the boundary. Sudden break of the function signalizes that some regions of the spacetime are unattainable for the $N = 2$ quasigeodesics.

be negative):

$$\mathcal{L}_{AB}^{ren} = \mathcal{L}_{AO_1}^{ren} + \mathcal{L}_{O_{2N}B}^{ren} + \sum_{i=1}^N \mathcal{L}_{O_{2i-2}O_{2i-1}}. \quad (4.73)$$

If $\mathcal{L}_{AO_1}^{ren} + \mathcal{L}_{O_{2N}B}^{ren} < 0$, and $|\mathcal{L}_{AO_1}^{ren} + \mathcal{L}_{O_{2N}B}^{ren}| > \sum_{i=1}^N \mathcal{L}_{O_{2i-2}O_{2i-1}}$, the Green function will get a contribution that does not vanish in the large Δ limit. For a large number of internal segments it is not likely, but neither is impossible: while all internal lengths are finite, the renormalized negative lengths might be of an arbitrarily huge absolute value:

$$L_{AO_1}^{ren} < 0, |L_{AO_1}^{ren}| \gg 1, \quad (4.74)$$

thus dominating over positive contributions.

In the case of a large conformal dimension it would mean that, if we were able to sum up contributions in all winding orders, the resulting Green function would have a shape of a comb with a number of peaks (in our calculations we discovered two of them). These peaks play a role

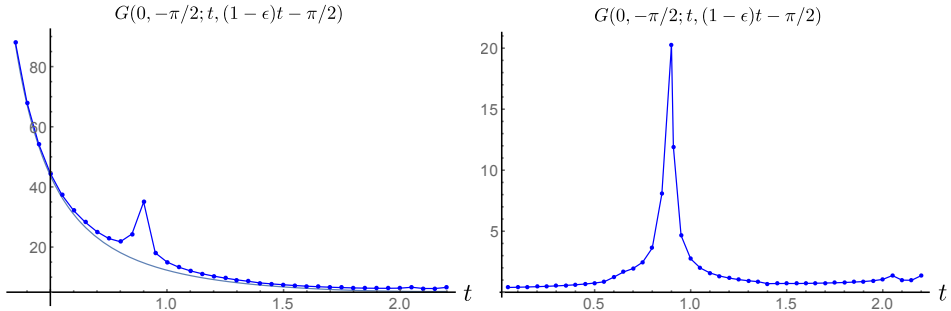


Figure 4.12. The retarded Green function at conformal weight $\Delta = 1$ at positive times. The left plot demonstrates how the non-trivial $N = 2$ windings modify the original Green function ($N = 1$ does not contribute when we consider the boundary theory within a single strip). The right plot represents the $N = 2$ winding contribution separately. We have made the Green’s function timelike to avoid dealing with the light-cone singularity. Here $\epsilon = 0.1$.

of “pit stops” for a particle travelling in time, - they form a set of easily reachable coordinates in time. Hence we deal with specific “negative time” revivals.

At positive times we have also discovered interesting features of the Green function. In the case of plain AdS_3 geometry the dual light-like Green function (shifted away from the singularity) is decaying in time. In presence of the causality violating conical defects we detected a new peak of a high weight, Fig.4.12, signaling a revival of the excitation.

4.6 Phases of the boundary field theory

We have calculated the Green function numerically up to $N = 4$ entanglements for the time machine geometry with $\alpha = \sqrt{3}\pi$ and $\psi = 1$. However it would be interesting to study how the properties of the Green function change upon changing the strength and rapidities of the conical defects. We constructed the leading order $N = 2$ contribution to the retarded Green function at negative times for $\alpha \in (1.1\pi, \dots 1.95\pi)$, and $\psi \in (0.1, \dots 1.5)$ with stepping $\Delta\alpha = 0.05\pi$, $\Delta\psi = 0.05$, paying special attention to the location in time and strength of the revival peak.

The results can be schematically summarized in a form of a phase diagram, Fig.4.13:

- If for a given value of α the rapidity ψ is not large enough to prevent the system from collapsing; the DeDeo-Gott geometry is forbidden (blue).
- If for a given value of α the rapidity ψ allows for the existence of the DeDeo-Gott time machine, but still not very large, we clearly see the effect of revival, and the peak is sharper the closer ψ is to the lower bound (yellow).
- If the rapidity is too large, the causality is violated, but excitations just decay and do not revive at negative times anymore (green).
- At very small values of α the retarded Green function does not exhibit any non-trivial features at negative time even in presence of the closed timelike curves (red). However, this feature is likely just an artifact of $N = 2$ approximation, and we do not expect it to be there for higher windings.

The profiles of the Green's function at negative times are presented on Fig.4.14(a,b) for $\alpha = 1.5\pi$ and $\alpha = 1.7\pi$ respectively. The fact that revivals are seen only at not very large rapidities (and the effect is stronger as closer ψ to its minimal possible value) is surprising and contrasts to how causality is broken in the bulk. The structure of CTC is defined by α and ψ , and the time jumps become stronger as the angle defects and rapidities are increased. Thus we rather should expect that for high ψ the time travelling along the CTC is more efficient in the sense that amplitudes of the *classical* free Green's function defined on the boundary are getting enhanced as $\alpha \psi$ grows. In the interacting holographic dual field theory the retarded Green's function is damped for larger α and ψ , so we can claim that causality in the boundary field theory is broken mildly as compared to the bulk.

Another interesting feature of this system is that while the overall weight of the Green function drastically decreases when the rapidity ψ is taken away from the “forbidden region” on the diagram, the actual past time penetration depth (i.e. the deepest reachable point at negative times where $G^{cr}(0, -\pi/2; t, -\pi/2) \neq 0$) increases (though very moderately), and this is in agreement with the “naive” intuition.

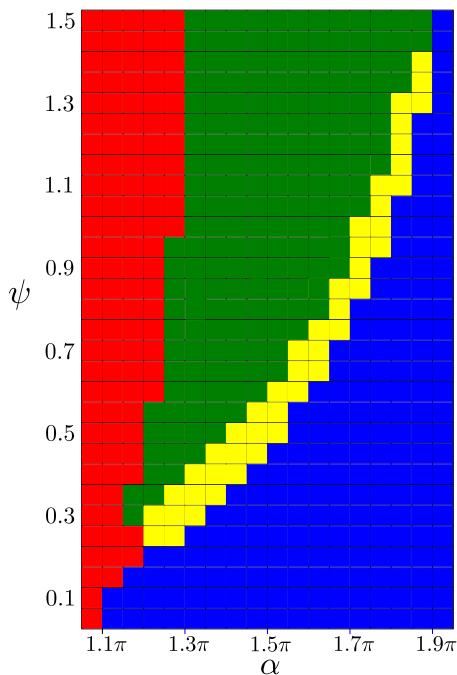


Figure 4.13. The four different “phases” of the boundary field theory. Blue spots depict the region of forbidden geometries, yellow spots are for the phase of negative time revivals, green spots form the region where the retarded Green function is non-zero at negative times, but does not exhibit reviving peaks in the large Δ limit. Red spots are where at the leading $N = 2$ order the boundary field theory retarded Green function does not demonstrate causality violation (i.e. $G^{cr}(0, -\pi/2; t, -\pi/2) \equiv 0, t < 0$) despite the presence of the CTC in the bulk. Everything is based on the numerical simulations of the leading $N = 2$ contribution to the retarded Green function. We expect higher order corrections to change the diagram qualitatively, but not quantitatively.

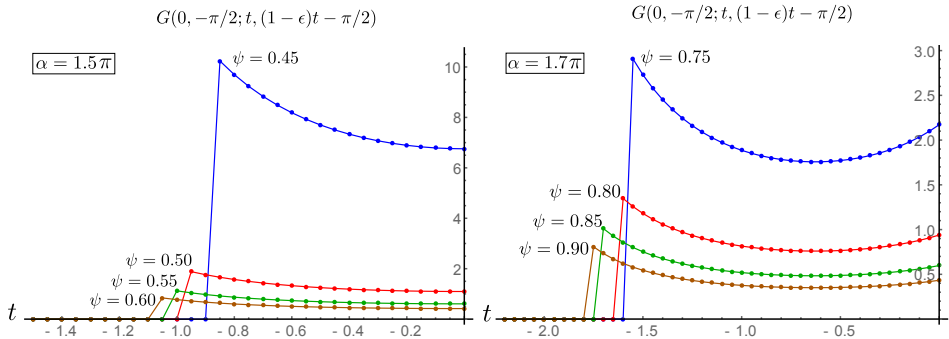


Figure 4.14. The negative time $N = 2$ contribution to the retarded Green's function at $\alpha = 1.5$, $\psi = 0.45, 0.50, 0.55, 0.60$ (left), and $\alpha = 1.7$, $\psi = 0.75, 0.80, 0.85, 0.90$ (right). Here $\Delta = 1$. On each of the plots the first three peaks are getting stronger and sharper as $\Delta \rightarrow \infty$ (the yellow region on the phase diagram), while the fourth one is getting suppressed in the same limit (the green region), so we do not consider it to be an actual revival of a non-causal excitation. Counterintuitively, the weight of the Green function drastically decreases when we increase α or/and ψ .

4.7 Conclusions

In this chapter we have analyzed properties of a two-point Green function in a (1+1)-dimensional field theory dual to the DeDeo-Gott time machine geometry. Using the geodesic approximation we have shown that *AdS/CFT* is capable of describing a quantum field theory when causality is violated, and have shown that the corresponding boundary propagator has remarkable features. We discovered that in presence of closed time-like curves in the *AdS* bulk a causal propagation of an excitation from the future to the past is possible on the boundary, and the retarded Green function exhibits peaks at certain negative times. At positive times analytic structure of the Green function also changes, and new singularities arise.

Surprisingly, we have found that as we increase the strength of the conical defects α and the rapidity ψ , the causality violation in the dual field theory is getting milder in the sense that the weight of the retarded Green's function at negative times decreases.

Contra to the previous results on the dynamics of physical systems in time machine backgrounds [23–26] our calculations have demonstrated

that sometimes it is possible to define evolution of an interacting theory in a time machine without imposing any additional self-consistency constraints. Despite the explicit non-causality the Green function does not have any uncontrollable pathologies.

Our considerations leave a number of open questions. First of all, we have to understand how to interpret the boundary state dual to the DeDeo-Gott geometry, - whether this quantum state is pathological or just exotic yet physical state. From the boundary point of view a single conical defect, if its angular deficit is $\alpha = 2\pi(1 - 1/N)$, can be thought of as state created by a non-local twist operator in a conformal field theory [33]. But what it means to have such an interplay of two independently boosted defects has to be clarified.

Another thing we have not touched on in the chapter is the entanglement structure of the boundary state. We focused on the properties of the retarded Green function, and thus analyzed the timelike quasigeodesics. However, even below the $\alpha = \pi$ threshold, when the CTC are not present in the system, due to the lensing it is possible to connect timelike separated boundary points just by standard continuous spacelike geodesics. If a certain generalization of the Ryu-Takayanagi conjecture [36] is true in this case, it would mean that the boundary state is timelike entangled [37]. Pursuing possible physical outcomes of this fact is an interesting direction for the future research.

Bibliography

- [1] K. Godel, “An Example of a new type of cosmological solutions of Einstein’s field equations of gravitation,” *Rev. Mod. Phys.* **21** (1949) 447.
- [2] W. J. van Stockum, “The gravitational feild of a distribution of particles rotating about an axis of symmetry,” *Proc. Roy. Soc. Edinburgh* **57** (1937) 135.
- [3] F. J. Tipler, “Rotating cylinders and the possibility of global causality violation,” *Phys. Rev. D* **9** (1974) 2203.
F. J. Tipler, “Causality violation in asymptotically flat space-times,” *Phys. Rev. Lett.* **37** (1976) 879.
- [4] M. S. Morris and K. S. Thorne, “Wormholes in space-time and their use for interstellar travel: A tool for teaching general relativity,” *Am. J. Phys.* **56** (1988) 395.
- [5] M. S. Morris, K. S. Thorne and U. Yurtsever, “Wormholes, Time Machines, and the Weak Energy Condition,” *Phys. Rev. Lett.* **61** (1988) 1446.
- [6] J. R. Gott, III, “Closed timelike curves produced by pairs of moving cosmic strings: Exact solutions,” *Phys. Rev. Lett.* **66** (1991) 1126.
- [7] A. Ori, “Formation of closed timelike curves in a composite vacuum/dust asymptotically-flat spacetime,” *Phys. Rev. D* **76** (2007) 044002 [gr-qc/0701024].
- [8] F. S. N. Lobo, “Time machines and traversable wormholes in modified theories of gravity,” *EPJ Web Conf.* **58** (2013) 01006 [arXiv:1212.1006 [gr-qc]].
- [9] O. Bertolami and R. Zambujal Ferreira, “Wormholes and Time-Machines in Nonminimally Coupled Matter-Curvature Theories of Gravity,” *EPJ Web Conf.* **58** (2013) 01008 [arXiv:1302.7125 [hep-th]].

- [10] S. M. Carroll, E. Farhi and A. H. Guth, Phys. Rev. Lett. **68** (1992) 263 [Phys. Rev. Lett. **68** (1992) 3368].
- [11] S. Deser, R. Jackiw and G. 't Hooft, Phys. Rev. Lett. **68** (1992) 267.
- [12] I. Y. Aref'eva and I. V. Volovich, "On the null energy condition and cosmology," Theor. Math. Phys. **155** (2008) 503 [hep-th/0612098].
- [13] V. A. Rubakov, "The Null Energy Condition and its violation," Phys. Usp. **57** (2014) 128 [arXiv:1401.4024 [hep-th]].
- [14] P. Creminelli, A. Nicolis and E. Trincherini, "Galilean Genesis: An Alternative to inflation," JCAP **1011** (2010) 021 [arXiv:1007.0027 [hep-th]].
- [15] P. Creminelli, M. A. Luty, A. Nicolis and L. Senatore, "Starting the Universe: Stable Violation of the Null Energy Condition and Non-standard Cosmologies," JHEP **0612** (2006) 080 [hep-th/0606090].
- [16] S. W. Hawking, "The Chronology protection conjecture," Phys. Rev. D **46** (1992) 603.
- [17] M. S. Costa, C. A. R. Herdeiro, J. Penedones and N. Sousa, "Hagedorn transition and chronology protection in string theory," Nucl. Phys. B **728** (2005) 148 [hep-th/0504102].
- [18] E. K. Boyda, S. Ganguli, P. Horava and U. Varadarajan, "Holographic protection of chronology in universes of the Godel type," Phys. Rev. D **67** (2003) 106003 [hep-th/0212087].
- [19] E. G. Gimon and P. Horava, "Over-rotating black holes, Godel holography and the hypertube," hep-th/0405019.
- [20] D. Brecher, P. A. DeBoer, D. C. Page and M. Rozali, "Closed time - like curves and holography in compact plane waves," JHEP **0310** (2003) 031 [hep-th/0306190].
- [21] M. M. Caldarelli, D. Klemm and P. J. Silva, "Chronology protection in anti-de Sitter," Class. Quant. Grav. **22** (2005) 3461 [hep-th/0411203].
- [22] M. M. Caldarelli, "Chronology protection in AdS/CFT," Fortsch. Phys. **54** (2006) 317 [hep-th/0602293].

- [23] O. V. Groshev, N. A. Gusev, E. A. Kuryanovich and I. V. Volovich, “On Solutions to the Wave Equation on Non-globally Hyperbolic Manifold,” arXiv:0903.0741 [math-ph].
- [24] F. Echeverria, G. Klinkhammer and K. S. Thorne, “Billiard balls in wormhole space-times with closed timelike curves: Classical theory,” Phys. Rev. D **44** (1991) 1077.
- [25] D. G. Boulware, “Quantum field theory in spaces with closed timelike curves,” Phys. Rev. D **46** (1992) 4421 [hep-th/9207054].
- [26] J. L. Friedman, N. J. Papastamatiou and J. Z. Simon, “Failure of unitarity for interacting fields on space-times with closed timelike curves,” Phys. Rev. D **46** (1992) 4456.
- [27] T. G. Mackay and A. Lakhtakia, “Towards a metamaterial simulation of a spinning cosmic string,” Phys. Lett. A **374** (2010) 2305 [arXiv:0911.4163 [physics.optics]].
- [28] M. Ringbauer, M. A. Broome, C. R. Myers, A. G. White and T. C. Ralph, “Experimental simulation of closed timelike curves,” Nature Commun. **5** (2014) 4145 [arXiv:1501.05014 [quant-ph]].
- [29] S. DeDeo and J. R. Gott, III, “An Eternal time machine in (2+1)-dimensional anti-de Sitter space,” Phys. Rev. D **66** (2002) 084020 [Erratum-ibid. D **67** (2003) 069902] [gr-qc/0212118].
- [30] S. Holst and H. J. Matschull, “The Anti-de Sitter Gott universe: A Rotating BTZ wormhole,” Class. Quant. Grav. **16** (1999) 3095 [gr-qc/9905030].
- [31] V. Balasubramanian and S. F. Ross, “Holographic particle detection,” Phys. Rev. D **61** (2000) 044007 [hep-th/9906226].
- [32] V. Balasubramanian, A. Naqvi and J. Simon, “A Multiboundary AdS orbifold and DLCQ holography: A Universal holographic description of extremal black hole horizons,” JHEP **0408** (2004) 023 [hep-th/0311237].
- [33] V. Balasubramanian, B. D. Chowdhury, B. Czech and J. de Boer, “Entwinement and the emergence of spacetime,” JHEP **1501** (2015) 048 [arXiv:1406.5859 [hep-th]].

- [34] V. Balasubramanian, A. Bernamonti, B. Craps, V. Keränen, E. Keski-Vakkuri, B. Müller, L. Thorlacius and J. Vanhoof, “Thermalization of the spectral function in strongly coupled two dimensional conformal field theories,” *JHEP* **1304** (2013) 069 [arXiv:1212.6066 [hep-th]].
- [35] P. Di Francesco, P. Mathieu, D. Senechal “Conformal Field Theory,” Springer-Verlag New York (1997) 890 p
- [36] S. Ryu and T. Takayanagi, “Aspects of Holographic Entanglement Entropy,” *JHEP* **0608** (2006) 045 [hep-th/0605073].
- [37] S. J. Olson and T. C. Ralph, “Entanglement between the future and past in the quantum vacuum,” *Phys. Rev. Lett.* **106** (2011) 110404 [arXiv:1003.0720 [quant-ph]].

Chapter 5

Discussion

In this thesis we have analyzed three completely different problems using the *AdS/CFT* correspondence. To conclude, let us discuss how these stories can be embedded in the wider context of the holographic theory of strongly coupled systems, and provide an outlook of possible directions for future research.

5.1 Holographic fermions and superconductivity

Among others, a natural and important goal of studies in the area of applications of gauge/string duality to condensed matter physics is to formulate a complete dynamical holographic theory of an unconventional superconductivity with an explicit fermionic pairing mechanism. However, what could be meant by pairing in holography requires clarification. As a weak/strong duality, the AdS/CFT correspondence helps to describe quantum field theories at strong 't Hooft gauge coupling λ_H by dualizing them to solutions of string theory at small string coupling constant g_s . In real solid state systems, the 't Hooft gauge coupling does not have an unambiguous phenomenological meaning, but we can say that in condensed matter-oriented holographic constructions that λ_H is responsible for the emergence of highly correlated collective excitations out of fundamental degrees of freedom in the field theory. In that sense, it is similar to the Coulomb interaction between fundamental bare electrons in a piece of metal that governs collective dynamics at the very microscopic level. However, if we wish to describe pairing in superconductivity, we should also include in our considerations another channel(s) of interactions, now responsible for coupling between these emergent composite operators, and would play the same role as phonons or spin waves play in real materials.

In Chapter 2 we introduced this explicit pairing channel via a Yukawa-like term in the bulk action that couples fermions to the order parameter. We have demonstrated that this leads to the opening of a superconducting

gap in the system and to condensation of the scalar order parameter. It is natural to make the dual bulk scalar field dynamical, and the strength of the interactions in this setup is then effectively controlled by the ratio of the Yukawa coupling and scaling dimension of the scalar: λ_Y/Δ_ϕ . In the regime of weak coupling, $\lambda_Y/\Delta_\phi \ll 1$, the boundary field theory exhibits properties of the conventional *BCS* superconductivity, while upon increasing the coupling it undergoes the BEC/BCS crossover.

However, this result should be considered as a very first step towards the ultimate goal. Our model should be further improved in the following ways.

- Because we were originally interested in a holographic reformulation of the Bardeen-Cooper-Schrieffer theory of superconductivity, we studied the superconducting instability in a model of a holographic Fermi-liquid, i.e. in a model with a sharp spectrum of fermionic quasi-particles. But if we are interested in an unconventional SC, we should take into account that fermionic degrees of freedom can be of a critical nature. So, to generalize our model, one can try to remove the IR cut-off and analyze the pairing of “unparticle” fermions.
- We have studied only the $T = 0$ ground state of the theory. On the other hand, it would be interesting to understand properties of the fermionic superconductivity at finite temperature and to study its thermal phase diagram.
- Our model accounts for interactions between fermions, the bulk gauge field, and the scalar order parameter, but we did not take into account the backreaction of the bulk fermions on the background metric. This could be important if one really wants to go beyond the probe limit and study superconductivity in a strongly correlated system. A first attempt to construct a setup with backreacting fermions (though without pairing and a dynamical scalar field) has been performed in [1, 2], and it is clear that to generalize it to a fully interacting case would be a very difficult numerical challenge.
- It would be interesting to analyze the transport properties of the model and to study the fermionic corrections to the electric conductivity. Also, it might be important to know how the model would behave once we introduce a lattice.

- We implemented the pairing while staying ignorant about its physical mechanism. Thus it would be interesting to formulate a more detailed “microscopic” theory where this interaction is caused by a non-trivial dynamical field.

5.2 Holography and the non-equilibrium quark-gluon plasma

Another important area of research in contemporary science is the physics of the quark-gluon plasma. When QCD matter is heated up to a very high temperature, $T \gtrsim 170\text{MeV} \sim 10^{12}K$, it undergoes a phase transition, and quarks and gluons, normally bounded within hadrons, deconfine: they start behaving as independent unbounded entities. Such an extremal and unusual state of matter opens room for studying properties of quantum matter that are inaccessible under normal circumstances. Experimentally the QGP can be produced in high energy collisions of heavy ions, like *Pb* and *Au*. A large number of constituent nucleons is crucial for creating a many-body state of matter.

The underlying Lagrangian for the quark-gluon plasma is just the well-known Lagrangian of QCD, but it is of little use: the experimentally produced QGP is a strongly coupled and highly non-equilibrium state of matter [3], and standard mathematical methods of quantum field theory are not applicable here. One can think about a holographic description of quark-gluon plasma formation in high energy heavy ions collisions. On the dual gravitational side, the relativistic ions are represented by gravitational shock waves. The collision leads to mutual stopping of the waves, and their kinetic energy transforms into rest energy, causing creation of a black hole. In the boundary field theory, this effect can be interpreted as the formation of a thermal deconfined state of matter, the QGP.

In Chapter 3 we have considered this model of colliding shock waves at non-zero chemical potential. Although in real experiments on heavy ion collisions the chemical potential is negligible, and all corresponding holographic models do not take it into account, it might be interesting to see if introducing non-zero charge density would lead to qualitatively correct phase diagram. In particular, it is expected in QCD that at higher density of hadronic matter, the temperature of the deconfinement phase transition becomes smaller, i.e. less energy is needed to produce the quark-gluon plasma. Surprisingly, in the simplest model of gravitational plane

waves we discovered an opposite tendency: larger chemical potential suppresses formation of QGP. It might indicate that already the chargeless models commonly used in holographic computations might require some modifications to be correct.

However, to really test our observation a further extensive analysis is required. In our calculations we limited ourselves by an analytic estimate of the size of the formed black hole based on a critical trapped surface calculation, that can be performed without simulations of the bulk gravitational field after the shock wave collision. But in order to fully understand the effect of non-zero chemical potential, complete real-time numerical simulations are required. With the advances in non-equilibrium numerical holography [4] this may be done in the near future.

5.3 Theoretical aspects of time travelling

Finally, in Chapter 4 we have applied the *AdS/CFT* correspondence to get an insight into a more fundamental issue in gravitational physics, and analyzed the behaviour of a two-point Green's function of a quantum field theory in a space with causality violation, by dualizing it to a space-time with closed time-like curves. In this case, the main advantage of the *AdS/CFT* was not that it is a weak/strong duality, but rather that it is a classical/quantum duality. Therefore the non-causal quantum dynamics could be mapped onto classical geometry, and the problem drastically simplifies. But our calculation leaves many open questions.

First of all, we considered a time machine solution to classical General Relativity in three dimensions. Is it possible to find a string theory embedding for this solution? Would this embedding preserve the closed time-like curves, or do holographic screens appear, restoring the causality, like happens for Gödel spacetimes in string theory [5, 6]?

In our model we relied on the geodesic approximation to avoid solving the field equations in a topologically non-trivial causality-violating background. On the other hand, because three dimensional gravity is purely topological and does not have propagating degrees of freedom, any solution is locally isometric to an empty *AdS*₃ and often can be represented as its factorization over some symmetry group. So we can not exclude that it is possible to represent the DeDeo-Gott solution that we considered in this form. Then an exact solution to a wave equation on this background could be easily generated.

Another issue is the field theoretical interpretation of the result. In the bulk we have a very simple configuration of two conical defects, so we might expect that it corresponds to a decent quantum state in the dual field theory. We do not know what that state is, but can try to speculate. In the case of three dimensions, bulk geodesics do not only contribute to the Green's functions, but also define the entanglement entropy of boundary regions, as conjectured by Ryu and Takayanagi [7]. Usually only equal-time entanglement is well-defined. However recently it has been proposed [8] to simulate CTC quantum mechanically by entangling a qubit to an older version of itself. Thus it could be possible that in our setup we deal with a field theoretical version of this non-equal time entanglement. Whether this conjecture is correct is a question for future investigation.

In this work, by solving several completely different problems, we tried to demonstrate that the holographic correspondence is a paradigm that has the power to provide intuition on totally diverse phenomenological concepts and systems by mapping them onto the same set of resonantly connected mathematical structures. A long way is ahead, a lot of problems remain to be addressed, and we still do not understand much about borders of the applicability of holography. If the boldest formulation of the holographic principle is true, and any quantum theory has a dual, the correspondence may very well become the Glass Bead Game of theoretical physics, in the original, literal meaning that Herman Hesse gave to this concept.

Bibliography

- [1] A. Allais, J. McGreevy and S. J. Suh, “A quantum electron star,” *Phys. Rev. Lett.* **108** (2012) 231602 [arXiv:1202.5308 [hep-th]].
- [2] A. Allais and J. McGreevy, “How to construct a gravitating quantum electron star,” *Phys. Rev. D* **88** (2013) 6, 066006 [arXiv:1306.6075 [hep-th]].
- [3] J. Adams *et al.* [STAR Collaboration], “Experimental and theoretical challenges in the search for the quark gluon plasma: The STAR Collaboration’s critical assessment of the evidence from RHIC collisions,” *Nucl. Phys. A* **757** (2005) 102 [nucl-ex/0501009].
- [4] P. M. Chesler and L. G. Yaffe, “Numerical solution of gravitational dynamics in asymptotically anti-de Sitter spacetimes,” *JHEP* **1407** (2014) 086 [arXiv:1309.1439 [hep-th]].
- [5] E. K. Boyda, S. Ganguli, P. Horava and U. Varadarajan, “Holographic protection of chronology in universes of the Godel type,” *Phys. Rev. D* **67** (2003) 106003 [hep-th/0212087].
- [6] E. G. Gimon and P. Horava, “Over-rotating black holes, Godel holography and the hypertube,” [hep-th/0405019].
- [7] S. Ryu and T. Takayanagi, “Holographic derivation of entanglement entropy from AdS/CFT,” *Phys. Rev. Lett.* **96** (2006) 181602 [hep-th/0603001].
- [8] M. Ringbauer, M. A. Broome, C. R. Myers, A. G. White and T. C. Ralph, “Experimental simulation of closed timelike curves,” *Nature Commun.* **5** (2014) 4145 [arXiv:1501.05014 [quant-ph]].

Samenvatting

Dit proefschrift is gewijd aan het toepassen van de holografische dualiteit op een kwalitatieve analyse van problemen in verschillende gebieden van de theoretische natuurkunde. Na een overzicht van de basisprincipes van deze correspondentie tussen een anti-de Sitter ruimte en een conforme veldentheorie in een dimensie lager (AdS/CFT) in hoofdstuk 1, nemen wij zijn concrete toepassingen in de fysica van de gecondenseerde materie, de kwantumchromodynamica, en de theorie van de niet-causale ruimtetijden ter hand.

In hoofdstuk 2 gebruiken we AdS/CFT methoden om een theorie te formuleren van BCS-achtige (Bardeen-Cooper-Schrieffer) supergeleiding gedreven door het paarsgewijs condenseren van fermionen in holografische systemen met Landau-achtige langlevende quasideeltjes. We tonen aan dat de duale theorie op de rand van AdS, dual aan een interagerende Dirac-Maxwell-Scalar theorie, zowel supergeleiding als de Bardeen-Cooper-Schrieffer/Bose-Einstein condensaat (BCS/BEC) crossover vertoont. Wanneer de scalaire en de fermionische velden ontkoppeld zijn, concurreren zij om de elektrische lading, en onderdrukken de fermionen het scalaire superfluid condensaat. Als er daarentegen sprake is van Yukawa koppeling, dragen de fermionen bij aan de totale condensaat waarde. Een opmerkelijk aspect van holografische fermionen is dat het bulk $U(1)$ ijkveld, dual aan de chemische potentiaal op de rand, een splitsing van de fermionische banden induceert (dit kan worden beschouwd als een bulk analoog van Rashba spin-baan splitsing), die op zijn beurt leidt tot het feit dat de paarvormings-symmetrie in de veldentheorie op de rand gelijk is aan $p + ip$. We merken ook op dat de standaard Gubser-Klebanov-Polyakov-Witten regel voor correlatiefuncties aan de theorie op de rand niet zonder wijzigingen kan worden gebruikt zodra de bulkvelden aan elkaar zijn gekoppeld.

In hoofdstuk 3 richten we onze aandacht op de niet-evenwicht fysica van de vorming van het quark-gluon plasma (QGP) dat in botsingen van zware ionen tot stand komt. We gebruiken ter vereenvoudiging compleet vlakke zwaartekrachts-schokgolven als een dual model voor de relativistische ionen in de veldentheorie op de rand en bestuderen hoe de aanwezigheid van een chemische potentiaal het proces van QGP forma-

tie beïnvloedt. Om de moeilijkheden van een dynamische simulatie van het bulksysteem met botsende schokgolven te omzeilen, concentreren we ons op de formatie van “trapped surfaces” (omsloten oppervlakken) die het mogelijk maken enkele eigenschappen van “het-te-vormen” zwart gat (duaal aan de deconfined toestand in de randtheorie) in te schatten, zonder de tijdsafhankelijke Einstein vergelijkingen op te hoeven lossen. We concluderen dat, vergeleken met het neutrale geval, elektrische lading de hoeveelheid hadrons geproduceerd in de botsing vermindert, en de temperatuur van de confinement/deconfinement overgang verhoogt.

In hoofdstuk 4 behandelen wij paradoxen behorende bij het reizen in de tijd. Met behulp van holografie kunnen wij de tweepunts Green’s functies in een niet-causale kwantumveldentheorie berekenen. Zulke theorieën zijn moeilijk vanuit basisprincipes te herleiden. De zwaartekracht-configuratie dual in deze theorie is een $(2 + 1)$ - dimensionale anti-de Sitter ruimtetijd met twee elkaar omcirkelende conische defecten. Dit resulteert in een ruimtetijd met gesloten tijdachtige krommen. Door toepassing van de AdS/CFT-correspondentie in zijn klassieke limiet, kunnen we de analyse van de kwantumdynamica zonder causaliteit vereenvoudigen tot simpelweg de analyse van klassieke pseudo-Riemann-metkunde van de bulk ruimtetijd. Ons basierend op de geodetische benadering kunnen we de Green’s functie in de theorie op de rand afleiden zonder extra zelf-consistentie eisen en wij tonen aan dat, zelfs in afwezigheid van de causaliteit, de evolutie van een kwantumveld zowel controleerbaar als niet-pathologisch kan zijn.

Tenslotte geven we in hoofdstuk 5 een overzicht van onze resultaten en plaatsen ze in een bredere context van de hedendaagse theoretische fysica.

Summary

The thesis is devoted to applications of holographic duality to qualitative analysis of problems in different areas of theoretical physics. After reviewing the basic principles of holography in the form of the anti-de Sitter/Conformal field theory (AdS/CFT) correspondence in Chapter 1, we proceed to its concrete applications in condensed matter physics, quantum chromodynamics, and the theory of non-causal spacetimes.

In chapter 2 we employ the AdS/CFT methods to formulate a theory of fermion driven ordering through pairing induced BCS-like superconductivity in holographic systems with Landau-like long-lived quasiparticles. We demonstrate that the AdS boundary dual of an interacting Dirac-Maxwell-scalar theory exhibits both superconductivity and the BCS/BEC crossover. If the scalar and fermionic field are decoupled from each other, they compete for the electric charge, and fermions suppress the scalar superfluid condensate. On the other hand, if the Yukawa coupling is switched on, fermions contribute additively to the total condensate value. A notable aspect of holographic fermions is that the bulk $U(1)$ gauge field dual to the boundary chemical potential also induces splitting of the fermionic bands (that might be considered as a bulk analogue of the Rashba spin-orbit splitting), which in turn leads to the fact that the pairing symmetry in the boundary field theory is $p + ip$. We also make an observation that the standard Gubser-Klebanov-Polyakov-Witten rule for the correlation functions cannot be used without modification once the bulk fields are coupled to each other.

In chapter 3 we turn our attention to the non-equilibrium physics of the formation of the quark-gluon plasma (QGP) in heavy ion collisions. For simplicity we use flat planar gravitational shock waves as a dual model of relativistic ions in the boundary field theory and study how a non-zero chemical potential affects the process of QGP formation. In order to circumvent the difficulties related to the full dynamical simulation of the bulk system of colliding shock waves, we stick to the formalism of trapped surfaces that allow us to obtain some estimates on properties of the “to-be-formed” black hole (dual to the deconfined boundary state) without solving the time-dependent Einstein equations. We find that as compared to the neutral case, electric charge reduces the multiplicity of

hadrons produced in the collision, and increases the temperature of the confinement/deconfinement transition.

In chapter 4 we address paradoxes of time traveling. Using holography we can calculate the two-point Green's functions in a non-causal quantum field theory. Such a theory is hard to construct *ab initio*, but its gravity dual is just a $(2 + 1)$ -dimensional anti-de Sitter spacetime with two orbiting conical defects. This results in a spacetime with closed timelike curves. Applying the AdS/CFT-correspondence in its classical limit, we can simplify the analysis of the quantum dynamics at broken causality to just the analysis of the classical pseudo-Riemannian geometry of the bulk spacetime. Relying on the geodesic approximation we can perform the derivation of the dual field theory Green's function without implying any additional self-consistency constraints and we show that evolution of a quantum field can be controllable and non-pathological even in absence of causality.

Finally, in chapter 5 we give a summary of our results and put them in a wider context of the contemporary theoretical physics.

List of Publications

The thesis is based on the following publications:

1. I. Y. Arefeva, A. A. Bagrov and E. O. Pozdeeva, “Holographic phase diagram of quark-gluon plasma formed in heavy-ions collisions,” *JHEP* **1205** (2012) 117 [arXiv:1201.6542 [hep-th]].
2. A. Bagrov, B. Meszema and K. Schalm, “Pairing induced superconductivity in holography,” *JHEP* **1409** (2014) 106 [arXiv:1403.3699 [hep-th]].
3. I. Arefeva, A. Bagrov, P. Säterskog and K. Schalm, “Holographic dual of a time machine,” [arXiv:1508.04440 [hep-th]].

Other publications by the author are

4. I. Y. Arefeva, A. A. Bagrov and E. A. Guseva, “Critical Formation of Trapped Surfaces in the Collision of Non-expanding Gravitational Shock Waves in de Sitter Space-Time,” *JHEP* **0912** (2009) 009 [arXiv:0905.1087 [hep-th]].
5. I. Y. Arefeva, A. A. Bagrov and L. V. Joukovskaya, “Critical Trapped Surfaces Formation in the Collision of Ultrarelativistic Charges in (A)dS,” *JHEP* **1003** (2010) 002 [arXiv:0909.1294 [hep-th]].
6. I. Arefeva, A. Bagrov and A. S. Koshelev, “Holographic Thermalization from Kerr-AdS,” *JHEP* **1307** (2013) 170 [arXiv:1305.3267 [hep-th]].
7. A. A. Bagrov, “Time machine creation in the ultra-relativistic proton collisions,” *Nucl. Phys. Proc. Suppl.* **216** (2011) 211.
8. I. Y. Arefeva, A. A. Bagrov and L. V. Joukovskaya, “Several aspects of applying distributions to analysis of gravitational shock waves in general relativity,” *St. Petersburg Math. J.* **22** (2011) 3, 337.

Curriculum Vitæ

I was born on 18 July 1987 in Zheleznodorozhny, a city in the Moscow Region in Russia. In 2003 I became a student at the Faculty of Physics of Moscow State University, and graduated in 2009 with a master degree *summa cum laude* from the department of quantum theory and high energy physics. Title of my master thesis was “Astrophysical sources of electromagnetic radiation as possible sources of gravitational waves”. In parallel, since the fall of 2005 I attended courses on modern mathematics and mathematical physics at the Steklov Mathematical Institute of the Russian Academy of Sciences.

In 2009 I enrolled a graduate program at the Steklov Institute. After spending the next two years as a PhD student there working on the theory of trans-Planckian collisions under supervision of Prof. Irina Arefeva, I became more interested in low energy physics and transferred to Leiden, the Netherlands, in September 2011 to do PhD research with Prof. Jan Zaanen and Prof. Koenraad Schalm on applications of the *AdS/CFT* correspondence to condensed matter physics at the Lorentz Institute for Theoretical Physics.

While in Leiden, I was a tutor for the courses on General Relativity and condensed matter theory.

During my study in Moscow and Leiden I have attended a number of schools and conferences in Russia, the Netherlands, Germany, Czech Republic, Switzerland, France, the United Kingdom, Greece, China, Austria, Iceland, and Sweden.

After graduation with a PhD degree, I will continue my academic career as a postdoctoral researcher at the Radboud University in Nijmegen, the Netherlands, with Prof. Mikhail Katsnelson.

Acknowledgments

First of all, I would like to express my deep gratitude to my advisors Koenraad Schalm and Jan Zaanen. By working with you I have not only drastically improved my professional skills but also developed a unique aesthetic perception of physics.

I very much like to mention Irina Arefeva, my former advisor from the Steklov Mathematical Institute and my long term collaborator. Thank you for bringing me into the world of theoretical physics.

The Lorentz Institute for Theoretical Physics is the place where I spent the happiest years of my life, and I am grateful to everyone who contributed to creating this pretty special atmosphere, in particular to Mihailo Cubrovic, Robert-Jan Slager, Louk Rademaker, Yan Liu, Ya-Wen Sun, Ke Liu, Jaakko Nissinen, Saso Grozdanov, Nick Poovuttikul, Mikhail Goykhman, Andrei Parnachev and Ana Achucarro. I am especially thankful to my collaborators Balazs Meszena, Nikos Kaplis, Petter Säterskog, Steffen Klug, and my officemate Richard Davison. I am indebted to Stephani Ribecco for helping me to always remain capable of doing research.

I thank the secretaries of the Lorentz Institute Trudy Geurds, Marianne Gouw, and Fran Ouwerkerk for their kind and professional assistance.

I thank my friends Olga Borovkova, Alexander Kuzmenkov, Marina and Alexey Volkov, Marina Vorontsova, Nikolay Kutrukhin, Anastasia Tarasyuk, Valentina Utochnikova and Natalia Yakovenko for being an important part of my life. You are those who inspire me to do science, and your role in shaping my personality is exceptional.

Professional development of myself as a scientist would have been impossible without the endless, decade-long discussions with my father Alexander on the philosophy and methodology of science, and without the enormous amounts of care and understanding from my mother Valentina. Anastasia, my dear sister, I put a very high value on our friendship.

Finally, I am infinitely thankful to my beloved wife Olga for constantly supporting me with her sincere will and ability to understand my thoughts and desires, and for sharing all important aspects of my worldview.